POLITECNICO DI TORINO

Master’s Degree in Civil Engineering

Master's Thesis

Progressive Collapse of structures



Supervisor:
Professor Valerio De Biagi

Co-supervisor:
Professor Foad Kiakojouri

Student:

Annapaola Di Fabio

September 2026

Contents

1 INTRODUCTION 3

2 TIPOLOGY OF PROGRESSIVE COLLAPSE 5

2.1 Types of progressive collapse 5

2.1.1 Pancake-type collapse 5

2.1.2 Zipper-type collapse 7

2.1.3 Domino-type collapse 9

2.1.4 Section-type collapse 12

2.1.5 Instability-type collapse 13

2.1.6 Mixed-type collapse 16

3 MAJOR COLLAPSES IN HISTORY 18

3.1 Ronan Point Collapse 18

3.2 Oklahoma City Collapse 19

3.3 World Trade Center Collapse 20

4 CASE STUDY 25

4.1 Difference between FEM and AEM 25

4.2 Design of the structure located in Turin 27

4.2.1 Properties of materials used 28

4.2.2 Properties of sections and floor used 30

4.2.3 Load case schematization 32

4.2.4 Load combination definition 34

4.2.5 Seismic action evaluation 36

4.2.6 Legend of seismic analysis results 38

4.2.7 Verification of reinforced concrete beam and column elements 39

4.3 Design of the structure located in L'Aquila 59

4.3.1 Properties of structural elements used 59

4.3.2 Load case schematization 60

4.3.3 Seismic action evaluation 61

4.3.4 Legend of seismic analysis results 63

4.3.5 Verification of reinforced concrete beam and column elements 63

5 ANALYSIS OF THE PROGRESSIVE COLLAPSE OF STRUCTURES 79

5.1 Analysis performed on ELS 80

5.2 Description of analysed scenario 83

5.3 Normal straining action distribution 92

6 CONCLUSIONS 95

7 BIBLIOGRAPHY 97

1 INTRODUCTION

Engineers started to recognize the dangers linked to progressive or disproportionate collapse after the 1968 incident involving Ronan Point, a 22-story residential building in London (Ministry of Housing and Local Government, 1968). First, a brief description of the difference between progressive and disproportionate collapse. Below are reported the definitions: progressive collapse is defined as "the spread of an initial local failure from element to element, eventually resulting in the collapse of an entire structure or a disproportionately large part of it" [1]. Disproportionate collapse is defined as "a collapse [that] results from small damage or a minor action leading to the collapse of a relatively large part of the structure" [2]. From the definition reported above it is clear that with the term "disproportionate" it is indicated that a small failure area can propagate to a large or uncontrollable area. "Progressive" instead refers to small failures that don't lead to the whole collapse of the structure, but the elements fail progressively. However, the two terms are often considered synonymous because progressive can cause disproportionate collapse. This slight difference is also discussed in Section 2.1.5

The collapse of the Twin Towers in New York on September 11, 2001, represents another significant turning point in the field of structural engineering, because it led to the adoption of new design measures to prevent progressive failure of structures. The 9/11 attack additionally led to a rising application of updated design standards to prevent progressive collapse of different structures. The events mentioned above have been crucial for a regulation point of view, in fact design guidance has been developed. In the United Kingdom, guidance is provided by the Building Regulations and associated Approved Documents, as well as by structural design standards such as BS 5950. In the United States, specific provisions for mitigating progressive collapse have been developed by the General Services Administration (GSA) and the Department of Defense (DoD).

In Italy it is possible to refer to NTC2018 or CNR-DT, that is widely recognised as an authoritative technical document.

The aim of the thesis is to understand how a structure designed in accordance with seismic regulations is more robust in the face of certain phenomena, such as impacts or explosions, by simulating its collapse. Having introduced the concept of robustness, it is now necessary to clarify its meaning by referring to two of the most important codes. According to the Eurocode BS EN 1990 [3]: "A structure shall be designed and executed in such a way that it will not be damaged by events such as explosion, impact, and the consequences of human errors, to an extent disproportionate to the original cause", instead considering the Building Regulations [4], the robustness requirements are identified based on the consequence class. The classes depend on the sizes and types of the building. Below are reported the table that summarizes the description above.

Consequence Class	**Robustness Requirement**
1	No additional measures needed.
2a	1. Horizontal ties. 2. Effective anchorage of suspended floors to walls in accordance to code of practice.
2b	1. Horizontal ties or effective anchorage of suspended floors to walls in accordance to code of practice. 2. Check that with the removal of a column or wall, the building remains stable and the area at any storey

	at risk of collapse does not exceed 15% of the floor area of that storey or 100 m2, whichever is smaller. If the collapse area limit is exceeded, such an element should be designed as a key element.
3	Systematic risk assessment of the building should be taken into account for all critical situations, and correspondent design measures should be taken.

Table 1.1

Keeping in mind the concept of robustness, it will be possible to observe in the following chapters the different behaviour of the structure: at the beginning designed taking into account only the static loads, subsequently considering also the seismic actions. The structure is the same, but the dimensions of the structural elements and the amount of reinforcement change according to the NTC2018 requirements building must fulfil. In the first case it is assumed that the structure is located in Turin, an area with low seismic risk; in the second case, instead, the building is placed in L'Aquila, where the seismic risk increases with respect to the previous one. The final step is the analysis of them after column removal using a specific software called ELS (Extreme Loading for Structures).

2 TIPOLOGY OF PROGRESSIVE COLLAPSE

The progressive collapse of structures is often disproportionate. In other words, the disproportion between a little triggering event and the subsequent collapse of a significant piece, or possibly the entire structure, is what defines it. Lastly, distinct collapse mechanisms can affect various types of buildings.

The contents of this section are primarily based on [5].

2.1 Types of progressive collapse

2.1.1 PANCAKE-TYPE COLLAPSE

Among the different mechanisms of progressive collapse observed in multi-storey buildings, the pancake collapse is characterised by the vertical propagation of structural failure. This mechanism develops when one or more structural components lose their ability to support the gravity loads, causing part of the building to detach from the remaining structure. Once this portion begins to fall, gravitational potential energy is converted into kinetic energy. The impact with the lower floors generates dynamic forces that may largely exceed the residual load-bearing capacity of the structure. As a result, the supporting elements below also fail, allowing the collapse to propagate progressively from one storey to the next until a partial or total structural collapse occurs.

The severity of this process depends mainly on the mass of the falling portion and the height through which it falls. As these parameters increase, the amount of kinetic energy released upon impact also increases, producing highly concentrated internal forces in the impacted region. If these forces exceed the resistance of the structural members or their connections, additional failures are triggered and the collapse front continues to advance. Although the propagation generally occurs downward, under certain conditions it may also extend upward into the remaining upper portion of the structure.

Several structural failure mechanisms can initiate or contribute to this loss of vertical load-bearing capacity. These include crushing, buckling or overturning of columns, failure of beam-to-column or floor-to-column connections, punching shear of floor slabs, or the collapse of horizontal structural members. In practice, progressive collapse is rarely associated with a single failure mode; instead, it usually results from the interaction of several damage mechanisms acting simultaneously or consecutively.

The term pancake collapse originates from the appearance of many low- and medium-rise buildings after collapse (Figure 2.1). In these structures, the energy released during the failure is generally lower than in tall buildings, causing the floor slabs to accumulate one above another while maintaining a recognisable stacked configuration. This arrangement resembles a stack of pancakes, from which the collapse mechanism derives its name. In contrast, very tall buildings develop significantly larger impact energies, often leading to much more extensive fragmentation of the structural system.



Figure 2.1 Pancake-type collapse of a ten-storey building triggered by an earthquake - Islamabad, Pakistan (From: [5])

The collapse of the World Trade Center towers in New York in 2001 is widely regarded as the best-known example of this collapse mechanism. The aircraft impacts caused severe local damage to the structural system and compromised the fire protection of several members. The subsequent fires further reduced the mechanical properties of the steel, progressively decreasing the vertical load-bearing capacity in the affected region. Once the damaged storeys could no longer sustain the weight of the structure above, the upper portion of each tower started to descend (Figure 2.2). The resulting impact on the lower, initially intact floors generated dynamic loads far greater than those considered in structural design, leading to a progressive loss of load-bearing capacity and ultimately to the complete collapse of both towers.

Post-collapse observations indicate that, during the progression of failure, the floor systems appeared to fail before the perimeter and core columns. In fact, portions of the external façade and parts of the central core remained standing temporarily after the main collapse had occurred. These observations suggest that the failure of floor systems or of the floor-to-column connections played a dominant role during the vertical propagation of the collapse. This interpretation is further supported by the work of Lalkovski, who re-examined the collapse sequence and questioned the hypothesis proposed by Bažant and co-workers, according to which the progressive failure was governed primarily by column collapse. Instead, Lalkovski argues that the initial collapse was more closely associated with instability and overturning of the perimeter and core columns, while the subsequent propagation mainly involved failures of the floor systems and their structural connections.

It should also be noted that the vertical collapse is not necessarily the first stage of the failure process. Before the loss of vertical load-bearing capacity becomes critical, structural damage may propagate horizontally due to the initial triggering event or the subsequent fire. In slender high-rise buildings, such as the World Trade Center towers, this horizontal progression is likely to precede the vertical collapse. Conversely, in less slender structures the horizontal and vertical failure mechanisms may develop simultaneously and interact with each other. For this reason, pancake collapse often occurs together with other progressive collapse mechanisms, particularly zipper-type and domino-type failures.

A further variation of the pancake collapse mechanism involves primarily the failure of the floor systems rather than the complete separation of structural segments. In this case, the slabs rotate while collapsing instead of falling vertically as detached bodies, and the dominant failure mechanism is governed by bending rather than

by the loss of vertical load-bearing capacity. The Ronan Point collapse is a well-known example of this behaviour, as the failure remained confined to one corner of the building while exhibiting characteristics that combine both pancake-type and domino-type collapse mechanisms.

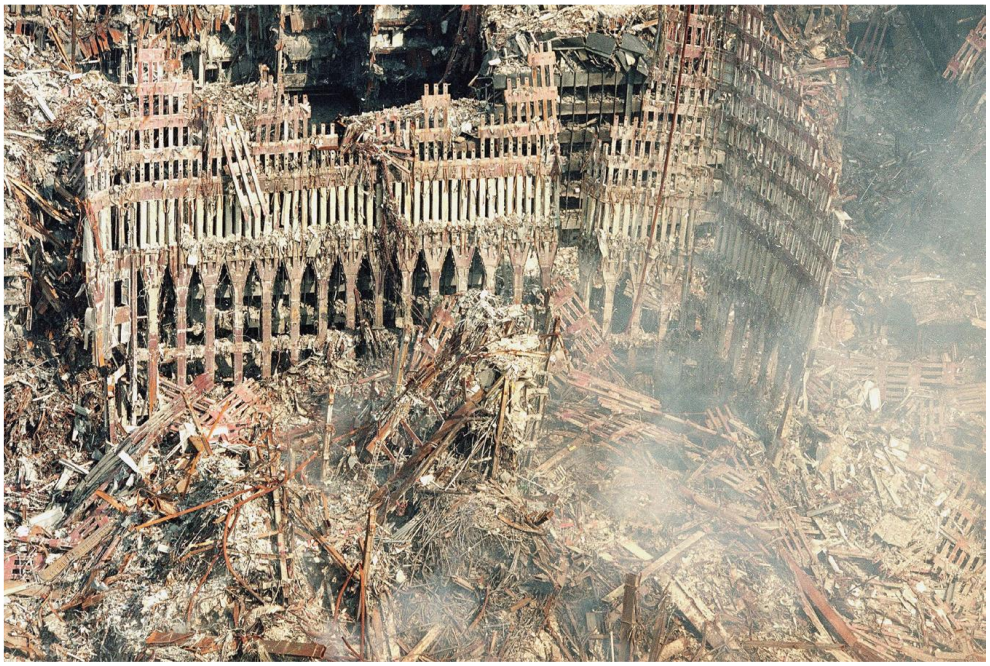


Figure 2.2 WTC 1 (north tower) after its collapse (New York, USA, 2001). At the centre, the last remaining staircase is seen where several firemen survived. (From: [5])

2.1.2 ZIPPER-TYPE COLLAPSE

The zipper-type collapse is a form of progressive structural failure in which the collapse propagates through the redistribution of internal forces following the local failure of one or more load-carrying elements. Unlike pancake collapse, where the propagation is mainly driven by impact forces generated by falling structural masses, zipper collapse develops because the loads previously resisted by the failed component are suddenly transferred to adjacent structural members. If these alternative load paths do not possess sufficient reserve capacity, they become overloaded and fail in succession, allowing the collapse to spread progressively throughout the structure.

This mechanism is typically associated with structural systems characterised by parallel load paths, where neighbouring elements perform similar structural functions. Following the initial failure, the remaining members are subjected to both a redistribution of static forces and an impulsive dynamic response caused by the sudden release of internal stresses. The combination of these effects may produce stress concentrations in adjacent elements, eventually causing them to exceed their load-bearing capacity. Consequently, the failure propagates transversely to the direction of the main internal forces rather than along it, distinguishing zipper-type collapse from pancake collapse.

The triggering event may involve the failure of a single structural component or a localised region within a structural element. Depending on the structural system, the initially failed component may be a hanger, a stay

cable, an anchorage, a column or a critical zone within a reinforced concrete slab, such as the punching shear region surrounding a column. Since the propagation mechanism is governed by force redistribution rather than by falling debris, impact forces generally play only a minor role or are completely absent.

One of the structural systems most vulnerable to this collapse mechanism is the cable-stayed bridge. In these structures, the rupture of a single stay cable may transfer additional tensile forces to neighbouring cables, potentially initiating a sequence of successive failures if adequate redundancy is not provided. For this reason, modern bridge design commonly includes specific loss-of-cable scenarios to verify the structural response after the sudden removal of an individual stay. A comparable sequence of failures was also observed during the collapse of the Tacoma Narrows Bridge in 1940 (Figure 2.3). Although the bridge was a suspension bridge rather than a cable-stayed bridge, the progressive failure followed a similar pattern. The extreme wind-induced oscillations caused several hangers to fail, after which the bridge deck progressively detached from the suspension system and ultimately collapsed.

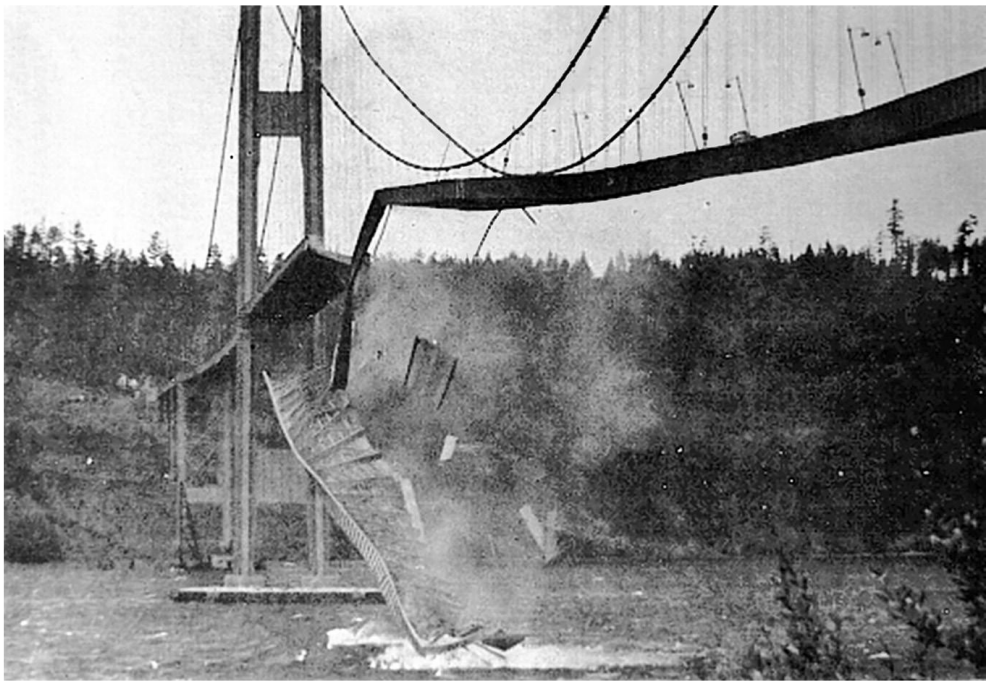


Figure 2.3 Failure progression of Tacoma Narrows suspension bridge (From: [6])

A similar redistribution mechanism has also been identified in building structures. The collapse of the suspended walkways at the Hyatt Regency Hotel in Kansas City is commonly cited as an example in which the failure of a relatively small number of critical connections triggered a disproportionate structural collapse. Likewise, several incidents involving suspended acoustic ceilings have been reported, where the rupture of only a few fixing points caused the progressive detachment of extensive ceiling areas. Comparable behaviour may also occur in anchored retaining walls if one or more ground anchors lose their load-carrying capacity, forcing the remaining anchors to sustain forces beyond their design resistance.

An important example involving reinforced concrete structures is the partial collapse of the Pipers Row Car Park in Wolverhampton in 1997 (Figure 2.4). Investigations indicated that the collapse originated from a punching shear failure around a single column within the flat slab system. The resulting redistribution of forces caused similar failures to develop around adjacent columns, producing a progressive sequence of punching failures. Although flexural cracking and membrane action also contributed to the structural response by pulling

the edge columns inward, the progressive punching shear mechanism is generally considered to have governed the collapse propagation.



Figure 2.4 Partial collapse of Pipers Row Car Park triggered by punching shear failure - Wolverhampton, UK (From: [5])

From a mechanical perspective, zipper-type collapse can be interpreted as the structural response to the sudden removal of a load-carrying element. Before failure, the internal forces carried by that element are in equilibrium with the surrounding structure. Once the element fails, these forces are instantaneously redistributed to the remaining structural system, generating a dynamic response that may significantly exceed the corresponding static effects. Although deterioration processes such as corrosion or fire may gradually reduce the resistance of a structural member, the final rupture usually occurs suddenly, making dynamic effects an essential aspect of the collapse mechanism.

The progression of zipper-type collapse therefore depends on the ability of the remaining structure to develop alternative load paths capable of accommodating the redistributed forces. If these alternative paths become overloaded, additional local failures occur, allowing the collapse to continue until a new stable equilibrium is reached or a much larger portion of the structure has failed.

2.1.3 DOMINO-TYPE COLLAPSE

The term “domino-type collapse” derives from the well-known sequential falling mechanism of domino tiles. The fundamental principle underlying this phenomenon is the loss of stability of an individual element which, after starting to rotate, transfers an action to the adjacent element, causing it to overturn in turn. The process can therefore be regarded as a sequence of closely interconnected events.

In an idealised configuration, the phenomenon begins with the overturning of an element about its lower edge. During the rotation, gravitational potential energy is progressively converted into kinetic energy. When the element reaches a sufficiently inclined position, its upper edge comes into contact with the lateral surface of the following element. The impact generates a horizontal force that contributes to the loss of stability of the impacted element. This action is not purely static, since it depends both on the geometric configuration of the system and on the velocity at which the impact takes place.

The adjacent element, subjected to this horizontal action, consequently exceeds its equilibrium condition and begins to rotate. The same mechanism is then repeated for the elements located along the propagation direction, resulting in a progressive sequence of overturning events.

A distinctive characteristic of this phenomenon concerns the orientation of the main forces with respect to the direction of collapse propagation. Before instability occurs, the elements are mainly subjected to vertical loads generated by their self-weight and other gravity-related actions, whereas collapse propagates through a predominantly horizontal action. The elements may therefore be considered, at least in the initial configuration, as components of a parallel load-bearing system. Unlike other progressive collapse mechanisms, in the domino case the direction of the action responsible for propagation does not coincide with that of the main loads for which the elements were originally designed.

This mechanism is therefore particularly relevant for structures characterised by relatively slender elements with limited resistance to overturning. Such a configuration may occur, for example, in structures consisting of a sequence of vertical elements that are either independent or partially connected. This condition may be encountered in some multi-span bridges when the height of the piers is large compared with the span length.

A representative example is the progressive collapse, caused by fire, of an approximately 270 m long wooden truss railway bridge located in Lampasas County, Texas (Figure 2.5). In this event, the failure propagated along the longitudinal direction of the bridge. The collapse mechanism involved deformation of the trusses around their central region, followed by their overturning and impact against the adjacent structural element. The impact initiated a similar process in the following span, resulting in the propagation of the collapse along the structure. The behaviour of the bridge nevertheless differs in some respects from the idealised configuration of a row of independent elements. The individual vertical structures were connected by the bridge spans, and each trestle did not behave as a single rigid body. Instead, its movement could be represented by two rigid portions connected by a hinge. Despite these differences, the observed propagation mechanism retained the main features of a domino-type collapse.



Figure 2.5 Collapse of a trestle bridge triggered by fire - Lampasas County, TX, USA (From: [5])

Another example can be found in the progressive collapse of overhead transmission line towers. Phenomena of this type have occasionally been observed in several countries. In 2005, near Münster, Germany, the accumulation of wet snow on the transmission lines caused the collapse of 82 towers. In this case, the collapse mechanism exhibits additional features that are not fully covered by the conventional domino model, making it necessary to adopt a more general definition. (Figure 2.6)

First, the transfer of the action responsible for propagation does not necessarily have to occur through direct contact between two consecutive elements. The interaction may instead be transmitted indirectly through intermediate components. In the case of transmission towers, for example, the electrical conductors provide a connection between successive structures. Consequently, the action responsible for propagation may take the form of either a pushing or a pulling force.

Furthermore, the direction in which collapse propagates does not necessarily have to coincide with the direction of overturning of the individual elements. A tower may lose stability in a direction transverse to the transmission line, while the action transferred to subsequent towers develops along the line itself. Therefore, the propagation and overturning directions may either coincide or differ, depending on the structural configuration and the governing instability mechanism.

Finally, when individual elements are connected to the ground through anchoring systems, progressive overturning may also require the loss of anchorage capacity or failure of the anchors. However, the phenomenon does not necessarily involve the movement of the entire structure starting from its foundations. Only a portion of the structure may overturn. Following a local collapse above foundation level, an upper portion of the structure may rotate around a plastic hinge located at the level of the damaged region

This interpretation is particularly useful for describing the behaviour observed in the case of the transmission towers that collapsed in Germany, where the instability mechanism appears to have also involved the rotation of upper portions of the structures following localised damage.

Overall, a domino-type collapse can therefore be identified by two fundamental aspects: the loss of stability and subsequent overturning of individual elements, and the ability of each element to transmit an action to neighbouring elements, leading to the propagation of the collapse. This mechanism highlights a structural vulnerability to actions that may differ significantly from the direction of the main loads considered during the design process.



Figure 2.6 Domino-type collapse of overhead transmission line towers - Münsterland, Germany (From: [5])

2.1.4 SECTION-TYPE COLLAPSE

Section-type collapse mainly concerns structures characterised by continuous structural components, such as shells, membranes and thin walled elements. Unlike conventional structures composed of discrete members, these systems can experience a failure that spreads directly through the material surrounding the initially damaged region.

The mechanism can be illustrated by considering a beam subjected to bending or a tensile member. If part of its cross section loses its load carrying capacity, the internal forces previously resisted by the damaged portion are redistributed through the remaining section. This produces higher stresses in the adjacent material and may lead to further failure. The process can therefore progressively extend across the section.

A similar behaviour can occur in shell and membrane structures, where the continuity of the material allows the effects of a local failure to spread directly to neighbouring regions. This represents the main characteristic of section-type collapse and distinguishes it from mechanisms involving separate structural elements.

The mechanism also presents similarities with zipper-type collapse because, in both cases, the initial failure causes a redistribution of internal forces towards the surrounding regions. The main difference is that section-

type collapse develops within a continuous structural system, whereas zipper-type collapse generally involves discrete structural members.

The behaviour of continuous structures following local damage is closely related to structural robustness. Redundancy, continuity and the capacity to redistribute loads can help prevent a local failure from developing into a disproportionate collapse. These aspects are particularly relevant when assessing the residual capacity of a structure after the loss of a local portion.

Therefore, section-type collapse can be regarded as a progressive reduction of the load-carrying capacity of a continuous structural region, driven mainly by stress redistribution around the initial damaged area.

A representative example of the failure propagation associated with continuous membrane structures can be observed in the tearing of a tensioned membrane containing an initial crack (Figure 2.7). As the applied displacement increases, the crack opens and the surrounding membrane undergoes significant deformation. The load is redistributed towards the regions adjacent to the damaged area, resulting in high tensile stresses near the crack tips. Once the local resistance is exceeded, the crack begins to propagate through the membrane. This behaviour illustrates the main physical features associated with section-type collapse, in which a local failure progressively extends into the surrounding continuous structural material. [7]

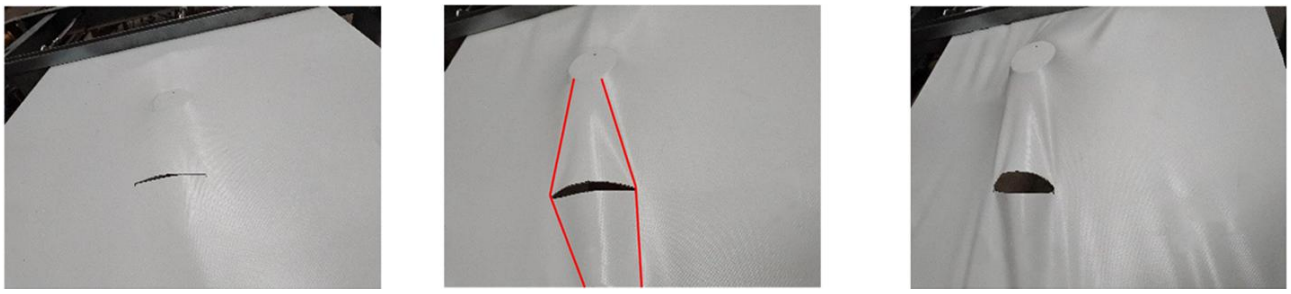


Figure 2.7 Progressive tearing of a tensioned membrane with an initial crack. Adapted from [7]

2.1.5 INSTABILITY-TYPE COLLAPSE

Structural instability is a failure mechanism in which a relatively small disturbance can produce a significant deformation or even lead to the loss of structural equilibrium. Such disturbances may be associated with geometrical imperfections, local damage or lateral actions. The phenomenon is particularly relevant for structural members subjected to compression, since a reduction in their restraint or stiffness may cause them to lose stability and buckle.

Structural systems are generally provided with bracing and stiffening elements to prevent this type of behaviour. Although these components may not always carry a large portion of the main structural loads, they play an important role in maintaining the stability of compressed members. Their failure can therefore have consequences that are considerably greater than the initial disturbance. For example, in trusses or framed structures, the loss of a brace may leave a compressed member insufficiently restrained and consequently vulnerable to buckling. Similarly, the failure of a stiffener in a plate can produce local instability and, under certain conditions, contribute to a larger structural failure.

The mechanism of an instability-type collapse can therefore be understood as a modification of the equilibrium conditions of the structure. Initially, the stabilising components prevent excessive deformation of the compressed members. If one of these components fails, the associated member becomes destabilised and may subsequently experience buckling under loads that were already present before the initial failure. A relatively small additional disturbance can then be sufficient to trigger a significant deformation.

The main stages of this mechanism can be summarised as follows:

- failure or loss of effectiveness of a bracing or stiffening component;
- destabilisation of the compressed member previously restrained by it;
- occurrence of buckling or another stability failure;
- either immediate structural collapse or propagation of the instability to other elements.

A distinction should be made between an instability-induced disproportionate collapse and a progressive instability-type collapse. If the loss of stability of a critical element, such as a main member of a truss tower, causes the entire structure to lose equilibrium almost immediately, the consequences may be disproportionate to the initial failure. However, if no successive failure of other elements occurs, the event cannot be considered progressive.

In other situations, the first instability can alter the conditions of neighbouring structural components and initiate further stability failures. For example, the deformation of one compressed member may cause the loss of effectiveness of another stabilising component, which in turn destabilises a second compressed member. The process can therefore continue through a sequence of successive instabilities. In this case, the collapse can be classified as a progressive instability-type collapse

This mechanism differs from other types of progressive collapse, particularly from domino- and zipper-type mechanisms. In a domino-type collapse, propagation generally occurs because the movement or overturning of one element produces an action on a neighbouring element. In a zipper-type collapse, instead, the failure of one component causes a redistribution of forces, potentially overloading other elements. In an instability-type collapse, the main phenomenon that propagates is instead the loss of stability: the failure of one component modifies the restraint conditions of another component and makes it susceptible to buckling.

An important example of progressive instability is represented by propagating buckles in pipelines (Figure 2.8). A local buckle developing in the cylindrical wall of a pipeline can extend progressively along the structure, affecting neighbouring portions of the pipe. The same component therefore performs both a load-bearing and stabilising function. Once a local portion becomes unstable, the resulting deformation modifies the conditions of the adjacent part, allowing the instability to continue propagating.



Figure 2.8 Propagating buckling of a pipe under external pressure (From: [5])

Experimental and numerical studies have investigated this phenomenon in offshore pipelines, showing that, after the initiation of a sufficiently severe local buckle, the deformation may propagate over considerable distances. The propagation behaviour depends on the geometry and mechanical properties of the pipeline and the applied loading conditions. [8]

The pipeline example also highlights an important characteristic of instability-type collapse: the main compressive or external loading responsible for the eventual failure is generally already present before the collapse begins. Therefore, the propagation mechanism is not necessarily associated with a new force transmitted from one failed element to another. Rather, it results from a progressive change in the stability conditions of the structure.

Energy transformations may also play a role in the collapse process. As a compressed element deforms, part of the potential energy associated with gravity or external pressure can be converted into elastic strain energy. When stability is lost, this stored energy can be released and contribute to the subsequent deformation. The importance of dynamic effects depends on the specific structural system and on the rate at which the instability develops.

For relatively slow stability failures, static analysis may provide a sufficiently accurate representation of the main mechanism. Conversely, when instability propagates rapidly, inertia and other dynamic effects can become significant. This is particularly relevant for propagating buckles, where the deformation moves along the structure and the interaction between different portions of the pipeline can influence the propagation process. [8]

It is therefore possible to distinguish two main forms of instability-type collapse. The first occurs when the instability of a critical element produces an immediate loss of structural equilibrium without a sequence of subsequent failures. The second involves progressive destabilisation, in which the instability of one part of the structure progressively creates the conditions for the instability of other parts. The defining characteristic of the latter mechanism is consequently not the transmission of a conventional propagating force, but the progressive modification of the stability conditions of the structure. The compressive forces acting on the destabilised elements are generally already present before the collapse, while the loss of restraint and stability propagates through the structure.

Finally, instability-type collapse is characterised by a marked disproportion between the magnitude of the initial disturbance and the resulting structural response. A small imperfection, local failure or loss of restraint may have limited consequences when the structure is far from its critical condition, but may produce very large deformations when the stability threshold is approached. This aspect establishes a conceptual connection

between instability and progressive collapse, since both mechanisms can transform a relatively limited initial event into a much larger structural response.

2.1.6 MIXED-TYPE COLLAPSE

The collapse mechanisms described above can generally be distinguished according to the way the failure is initiated and subsequently propagated. However, some structural failures cannot be attributed to a single mechanism, since different collapse modes may occur simultaneously or consecutively during the same event. These cases are generally classified as mixed-type collapses and are characterised by the interaction of different propagation mechanisms.

A well-known example is the Sampoong Department Store collapse in Seoul in 1995, which exhibited both zipper-type and pancake-type characteristics. The building consisted of a flat-slab system, and the irregular arrangement of some columns contributed to an inadequate capacity for transferring vertical loads from the slabs to the columns. Following the initial failure of a column, the load carried by it was redistributed towards neighbouring structural elements through alternative load paths. However, these elements were unable to sustain the additional demand, leading to a progressive punching shear failure that extended horizontally across the upper floor. This stage can be associated with a zipper-type mechanism, since the failure propagated from one structural element to the next as a consequence of load redistribution. Subsequently, the loss of support caused the upper slab to detach and fall onto the floor below. The impact generated by the falling slab produced further punching shear failures, causing the collapse to propagate downwards and giving rise to a pancake-type mechanism.



Figure 2.9 Mixed-type collapse of Sampoong Superstore - Seoul, South Korea (From: [5])

Another case presenting mixed characteristics is the partial collapse of the Alfred P. Murrah Federal Building in Oklahoma City in 1995. The event can mainly be associated with a pancake-type mechanism, but some features also suggest the presence of a domino-type component. In particular, portions of the structure that had fallen were still connected to the remaining structure through continuous reinforcement. These connections could have transmitted horizontal tensile forces to adjacent structural elements, potentially contributing to their

displacement or overturning. The fact that the collapse reportedly stopped near a discontinuity in the reinforcement supports the hypothesis that these forces may have influenced the propagation of the failure.

Therefore, mixed-type collapse can be understood as a failure process in which different propagation mechanisms interact during the same event. The progression may occur horizontally, as in zipper, stability or domino-type mechanisms, vertically, as typically observed in pancake-type collapse, or through a combination of these directions. The relative importance of each mechanism may also change as the collapse develops. Consequently, the behaviour of mixed-type collapses is generally more complex than that of the individual collapse types and cannot always be described using a single simplified mechanism.

As suggested by [5], it is possible to group the different collapses in classes, as showed in the following table.

Collapse class	**Collapse types**	**Main characteristics**
Redistribution class	Zipper-type, Section-type	Failure of a structural element causes a redistribution of the forces previously carried by the damaged region towards the remaining parts of the structure. This redistribution may overload neighbouring or adjacent elements and promote further failure.
Impact class	Pancake-type, Domino-type	Gravitational potential energy is converted into kinetic energy as structural elements fall or overturn. The resulting impact can transfer energy to the remaining structure and trigger further failures
Instability class	Instability-type	Loss of stability occurs in compressed elements after the failure or loss of effectiveness of bracing or stabilising components. The collapse is therefore governed primarily by destabilisation and buckling rather than by impact or direct force redistribution.
Mixed class	Mixed-type	Two or more collapse mechanisms interact during the same failure event. Different mechanisms may occur successively or simultaneously, and their interaction can influence both the direction and the extent of collapse propagation.

Table 2.1 Classification of progressive collapse mechanisms according to [5]

3 MAJOR COLLAPSES IN HISTORY

Throughout history, structural collapses have marked turning points in the fields of engineering and public safety, leading to changes in engineering standards and the introduction of new restrictions in the regulations used up to that point.

This chapter presents a description of some of the most significant structural failures in history. In addition to the technical aspects, the chapter also covers the evolution of regulations.

3.1 Ronan Point Collapse

Ronan Point (Ministry of Housing and Local Government, 1968) was a 22-storey tower block in Newham, East London. In 1968, the occupant of the apartment 90 on the 18th floor lit a match for her stove to brew her morning cup of tea. A gas explosion, caused by a leak, demolished a load-bearing wall, which then triggered the collapse of an entire corner of the building (Figure 3.1). The partial collapse of the structure killed four people and injured 17. [9]

The collapse sheared off the living room portion of the apartments, leaving the bedrooms intact except for floors 17–22, where all the fatalities occurred.



Figure 3.1 Ronan Point collapse (From [6])

The Ronan Point tower was built using an old technique, developed in Denmark, known as large panel system (LPS) or Larsen–Neilsen system. In this solution all the walls, floors and stairways were precast, but the

concrete prefabricated sections were cast off site and bolted together to build the structure. Further ties were not taken into consideration. The only load considered during the design process was the wind action, but accidental loads, such as blast, were not taken into account. [6]

The explosion was not significant in magnitude. The resident's hearing had not been damaged. This suggested that the pressure was less than 70 kPa. "The Building Research Station and Imperial College of London performed an extensive battery of tests to discover how much internal force Ronan Point could withstand. The results indicated that the walls could be displaced by a pressure of only 19.3 kPa (Levy and Salvadori 1992). It was estimated that the kitchen and living room walls were moved by a pressure of only 1.7 kPa, while the exterior wall was displaced with a pressure of 21 kPa." [9]

Moreover, the design of the Ronan Point did not provide alternative load paths for the upper floors if a lower level collapsed, due to building's lack of structural redundancy. Another reason was the poor quality of the workmanship of the steel connecting plates that joined the walls; the workers had not tightened the nuts of the connecting studs.

The collapse of the southeast corner of Ronan Point prompted changes to building codes. Building codes now consider the possibility of progressive collapses and the forces resulting from an internal explosion. The codes also require minimum levels of ductility and redundancy. [9]

3.2 Oklahoma City Collapse

On April 19, 1995, a truck bomb exploded in front of the Alfred P. Murrah Federal Building in Oklahoma City, and since then it has been considered one of the largest terrorist attacks in American history. The bomb was detonated in a rental truck parked in a loading lane within a distance of about 4.3 m on the north side of the Murrah Building. The resulting shock wave, equivalent to approximately 1800 kg of TNT, severely damaged the structure, causing the destruction of one-third of the Murrah Building (Figure 3.2). The entire north face of the structure collapsed, and the rest of structure received extensive damage. [6]

Once again, this tragic event led to significant changes in regulations and security measures, including more rigorous criteria.

The Alfred P. Murrah Federal Building was a reinforced concrete structure with a nine-storey office building, two one-storey wings, and a multilevel car park. The moment frame together with a cast in place concrete core in the south side work to ensure the lateral stability of the structure. To allow street-level access to the first floor, the second floor was recessed. As a result, a large transfer beam was placed on the third floor to support the load of all floors above. Two-storey-high columns, spaced 12.3 m, carried this beam (Figure 3.3). This arrangement did not provide the sufficient safety against explosion, because this transfer beam was the key element supporting the gravity load of the upper levels. [10]

From the same figure it is possible to notice that a column collapsed directly due to the explosion, which was the column nearest to the detonation position. In addition, the large blast wave led to the shear failure of the adjacent columns. Therefore, the transfer beam lost support due to the failure of these three columns. The high load from level three and above caused the failure of the beam. Since this beam had a key role, being the carrier of the gravity loads from level 3 upward, its collapse triggered a progressive failure of the structures along the north face.



Figure 3.2 Murrah Federal Building bombing (From: [11])

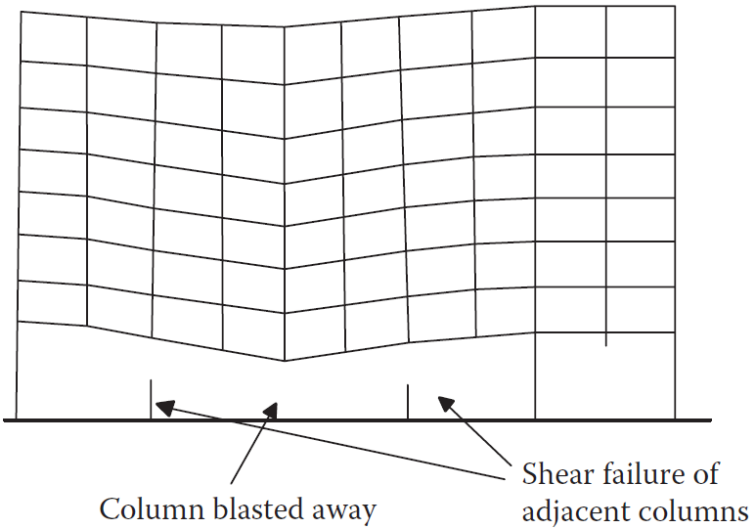


Figure 3.3 Damage of ground-level columns of the Murrah Federal Building (From: [12])

3.3 World Trade Center Collapse

Construction began in 1968 and in 2001 the WTC complex had become an integral part of Manhattan. It was composed of seven buildings, in the southwest of the city (Figure 3.4). The two towers, WTC1 (north tower) and WTC2 (south tower), composed by 110 stories, were the higher of the city. WTC 3, a Marriott Hotel, was

22 stories tall, WTC 4 (South Plaza Building) and WTC 5 (North Plaza Building) were each 9-story office buildings, and WTC 6 (U.S. Customs House) was an 8-story office building. These buildings were built around a Plaza named in honor of Austin Tobin. WTC 7 was a 47-story office building on Port Authority land across Vesey Street on the north side of the Plaza complex. [13]

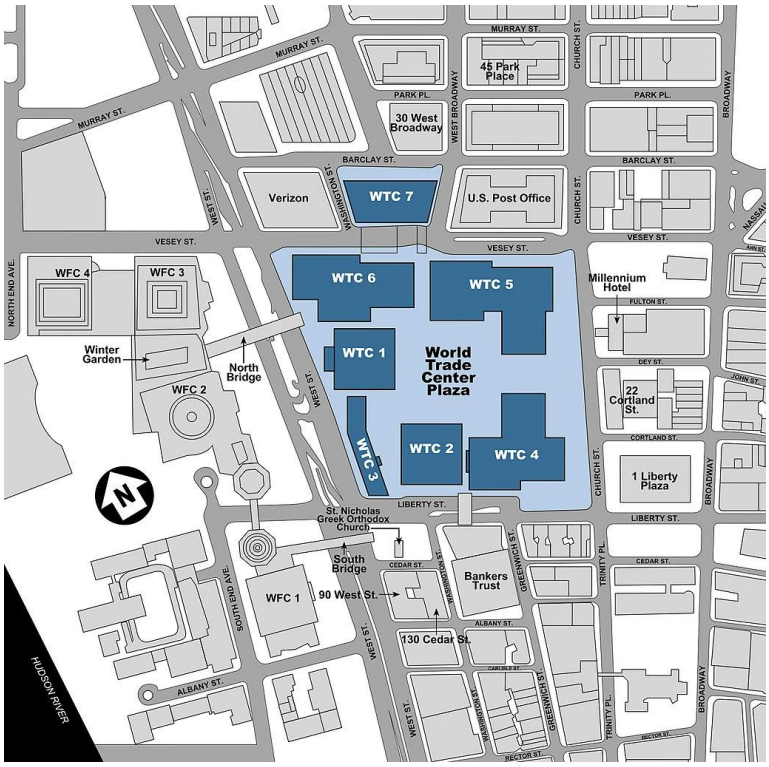


Figure 3.4 The World Trade Center (From: [14])

On September 11, 2001, the Twin Towers (referred to as WT1 and WTC2) collapsed after being hit by two hijacked airplanes. Some days later, another building, the WTC7 collapsed due to the fires set by the falling debris from the Twin Towers.

The towers of WTC1 and WTC2 were designed as tube-in-tube structures, as shown below. There were four major structural subsystems in the towers [13]:

- exterior wall: vertical square tube of 236 narrow columns, 59 of each face from the 10th floor to the 107th floor.
- core: the long axis of the core in WTC 1 was oriented in the east-west direction, while the long axis of the core in WTC 2 was oriented in the north-south direction. In the core there were 47 heavy columns. (Figure 3.5)
- floor system: composite floor truss system.
- hat truss: it was located from the 107th floor to the roof of each tower. It was a set of steel braces, called "hat truss"

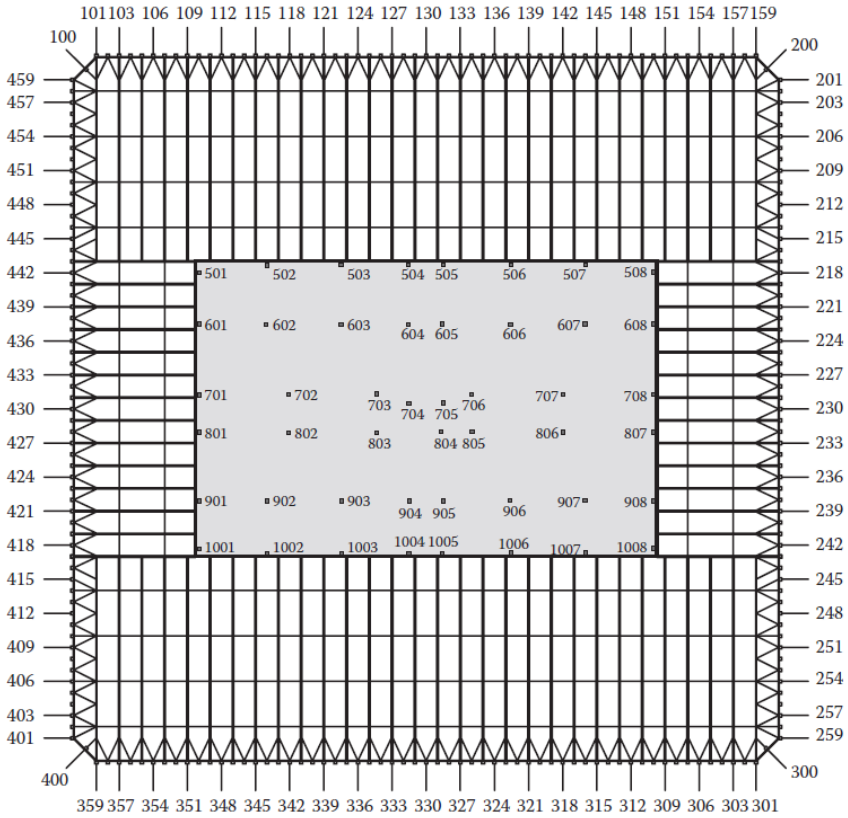


Figure 3.5 Layout for WTC1 (From: [13])

At 8:46:30 a.m. EDT, five hijackers flew American Airlines Flight 11 (AA 11) with 11 crew and 76 passengers into the north face of WTC 1. When it hit the north tower, it likely contained about 10,000 gal (66,000 lb), evenly distributed between the right- and left-wing tanks. The total weight of the aircraft was estimated to be 283,600 lb.

The plane flew almost directly toward the north tower descending at an angle of about 10 degrees at the moment of impact. The plane struck the tower on the 96th floor but the consequences extended from the 93rd floor to the 99th floor. After the Boeing 767 hit the tower, the fuel was transformed into flammable droplets that easily ignited thanks to the hot debris and electronic devices. The flames caused explosions visible from a distance, but only a small portion of the fuel burned immediately; the rest remained in the building, contributing to the prolonged fires.



Figure 3.6 Aircraft entry hole on the north side of WTC 1, photographed 30 s after impact (From: [13])

There was no way to fight the fires, also because the pipes that brought water to the automatic sprinklers had broken, and water was running down the stairs. The perimeter columns, floor and core columns were immersed in these hot gases and began to weaken. Where the insulation was dislodged, the temperature of the steel increased rapidly, in contrast to steel members where insulation was intact. When a steel column is heated, its ability to support gravity loads and resist lateral loads decreases. At about 300 °C, steel loses 20 percent of its yield strength. The fires heated the slabs between the 93rd and 97th floors, especially on the south side, because there the beams lost the fireproofing. The heat caused the floors to sag, which began to pull the connected structures inward. The conditions continued to deteriorate in fact FDNY units were hindered by the chaotic situation.

WTC2 suddenly collapsed, slowing the evacuation of WTC1 due to dust, smoke and debris and enhancing the fires in the North Tower. “By 10:23 a.m., the south exterior wall had bowed inward as much as 55 in.”. [13]

The tower was failing: the central core, the slabs and the perimeter wall were largely weakened. The upper part of the tower, above the impact zone, began to lean toward the south like a rigid block, and shortly thereafter collapsed onto the lower floors. In just 12 seconds, the entire building collapsed completely, leaving only rubble.

The collapse of WTC2 (Figure 3.7) was similar and also determined by the time for the fires to weaken the perimeter columns and floors on the east and south sides of the building. Since the aircraft impact damage to the core was more severe in WTC 2 than in WTC 1, it collapsed in a shorter amount of time.



Figure 3.7 Hijacked flight 175 seconds before crashing into the South Tower (From: [15])

4 CASE STUDY

After carefully reviewing the introductory and historical sections, it is possible now to focus on the case study: the dimensioning of a small building, considering the different parameters to be adopted if the structure is located in Turin or in L'Aquila, and the subsequent study of their behaviour following column removal. For the dimensioning and subsequent verification of the structure it is used 2si PRO_SAP (**PRO**fessional **S**tructural **A**nalysis **P**rogram)

PRO_SAP is a structural analysis and design software based on the Finite Element Method (FEM). It is used to model, analyse, and verify structures made of reinforced concrete, steel, timber, masonry, and other materials, for both new buildings and existing structures. Instead, another software programme was used to analyse behaviour following column removal: ELS (Extreme Loading Structure). Its operation is based on the theory of applied elements.

Before starting with the description of the structure it is necessary to clarify the difference between FEM and Applied Element Method (AEM).

4.1 Difference between FEM and AEM

The study of structural collapse behaviour is essential for understanding failure mechanisms and reducing the consequences of extreme events, such as earthquakes. From a numerical point of view, structures may experience both small and large displacements before collapse. While geometric changes can be neglected in the small displacement range, important phenomena such as column instability (buckling) require an analysis based on large displacement theory. The Finite Element Method (FEM) has traditionally been the main approach used for studying structural instability, allowing the evaluation of critical loads, buckling modes, and post-buckling behaviour. However, since FEM is based on the assumption of a continuous material, it presents some difficulties in reproducing the separation of structural components and the propagation of fractures, especially when the location of failure is unknown in advance.

To overcome these limitations, alternative numerical approaches have been developed, including the Modified/Extended Distinct Element Method (MDEM/EDEM) and the Rigid Body and Spring Model (RBSM), which are better suited to represent large deformations and discontinuous behaviour. Nevertheless, these methods still present some limitations regarding accuracy in the initial deformation stage and computational efficiency. [16]

The Applied Element Method (AEM) was developed to combine the advantages of continuous and discontinuous numerical approaches. In this method, the structure is divided into virtual elements connected by springs, each of which represents the stresses, deformations, and possible failure mechanisms of the corresponding structural portion. The main advantage of AEM is its ability to reproduce the complete structural response, from the initial loading phase to the final collapse, including nonlinear phenomena such as crack initiation and propagation, element separation, and progressive failure.

Unlike other numerical methods, AEM does not require the definition of the geometric stiffness matrix, which increases its flexibility in analysing different structural systems and loading conditions. Comparisons between numerical results and theoretical or experimental solutions have demonstrated good accuracy both in the small deformation range and in large deformation scenarios. Therefore, AEM represents a suitable method for investigating instability phenomena and progressive structural collapse.

In the Applied Element Method (AEM), structures are modelled using three-dimensional solid elements connected through normal and shear springs along their interfaces, as it is possibile to observe in the Figure 4.1. Unlike traditional FEM approaches, where structures are commonly simplified into frame and shell elements, AEM uses solid elements that allow a more realistic simulation of contact, separation, and interaction between structural components during collapse.

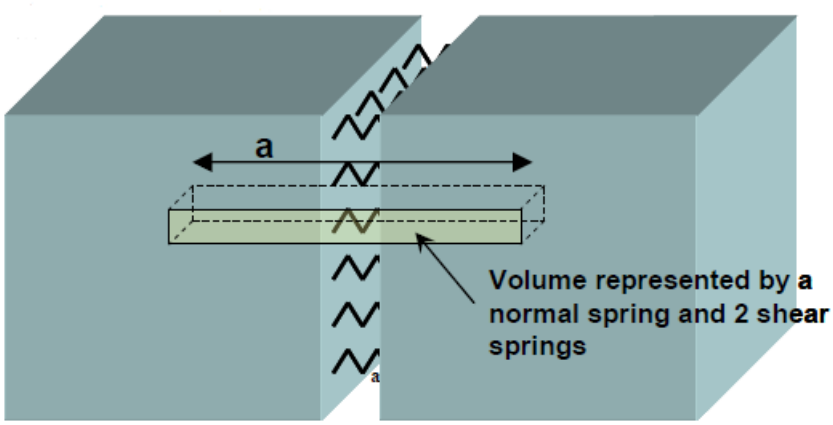


Figure 4.1 Element shape and spring distribution for AEM (From: [17])

The degrees of freedom of each element are defined at its centre of gravity, where the unknown displacements and rotations are calculated. For regular structures, cuboidal elements are generally adopted, while more complex geometries can be represented using irregular hexahedral elements. This flexibility allows the modelling of structures with complicated shapes and different levels of detail. One of the main advantages of AEM in progressive collapse analysis is its ability to simulate crack initiation, propagation, and separation between elements without requiring the failure path to be defined in advance. This differs from conventional FEM approaches, where nodal compatibility assumptions can make the prediction of fracture location more difficult.

The accuracy of an AEM model depends on the quality of the discretisation. Smaller elements should be used in areas with high stress concentrations, while larger elements can be adopted in less critical regions. Regular element shapes and gradual variations in mesh size are recommended to ensure reliable results. Additionally, adjacent element faces must be correctly aligned to generate the connecting springs and properly reproduce the structural behaviour.

4.2 Design of the structure located in Turin

The following paragraphs include a description of the structure and of the general criteria for analysis and verification, according to point § 10.1 of DM 17/01/18.

The structure is located in the city of Turin, in the Piedmont region, at geographical coordinates longitude 7.674 and latitude 45.070.

The structure has been classified as Use Class II, corresponding to ordinary buildings intended for standard use conditions. The nominal design working life of the structure (Vn) is assumed to be 50 years, with a use parameter equal to 1.0, resulting in a reference period (Vr) of 50 years for the evaluation of structural actions and safety verifications.

From a geometric point of view, the structure has plan dimensions of 15 m × 12 m, while the overall structural height is equal to 9.90 m (Figure 4.2). These dimensional characteristics have been considered in the structural analysis and verification procedures carried out in accordance with the standards.

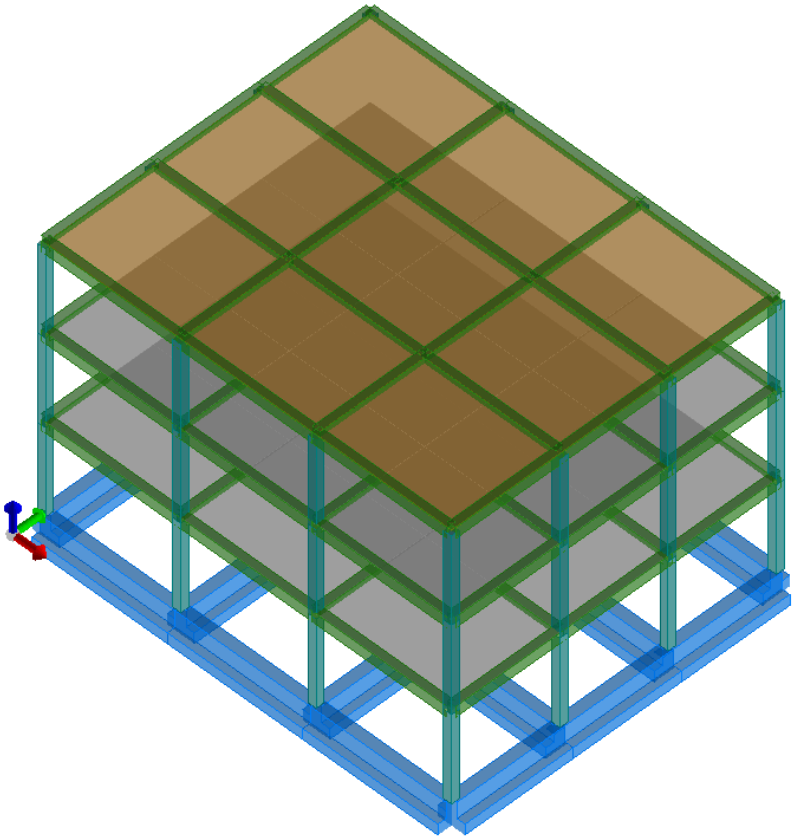


Figure 4.2 Structure located in Turin

The structural elements are controlled for safety according to the construction theory methods.

To estimate the tensile-deformation state induced by the static loads, the structural analysis is carried out according to the displacement method, instead, to estimate the tensile-deformation state induced by the dynamic loads (among which the seismic load), the structural analysis is carried out according to the method of the modal analysis and response spectra in terms of acceleration.

The structural analysis is carried out according to finite element method. This method schematize the structure by using elements connected in a fixed number of points, i.e. nodes. The nodes are defined according to three Cartesian coordinates within global reference system.

The unknowns of the problem (within the methods of displacements) are represented by the nodal degrees of freedom referred to a global reference system. These unknowns include the translational displacements along the X, Y, and Z axes, as well as the rotational components around the same axes.

The problem is solved by means of a system of linear algebraic equations, whose know terms represent the loads applied to the structure and appropriately concentrated on nodes:

$$K * u = F \tag{1}$$

where K represents the global stiffness matrix of the structure, u is the vector of nodal displacements, and F is the vector of nodal forces.
The element actions and/or tensions, which are generally referred to the local reference system, are deduced from the displacements obtained by means of the problem solution. The utilized reference system is composed of a clockwise system of Cartesian coordinates XYZ. Axis Z is assumed as vertical and directed upwards.

The numerical structural model developed for the analysis is composed of 64 nodes and 144 two-dimensional structural elements (D2 elements), including trusses, beams, and columns. In addition, the model includes 27 slab elements representing the floor diaphragms. The structure is characterized by the presence of columns and beams, while the floor system has been modeled as a rigid diaphragm in its plane. The foundation system has been represented through foundation beams, allowing the interaction between the superstructure and the supporting elements to be properly taken into account in the analysis.

4.2.1 PROPERTIES OF MATERIALS USED

The program allows to utilize various materials. The material types foreseen by the program are listed below:

- material of r.c. type
- material of steel type
- material of masonry type
- material of wooden type
- material of general type

The materials utilized in the present simulation are identifiable by means of identification symbol and numerical code (the latter is actually indicated in the description of the structural elements). The table shows the following data for each material:

Young	modulus of normal elasticity
Poisson	transversal shrinkage factor
G	modulus of tangential elasticity
Gamma	specific weight
Alfa	thermal expansion factor

The above stated data are utilized to simulate the static performance and to determine inertial and thermal loads.

Following data are indicated for the materials of type:

1	***R.C.***	**Rck**	cubic specific strength
		Fctm	average simple tensile strength
2	***Steel***	**Ft**	breaking tensile strength
		Fy	yield tension
		Fd	estimated strength
		Fdt	estimated strength for thickness t>40 mm
		Sadm	allowed tension
		Sadmt	allowed tension for thickness t>40 mm

Table 4.1 Concrete and steel strength parameters

The report shows both the characteristic and mean values using one and/or the other in relation to the requests for legislation in use and the type of verification.

Id	**Type / Notes**	**V. charact.**	**V. mean**	**Young**	**Poisson**	**G**	**Alpha**
1		*kN/m2*	*kN/m2*	*kN/m2*		*kN/m2*	
	Concrete class C25/30			3.145e+07	0.20	1.310e+07	1.00e-05
	Strength Rc	30000					
	Strength fctm		2560				

Table 4.2 Concrete material properties

Reinforced concrete beams		**Reinforced concrete columns**	
Ultimate limit states		**Ultimate limit states**	
Yield strength fy [daN/cm2]	4500.00	Yield strength fy [daN/cm2]	4500.00
fy stirrups strength [daN/cm2]	4500.00	fy stirrups strength [daN/cm2]	4500.00
Steel Type	C type	Steel Type	C type
Gamma s coefficient	1.15	Gamma s coefficient	1.15
Gamma c coefficient	1.50	Gamma c coefficient	1.50
Allowable stresses		**Allowable stresses**	
Allowable stress steel [daN/cm2]	2600.00	Allowable stress steel [daN/cm2]	2600.00
Stirrups		**Stirrups**	
Min spacing [cm]	5.00	Min spacing [cm]	5.00
Diameter [cm]	12.00	Diameter [cm]	12.00
Max spacing [cm]	30.00	Max spacing [cm]	25.00
Ctg(Theta) Max	2.50	Ctg(Theta) Max	2.50

Table 4.3 Design parameters for reinforced concrete beams and columns

4.2.2 PROPERTIES OF SECTIONS AND FLOOR USED

The sections utilized for simulation are identifiable by means of reference symbol and numerical code. For each section the following data are here reported:

Area	section area
A V2	section area/shear factor for shear in direction 2
A V3	section area/shear factor for shear in direction 3
Jt	stiffness torsional factor
J2-2	moment of inertia of the section referred to axis 2
J3-3	moment of inertia of the section referred to axis 3
W2-2	section modulus referred to axis 2
W3-3	section modulus referred to axis 3

The following table shows only the sections used in the design of the structure and the respective properties:

Id	Type	Area	A V2	A V3	Jt	J 2-2	J 3-3	W 2-2	W 3-3
		cm2	*cm2*	*cm2*	*cm4*	*cm4*	*cm4*	*cm3*	*cm3*
13	T: bi=12.00 ht=24.00 bs=50.00 hs=4.00	440.00	0.0	0.0	1.048e+04	4.455e+04	2.398e+04	1781.87	1551.37
17	Column Rettangular: b=30 h=30	900.00	750.00	750.00	1.139e+05	6.750e+04	6.750e+04	4500.00	4500.00
18	Foundation Reverse T: bi=100 ht=100 bs=40 hi=40	6400.00	0.0	0.0	3.191e+06	3.653e+06	5.003e+06	7.307e+04	8.169e+04
19	Beam Rettangular: b=30 h=40	1200.00	1000.00	1000.00	1.946e+05	9.000e+04	1.600e+05	6000.00	8000.00

Table 4.4 Geometric and section properties of structural elements

The program utilizes three or more nodes elements generally known as floor. Each floor element is identifiable with a polygon of nodes 1, 2, ..., N.

The floor element is used first of all for simulation of loads applied to the structural elements. Secondly, it can be utilized for the correct distribution of the horizontal forces acting within the plane of the element.

Loads assigned on floor elements, which are collected into an archive, are assigned directly on element using the information given by the user in the archive of floors (e.g. psi factors). The following table reports data used for the definition of loads and seismic masses.

Id.Arch.	Number of the archive
Type	Load typology ***Variab.*** Generic live load ***Var. rid.*** Generic live load with a reduction in function of the area of the floor (c.5.5. …) ***Snow*** Snow load on roofs
G1	Dead load (self weight of the floor)
G2	Dead load of non structural elements
Q	Live load
Fact. A	Live load reduction factor (0.5 or 0.75) for “Var.rid.” typology

S seis.	Live load reduction factor for seismic masses definition according to Italian D.M. 96
Psi 0	Psi factor for ***characteristic load combinations***
Psi 1	Psi factor for ***frequent load combinations***
Psi 2	Psi factor for ***quasi permanent load combinations***
Psi S 2	Psi factor for ***seismic masses definition***
Fact. Fi	Correlation coefficient for loads on buildings

Table 4.5 Definition of loads and seismic mass

Each element is characterized by a group of properties. In particular, for each element, it is reported:

Elem	Number of the element
Type	Behaviour code ***S*** the element assign only loads to the structure ***C*** the element assign loads and models a rigid plane ***P*** panel element ***M*** monodirectional load assignment ***B*** two directions load assignment
Id.Arch.	Number of the archive
Mat	Material assigned to the element
Thickness	Thickness of the element
Load framing	Angle between X axis and the principal direction of the floor
G1	Dead load of the floor (including self weight)
G2	Dead load of non structural elements
Q	Live load on the floor
Nodes	Number of the nodes which define the element (5 per row)

Table 4.6 Properties for each element

In the present structure only the following two types of floor are used. The n.11 “Variable” type is used on the first and second floors, while the n.10 “Snow” type is used on the top floor.

Each floor consists of 9 elements; as shown in the tables below, elements 1 to 18 exhibit the properties of floor type n.11 “Variable”.

ID Arch	Type	G1	G2	Q	S seis.	Psi 0	Psi 1	Psi 2	Psi S2	Fact. Fi
		kN/m2	*kN/m2*	*kN/m2*						
11	Variab.	4.85	2.32	2.00	1.00	0.70	0.50	0.30	0.30	1.00
10	Snow	4.85	2.32	1.23	1.00	0.50	0.20	0.0	0.0	1.00

Table 4.7 Types of loads

Elem.	Type	ID Arch.	Thickness	Load framing	G1	G2	Q
			cm		*kN/m2*	*kN/m2*	*kN/m2*
1-18	CB	11	20	90	4.85	2.32	2.00
19-27	CB	10	20	90	4.85	2.32	1.23

Table 4.8 Properties of each element

4.2.3 LOAD CASE SCHEMATIZATION

The program allows the usage of various load cases. The following 11 load cases are considered:

	Name	Type	Description
1	Ggk	A	load case including the structure dead weight
2	Gk	NA	load case including permanent loads
3	Qk	NA	load case including live loads
4	Gsk	A	load case including floor and roof permanent loads
5	Qsk	A	load case including floor and roof live loads
6	Qnk	A	load case including roof snow live loads
7	Qtk	SA	load case including structure temperature change
8	Qvk	NA	load case including structure wind loads
9	Esk	SA	seismic load case by the way of the equivalent static analysis
10	Edk	SA	seismic load case by the way of the dynamic analysis
11	Etk	NA	load case including forces due to earth pressure seismic increment
12	Pk	NA	load case including loads due to constraints subsiding, and prestressing.

Table 4.9 Load cases

Where:

- (A) stands for automatic load cases: the user won't be asked to enter data;
- (SA) stands for semi-automatic load cases: the user will be asked to enter a minimum part of data;
- (NA) non-automatic load cases: the user will be asked to enter generic loads for the structural elements.

The Table 4.14 shows the load cases affecting the structure and their related data, i.e.: the Type Number, the Identification Code and the Load Case Reference Value (where requested).

For the seismic load cases (9-Esk and 10-Edk), the input angle values, the seismic intensity, the structure and foundation coefficients are shown; finally, the related mass rate, for each load case participating to the seismic mass definition, is shown.

Let us point out that in the load cases 5-Qsk and 6-Qnk, each floor or roof element in the model is assumed wholly participating to the seismic mass definition (see the Sksol value in the floor element chapter) and therefore, their participating mass rate is assumed to be 1.

- ***Snow load calculation:***
  The snow load on roofs is calculated based on the following parameters:
  - Zone: macro area resulting from the subdivision of the national territory;
  - Exposure: topographical area exposed to wind;
  - Ce: wind exposure coefficient;
  - TR: design return period expressed in years;
  - as: site altitude;
  - qsk: characteristic value of snow load on the ground (for Tr = 50 years);

Zone	**Exposure**	**Ce**	**TR**	**as**	**qsk**
Alpine I	Normal zone	1,00	50 years	239 m	153,98

Table 4.10 Snow load

Considering the parameters reported above, the snow load is: Qnk = 1.23 kN/mq

- ***Wind load calculation:***
  Wind velocity is calculated with reference to the following parameters:
  - Zone: macro-area derived from the subdivision of the national territory (NTC – Table 3.3.I);
  - Vb,0: basic wind velocity of the zone (NTC – Table 3.3.I);
  - a0: base altitude of the zone (NTC – Table 3.3.I);
  - ks: parameter depending on the zone where the structure is located (NTC – Table 3.3.I);
  - as: site altitude;
  - TR: design return period expressed in years;
  - Vb: reference wind velocity calculated as follows:
    $V_b = V_{b,0}$ for $a_s \leq a_0$
    $V_b = V_{b,0}*[1 + k_s ((a_s / a_0) - 1)]$ for $a_0 < a_s \leq 1500$ m
    for as > 1500 m, values shall be obtained from appropriate documentation or proven investigations; such values shall not be lower than those prescribed for as = 1500 m;
  - Cr: return coefficient as a function of the return period TR;
  - Vr: reference wind velocity corresponding to the return period TR.

Zone	Vb,0	a0	ks	as	TR	Vb	Cr	Vr
1	25 m/s	1000 m	0,40	239 m	50 years	25,00 m/s	1,000	25,00 m/s

Table 4.11 Wind load

Reference dynamic pressure:

$$q_r = \frac{\rho V_r^2}{2} = 0.39\ kN/mq \tag{2}$$

where: ρ is the air density (conventionally assumed constant and equal to 1.25 kg/m³).

Exposure: Category V – Inland areas up to 500 m above sea level
From which the parameters of Table 3.3.II of the NTC are derived:

Kr	z0	zmin
0.23	0.70 m	12 m

Table 4.12

Terrain roughness class: A (NTC – Table 3.3.III)
Urban areas with at least 15% of the surface covered by buildings whose average height exceeds 15 m.

Wind action on structures is determined by the following parameters:

- Cp: pressure coefficient;
- Cd: dynamic coefficient;
- Ct: topographic coefficient;
- Ce: exposure coefficient (function of *z*, *z0* and *Ct*);
- z: height above ground level.

Cp	Cd	Ct	Ce	z
1.00	1.00	1.00	1.48	9.90 m

Table 4.13 Wind calculation parameters

Wind pressure:

$$p = q_r \, C_e \, C_p \, C_d = 0.58 \frac{kN}{mq} \tag{3}$$

The load case table and the related notes for each load case are shown below:

LC	Type	ID code	Notes
1	Ggk	LC=Ggk (self-weight of the structure)	
2	Gsk	LC=G1sk (permanent loads on floors and roof)	
3	Gsk	LC=G2sk (permanent loads on floors and roof n.c.d.)	
4	Qsk	LC=Qsk (variable loads on floors)	
5	Qnk	LC=Qnk (snow load)	
6	Edk	LC=Ed (dynamic ULS) alfa=0.0 (ecc. +)	modal mass:1.00 for 1 LC=Ggk (self-weight of the structure)
			modal mass:1.00 for 2 LC=G1sk (permanent loads on floors and roof)
			modal mass:1.00 for 3 LC=G2sk (permanent loads on floors and roof n.c.d.)
			modal mass:1.00 for 4 LC=Qsk (variable loads on floors)
			modal mass:1.00 for 5 LC=Qnk (snow load)
7	Edk	LC=Ed (dynamic ULS) alfa=0.0 (ecc. -)	as previous seismic LC
8	Edk	LC=Ed (dynamic ULS) alfa=90.00 (ecc. +)	as previous seismic LC
9	Edk	LC=Ed (dynamic ULS) alfa=90.00 (ecc. -)	as previous seismic LC
10	Edk	LC=Ed (dynamic ULS) alfa=0.0 (ecc. +)	as previous seismic LC
11	Edk	LC=Ed (dynamic ULS) alfa=0.0 (ecc. -)	as previous seismic LC
12	Edk	LC=Ed (dynamic ULS) alfa=90.00 (ecc. +)	as previous seismic LC
13	Edk	LC=Ed (dynamic ULS) alfa=90.00 (ecc. -)	as previous seismic LC

Table 4.14 Load cases

4.2.4 LOAD COMBINATION DEFINITION

The program combines various load case types according to the regulations foreseen by the acting standards and norms currently in force. The foreseen combinations are provided for the structure safety control, in the course of which the structure resistance to displacements and stresses is checked.
The first combination table reported below includes the following information: number, type, and identification code.

For limit state checks, the following action combinations are defined:

- Fundamental combination for ULS
  $gG1 \times G1 + gG2 \times G2 + gP \times P + gQ1 \times Qk1 + gQ2 \times y02 \times Qk2 + gQ3 \times y03 \times Qk3 + \ldots$
- Rare combination for SLS
  $G1 + G2 + P + Qk1 + y02 \times Qk2 + y03 \times Qk3 + \ldots$
- Frequent combination for SLS

$G1 + G2 + P + y11 \times Qk1 + y22 \times Qk2 + y23 \times Qk3 + ...$

- Quasi-permanent combination for SLS
  $G1 + G2 + P + y21 \times Qk1 + y22 \times Qk2 + y23 \times Qk3 + ...$
- Seismic combination
  $E + G1 + G2 + P + y21 \times Qk1 + y22 \times Qk2 + ...$
- Exceptional combination
  $G1 + G2 + Ad + P + y21 \times Qk1 + y22 \times Qk2 + ...$

Where:

Use/Action	**ψ₀**	**ψ₁**	**ψ₂**
Category A – Residential	0.70	0.50	0.30
Category B – Offices	0.70	0.50	0.30
Category C – Areas susceptible to crowding	0.70	0.70	0.60
Category D – Commercial areas	0.70	0.70	0.60
Category E – Libraries, archives, warehouses…	1.00	0.90	0.80
Category F – Garages and parking (vehicles ≤ 30 kN)	0.70	0.70	0.60
Category G – Garages and parking (vehicles > 30 kN)	0.70	0.50	0.30
Category H – Roofs	0.00	0.00	0.00
Wind	0.60	0.20	0.00
Snow at altitude ≤ 1000 m	0.50	0.20	0.00
Snow at altitude > 1000 m	0.70	0.50	0.20
Thermal variations	0.60	0.50	0.00

Table 4.15 Coefficients for the action combinations

In the verifications, two alternative design approaches can be adopted:

- Approach 1: two different combinations of partial safety factors are considered for the actions, for the materials, and for the global resistance (Combination 1 with factors A1 and Combination 2 with factors A2).
- Approach 2: a single combination is defined for the actions, for the material strength, and for the global resistance (with factors A1).

		Coefficient γf	**EQU**	**A1**	**A2**
Permanent loads	Favorable Unfavorable	γG1	0,9 1,1	1,0 1,3	1,0 1,0
Non-structural permanent loads	Favorable Unfavorable	γG2	0,8 1,5	0,8 1,5	0,8 1,3
Variable loads	Favorable Unfavorable	γQi	0,0 1,5	0,0 1,5	0,0 1,3

Table 4.16 Design approaches

A total of 78 load combinations were considered in the analysis, including Ultimate Limit State (ULS) combinations and Seismic Serviceability Limit State (SLS) combinations. The combinations were identified according to the corresponding design approach and verification type.

4.2.5 SEISMIC ACTION EVALUATION

Seismic action on building is computed from "seismic base hazard" for ideal condition of rigid soil and horizontal surface. Now seismic hazard, for a reference grid and for return periods, is available from website http://esse1.mi.ingv.it/.

Seismic action is defined for a reference period Vr (product of nominal life of the structure by use coefficent as reported in the table Structure Parameters). For the reference period Vr and the related probability Pver for limit states, the code obtains return period Tr and seismic hazard parameters (see Table 4.17):

- ag: maximum ground orizontal acceleration;
- Fo: maximum amplification factor for orizontal acceleration spectrum;
- T*c: initial period for costant velocity in the orizontal acceleration spectrum;

Use class	Life Vn [year]	Use Coeff.	Period Vr [year]	Kind of soil	Kind of surface
II	50.0	1.0	50.0	B	T1

Table 4.17 Structure parameters

From the seismic hazard parameters the code computes:

- S factor for soil and kind of surface as: $S = S_s * S_t$
- F_0 maximum amplification factor for orizontal acceleration spectrum
- F_V maximum amplification factor for vertical acceleration spectrum
- T_B initial period for costant acceleration
- T_C initial period for costant velocity
- T_D initial period for costant displacement

The horizontal acceleration spectrum, S_e, is definied by the espressions below:

$$0 \le T < T_B \qquad S_e(T) = a_g * S * \eta * F_0 * \left[\frac{T}{T_B} + \frac{1}{\eta * F_0} * \left(1 - \frac{T}{T_B}\right)\right] \tag{4}$$

$$T_B \le T < T_C \qquad S_e(T) = a_g * S * \eta * F_0 \tag{5}$$

$$T_C \le T < T_D \qquad S_e(T) = a_g * S * \eta * F_0 * \left(\frac{T_C}{T}\right) \tag{6}$$

$$T_D \le T \qquad S_e(T) = a_g * S * \eta * F_0 * \left(\frac{T_C * T_D}{T^2}\right) \tag{7}$$

Where, for subsoil category A, the coefficients S_s and C_c are equal to 1; whereas for subsoil categories B, C, D, and E, the coefficients S_s and C_c are calculated using the expressions given in the following Table 4.18.

Subsoil category	S_s	C_c
A	1,00	1,00
B	$1{,}00 \le 1{,}40 - 0{,}40 * F_0 * \frac{a_g}{g} \le 1{,}20$	$1{,}10 * (T_C{}^*)^{-0{,}20}$

C	$1{,}00 \leq 1{,}70 - 0{,}60 * F_0 * \frac{a_g}{g} \leq 1{,}50$	$1{,}05 * (T_C{}^*)^{-0{,}33}$
D	$0{,}90 \leq 2{,}40 - 1{,}50 * F_0 * \frac{a_g}{g} \leq 1{,}80$	$1{,}25 * (T_C{}^*)^{-0{,}50}$
E	$1{,}00 \leq 2{,}00 - 1{,}10 * F_0 * \frac{a_g}{g} \leq 1{,}60$	$1{,}15 * (T_C{}^*)^{-0{,}40}$

Table 4.18 Coefficients calculation

To account for topographic conditions and in the absence of specific local seismic response analyses, the values of the topographic coefficient S_T given in the Table 4.19 are used.

Topographic category	$\boldsymbol{S_T}$
T1	1,0
T2	1,2
T3	1,2
T4	1,4

Table 4.19

The vertical acceleration spectrum, S_{ve}, is definied by the espressions below:

$$0 \leq T < T_B \qquad S_{ve}(T) = a_g * S * \eta * F_v * \left[\frac{T}{T_B} + \frac{1}{\eta * F_0} * \left(1 - \frac{T}{T_B}\right)\right] \tag{8}$$

$$T_B \leq T < T_C \qquad S_{ve}(T) = a_g * S * \eta * F_v \tag{9}$$

$$T_C \leq T < T_D \qquad S_{ve}(T) = a_g * S * \eta * F_v * \left(\frac{T_C}{T}\right) \tag{10}$$

$$T_D \leq T \qquad S_{ve}(T) = a_g * S * \eta * F_v * \left(\frac{T_C * T_D}{T^2}\right) \tag{11}$$

Values of the coefficients S_s, T_B, T_C and T_D are showned in the following table:

Subsoil category	$\boldsymbol{S_s}$	$\boldsymbol{T_B}$	$\boldsymbol{T_C}$	$\boldsymbol{T_D}$
A, B, C, D, E	1,0	0,05 s	0,15 s	1,0 s

Table 4.20 Seismic spectrum parameters

LS	$\boldsymbol{P_{ver}}$	$\boldsymbol{T_r}$	$\boldsymbol{a_g}$	$\boldsymbol{F_0}$	$\boldsymbol{T * c}$
		Years	*g*		*sec*
SLO	81.0	30.1	0.024	2.576	0.180
SLD	63.0	50.3	0.029	2.587	0.194
SLV	10.0	474.6	0.056	2.758	0.270
SLC	5.0	974.8	0.067	2.806	0.290

Table 4.21 Seismic parameters for the considered limit states

LS	a_g	S	F_0	F_v	T_B	T_C	T_D
	g				*sec*	*sec*	*sec*
SLO	0.024	1.200	2.576	0.535	0.093	0.279	1.695
SLD	0.029	1.200	2.587	0.599	0.099	0.296	1.718
SLV	0.056	1.200	2.758	0.883	0.129	0.386	1.825
SLC	0.067	1.200	2.806	0.979	0.136	0.409	1.867

Table 4.22 Seismic response spectrum parameters

Mode	Frequency	Period	X effective M x g	%	Y effective M x g	%	Z effective M x g	%	RZ effective M x g	%
	1/sec	*sec*	*kN*		*kN*		*kN*		*kN m2*	
1	1.32	0.76	4692.00	88	0.00	0	0.0	0	0.00	0
2	1.33	0.75	0.00	0	4701.00	88	0.0	0	0.00	0
3	1.62	0.62	0.00	0	0.00	0	0.0	0	1.88E+09	89
4	3.93	0.25	0.00	9	342.40	0	0.0	0	0	0
5	3.99	0.25	441.10	0	0.00	9	0.0	0	0.0938	0
6	4.19	0.24	0.00	0	0.00	0	0.0	0	853940	8

Table 4.23 Modal properties of the structure

4.2.6 LEGEND OF SEISMIC ANALYSIS RESULTS

The program allows to analyse various seismic configurations.

Actually the following load cases are provided:

- Esk: seismic load case with an equivalent static analysis
- Edk: seismic load case with a dynamic analysis

Each load case is characterized by an input angle and a configuration of masses which determine the comprehensive seismic force.

In the case of elements designed in a non-dissipative field, the stresses calculated with a qND factor obtained in accordance with point 7.3.2 are adopted, depending on the behaviour factor q used for the structure:

$$1 < q_{ND} = \frac{2}{3} * q \ < \ 1.5 \tag{12}$$

Below the behaviour factors according to the D.M. 17/10/2018

The structure is classified as a new building with regularity both in plan and in height. The adopted ductility class is CD “B”. The structural system is made of reinforced concrete and consists of frame structures, coupled wall structures, and mixed systems. The αu/α1 ratio has been defined according to the value specified by the applicable code provisions, with reference to multi-storey and multi-bay frame structures

a_u/a_1	1.300
$q_0 = 3.000\ a_u/a_1$	3.900
k_w	1.000

K_R	1.0
$q_D = q_0 \bullet k_w \bullet K_R$	3.900

Table 4.24 Seismic behavior factor parameters

	Dissipative
q SLU x	3.900
q SLU y	3.900
q SLU z	1.500

Table 4.25 Behaviour factors for ULS

4.2.7 VERIFICATION OF REINFORCED CONCRETE BEAM AND COLUMN ELEMENTS

The table shows the identification number and verification code for each element, with the abbreviations OK or NV.

The design was carried out using the Limit State (LS) method. Accordingly, the following information is reported: the x/d ratio, the proportional stress checks, and the average compression check, together with the load combinations corresponding to the reported values. Furthermore, the structure exhibits dissipative behaviour and has been designed according to the resistance hierarchy criterion. Therefore, the overstrength and beam–column joint checks are also reported.

For checks on the LS of the columns, there is the Table 4.27 with the symbols described below:

M_C X Y	Pier line number (P) and plan coordinates (X, Y)
Column	Column identification number (element D2)
Elevation	Elevation of the verification section
%Af	Percentage of reinforcement area with respect to the concrete area
Slenderness ratio	Slenderness ratio λ / λ*: value greater than 1 for slender members when the verification is carried out using the direct equilibrium method
Longitudinal reinforcement	Number and diameter (d) of longitudinal reinforcement bars, distinguished into corner bars and side bars at positions nL1 and nL2
N/M check	Axial force–bending interaction check with ratio Ed/Rd: value ≤ 1 for a satisfactory verification
Seismic N check	Seismic axial compression check considering concrete only, with ratio Nsd/Nrd, where Nrd is calculated in accordance with Clause 7.4.4.2.1: value ≤ 1 for a satisfactory verification
Stirrups	Data of the stirrup region under verification, specifically: number of legs, diameter, spacing, and length L of the region
V/T check	Shear/torsion check with ratio Ved/Vrd: value ≤ 1 for a satisfactory verification

Table 4.26 Legend of symbols

To facilitate the interpretation of the table below, which summarizes the reinforcement provided in each column and the corresponding verification checks, the figure showing the column numbering is presented below.

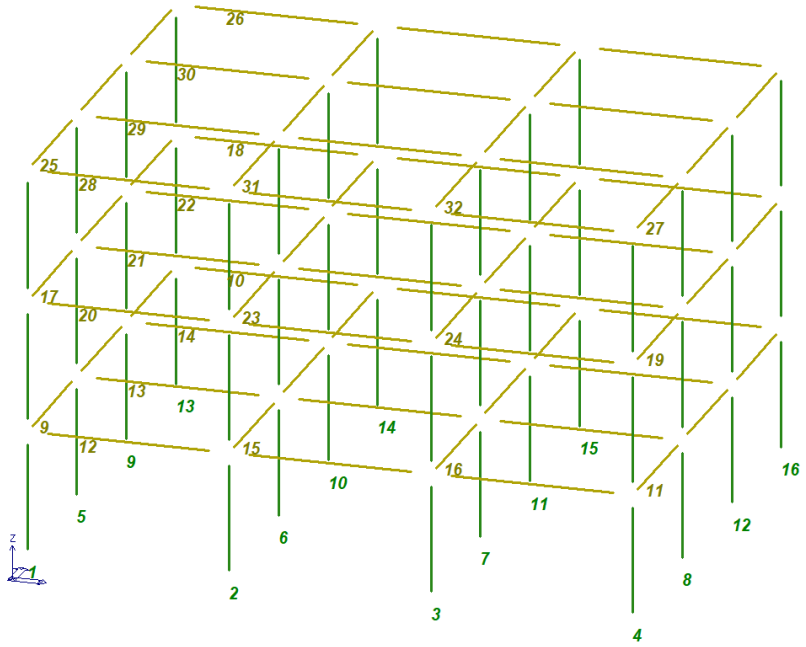


Figure 4.3 Column and Beam numbering

M_C = 1 X = 0.0 Y = 119.8									
Column	***Elevation***	***%Af***	***Slend. Ratio***	***Long. Reinf.***	***N/M check***	***S. N check***	***Stirrups***	***V/T check rc***	***V/T check steel***
	cm						L=cm		
13	0	0.89	0.68	4d16 0+0 d16	0.33	0.22	2+2d10/12 L=62	0.24	0.14
	165	0.89	0.68	4d16 0+0 d16	0.12	0.22	2+2d10/15 L=205	0.24	0.16
	330	0.89	0.68	4d16 0+0 d16	0.35	0.21	2+2d10/12 L=62	0.25	0.14
77	330	0.89	0.55	4d16 0+0 d16	0.42	0.14	2+2d10/12 L=62	0.26	0.13
	495	0.89	0.55	4d16 0+0 d16	0.08	0.14	2+2d10/15 L=205	0.26	0.15
	660	0.89	0.55	4d16 0+0 d16	0.43	0.14	2+2d10/12 L=62	0.26	0.13
117	660	0.89	0.38	4d16 0+0 d16	0.46	0.07	2+2d10/12 L=62	0.25	0.11
	825	0.89	0.38	4d16 0+0 d16	0.07	0.06	2+2d10/15 L=205	0.25	0.13
	990	0.89	0.38	4d16 0+0 d16	0.57	0.06	2+2d10/12 L=62	0.25	0.11
M_C = 2 X = 500.0 Y = 119.8									
Column	***Elevation***	***%Af***	***Slend. Ratio***	***Long. Reinf.***	***N/M check***	***Seis N check***	***Stirrups***	***V/T check rc***	***V/T check steel***
14	0	0.89	0.94	4d16 0+0 d16	0.34	0.41	2+2d10/8 L=56	0.27	0.11
	165	0.89	0.94	4d16 0+0 d16	0.21	0.4	2+2d10/15 L=218	0.27	0.2
	330	0.89	0.94	4d16 0+0 d16	0.33	0.4	2+2d10/8 L=56	0.27	0.11
78	330	0.89	0.76	4d16 0+0 d16	0.35	0.27	2+2d10/12 L=62	0.27	0.15
	495	0.89	0.76	4d16 0+0 d16	0.15	0.26	2+2d10/15 L=205	0.27	0.18
	660	0.89	0.76	4d16 0+0 d16	0.36	0.26	2+2d10/12 L=62	0.27	0.15
118	660	0.89	0.53	4d16 0+0 d16	0.34	0.12	2+2d10/12 L=62	0.24	0.12

	825	0.89	0.53	4d16 0+0 d16	0.08	0.12	2+2d10/15 L=205	0.24	0.15
	990	0.89	0.53	4d16 0+0 d16	0.4	0.12	2+2d10/12 L=62	0.24	0.12
M_C = 3 X = 1000.0 Y = 119.8									
Column	***Elevation***	***%Af***	***Slend. Ratio***	***Long. Reinf.***	***N/M check***	***Seis N check***	***Stirrups***	***V/T check rc***	***V/T check steel***
15	0	0.89	0.94	4d16 0+0 d16	0.34	0.41	2+2d10/8 L=56	0.27	0.11
	165	0.89	0.94	4d16 0+0 d16	0.21	0.4	2+2d10/15 L=218	0.27	0.2
	330	0.89	0.94	4d16 0+0 d16	0.33	0.4	2+2d10/8 L=56	0.27	0.11
79	330	0.89	0.76	4d16 0+0 d16	0.35	0.27	2+2d10/12 L=62	0.27	0.15
	495	0.89	0.76	4d16 0+0 d16	0.15	0.26	2+2d10/15 L=205	0.27	0.18
	660	0.89	0.76	4d16 0+0 d16	0.36	0.26	2+2d10/12 L=62	0.27	0.15
119	660	0.89	0.53	4d16 0+0 d16	0.34	0.12	2+2d10/12 L=62	0.24	0.12
	825	0.89	0.53	4d16 0+0 d16	0.08	0.12	2+2d10/15 L=205	0.24	0.15
	990	0.89	0.53	4d16 0+0 d16	0.4	0.12	2+2d10/12 L=62	0.24	0.12
M_C = 4 X = 1500.0 Y = 119.8									
Column	***Elevation***	***%Af***	***Slend. Ratio***	***Long. Reinf.***	***N/M check***	***Seis N check***	***Stirrups***	***V/T check rc***	***V/T check steel***
16	0	0.89	0.68	4d16 0+0 d16	0.33	0.22	2+2d10/12 L=62	0.24	0.14
	165	0.89	0.68	4d16 0+0 d16	0.12	0.22	2+2d10/15 L=205	0.24	0.16
	330	0.89	0.68	4d16 0+0 d16	0.35	0.21	2+2d10/12 L=62	0.25	0.14
80	330	0.89	0.55	4d16 0+0 d16	0.42	0.14	2+2d10/12 L=62	0.26	0.13
	495	0.89	0.55	4d16 0+0 d16	0.08	0.14	2+2d10/15 L=205	0.26	0.15
	660	0.89	0.55	4d16 0+0 d16	0.43	0.14	2+2d10/12 L=62	0.26	0.13
120	660	0.89	0.38	4d16 0+0 d16	0.46	0.07	2+2d10/12 L=62	0.25	0.11
	825	0.89	0.38	4d16 0+0 d16	0.07	0.06	2+2d10/15 L=205	0.25	0.13
	990	0.89	0.38	4d16 0+0 d16	0.57	0.06	2+2d10/12 L=62	0.25	0.11
M_C = 5 X = 0.0 Y = 519.8									
Column	***Elevation***	***%Af***	***Slend. Ratio***	***Long. Reinf.***	***N/M check***	***Seis N check***	***Stirrups***	***V/T check rc***	***V/T check steel***
9	0	0.89	0.91	4d16 0+0 d16	0.36	0.38	2+2d10/8 L=56	0.28	0.1
	165	0.89	0.91	4d16 0+0 d16	0.2	0.37	2+2d10/15 L=218	0.28	0.19
	330	0.89	0.91	4d16 0+0 d16	0.41	0.37	2+2d10/8 L=56	0.28	0.1
73	330	0.89	0.73	4d16 0+0 d16	0.54	0.24	2+2d10/12 L=62	0.3	0.15
	495	0.89	0.73	4d16 0+0 d16	0.14	0.24	2+2d10/15 L=205	0.3	0.18
	660	0.89	0.73	4d16 0+0 d16	0.51	0.24	2+2d10/12 L=62	0.3	0.15
113	660	0.89	0.51	4d16 0+0 d16	0.68	0.11	2+2d10/12 L=62	0.28	0.12
	825	0.89	0.51	4d16 0+0 d16	0.1	0.11	2+2d10/15 L=205	0.28	0.14
	990	0.89	0.51	4d16 0+0 d16	0.81	0.1	2+2d10/12 L=62	0.28	0.12
M_C = 6 X = 500.0 Y = 519.8									
Column	***Elevation***	***%Af***	***Slend. Ratio***	***Long. Reinf.***	***N/M check***	***Seis N check***	***Stirrups***	***V/T check rc***	***V/T check steel***
10	0	0.89	1.25	4d16 0+0 d16	0.79	0.67	2+2d10/5 L=55	0.29	0.08
	165	0.89	1.25	4d16 0+0 d16	0.78	0.67	2+2d10/15 L=220	0.29	0.23
	330	0.89	1.25	4d16 0+0 d16	0.78	0.66	2+2d10/5 L=55	0.29	0.08
74	330	0.89	1	4d16 0+0 d16	0.45	0.44	2+2d10/8 L=56	0.34	0.15
	495	0.89	1	4d16 0+0 d16	0.45	0.44	2+2d10/15 L=218	0.34	0.28

	660	1.79	1	4d16 2+2 d16	0.85	0.43	2+2d10/8 L=56	0.34	0.15
114	660	0.89	0.71	4d16 0+0 d16	0.72	0.21	2+2d10/12 L=62	0.23	0.14
	825	0.89	0.71	4d16 0+0 d16	0.13	0.21	2+2d10/15 L=205	0.23	0.17
	990	0.89	0.71	4d16 0+0 d16	0.2	0.2	2+2d10/12 L=62	0.23	0.14
M_C = 7 X = 1000.0 Y = 519.8									
Column	***Elevation***	***%Af***	***Slend. Ratio***	***Long. Reinf.***	***N/M check***	***Seis N check***	***Stirrups***	***V/T check rc***	***V/T check steel***
11	0	0.89	1.25	4d16 0+0 d16	0.79	0.67	2+2d10/5 L=55	0.29	0.08
	165	0.89	1.25	4d16 0+0 d16	0.78	0.67	2+2d10/15 L=220	0.29	0.23
	330	0.89	1.25	4d16 0+0 d16	0.78	0.66	2+2d10/5 L=55	0.29	0.08
75	330	0.89	1	4d16 0+0 d16	0.45	0.44	2+2d10/8 L=56	0.34	0.15
	495	0.89	1	4d16 0+0 d16	0.45	0.44	2+2d10/15 L=218	0.34	0.28
	660	1.79	1	4d16 2+2 d16	0.85	0.43	2+2d10/8 L=56	0.34	0.15
115	660	0.89	0.71	4d16 0+0 d16	0.72	0.21	2+2d10/12 L=62	0.23	0.14
	825	0.89	0.71	4d16 0+0 d16	0.13	0.21	2+2d10/15 L=205	0.23	0.17
	990	0.89	0.71	4d16 0+0 d16	0.2	0.2	2+2d10/12 L=62	0.23	0.14
M_C = 8 X = 1500.0 Y = 519.8									
Column	***Elevation***	***%Af***	***Slend. Ratio***	***Long. Reinf.***	***N/M check***	***Seis N check***	***Stirrups***	***V/T check rc***	***V/T check steel***
12	0	0.89	0.91	4d16 0+0 d16	0.36	0.38	2+2d10/8 L=56	0.28	0.1
	165	0.89	0.91	4d16 0+0 d16	0.2	0.37	2+2d10/15 L=218	0.28	0.19
	330	0.89	0.91	4d16 0+0 d16	0.41	0.37	2+2d10/8 L=56	0.28	0.1
76	330	0.89	0.73	4d16 0+0 d16	0.54	0.24	2+2d10/12 L=62	0.3	0.15
	495	0.89	0.73	4d16 0+0 d16	0.14	0.24	2+2d10/15 L=205	0.3	0.18
	660	0.89	0.73	4d16 0+0 d16	0.51	0.24	2+2d10/12 L=62	0.3	0.15
116	660	0.89	0.51	4d16 0+0 d16	0.68	0.11	2+2d10/12 L=62	0.28	0.12
	825	0.89	0.51	4d16 0+0 d16	0.1	0.11	2+2d10/15 L=205	0.28	0.14
	990	0.89	0.51	4d16 0+0 d16	0.81	0.1	2+2d10/12 L=62	0.28	0.12
M_C = 9 X = 0.0 Y = 919.8									
Column	***Elevation***	***%Af***	***Slend. Ratio***	***Long. Reinf.***	***N/M check***	***Seis N check***	***Stirrups***	***V/T check rc***	***V/T check steel***
5	0	0.89	0.91	4d16 0+0 d16	0.36	0.38	2+2d10/8 L=56	0.28	0.1
	165	0.89	0.91	4d16 0+0 d16	0.2	0.37	2+2d10/15 L=218	0.28	0.19
	330	0.89	0.91	4d16 0+0 d16	0.41	0.37	2+2d10/8 L=56	0.28	0.1
69	330	0.89	0.73	4d16 0+0 d16	0.54	0.24	2+2d10/12 L=62	0.3	0.15
	495	0.89	0.73	4d16 0+0 d16	0.14	0.24	2+2d10/15 L=205	0.3	0.18
	660	0.89	0.73	4d16 0+0 d16	0.51	0.24	2+2d10/12 L=62	0.3	0.15
109	660	0.89	0.51	4d16 0+0 d16	0.68	0.11	2+2d10/12 L=62	0.28	0.12
	825	0.89	0.51	4d16 0+0 d16	0.1	0.11	2+2d10/15 L=205	0.28	0.14
	990	0.89	0.51	4d16 0+0 d16	0.81	0.1	2+2d10/12 L=62	0.28	0.12
M_C = 10 X = 500.0 Y = 919.8									
Column	***Elevation***	***%Af***	***Slend. Ratio***	***Long. Reinf.***	***N/M check***	***Seis N check***	***Stirrups***	***V/T check rc***	***V/T check steel***
6	0	0.89	1.25	4d16 0+0 d16	0.79	0.67	2+2d10/5 L=55	0.29	0.08
	165	0.89	1.25	4d16 0+0 d16	0.78	0.67	2+2d10/15 L=220	0.29	0.23
	330	0.89	1.25	4d16 0+0 d16	0.78	0.66	2+2d10/5 L=55	0.29	0.08
70	330	0.89	1	4d16 0+0 d16	0.45	0.44	2+2d10/8 L=56	0.34	0.15

	495	0.89	1	4d16 0+0 d16	0.45	0.44	2+2d10/15 L=218	0.34	0.28
	660	1.79	1	4d16 2+2 d16	0.85	0.43	2+2d10/8 L=56	0.34	0.15
110	660	0.89	0.71	4d16 0+0 d16	0.72	0.21	2+2d10/12 L=62	0.23	0.14
	825	0.89	0.71	4d16 0+0 d16	0.13	0.21	2+2d10/15 L=205	0.23	0.17
	990	0.89	0.71	4d16 0+0 d16	0.2	0.2	2+2d10/12 L=62	0.23	0.14
M_C = 11 X = 1000.0 Y = 919.8									
Column	***Elevation***	***%Af***	***Slend. Ratio***	***Long. Reinf.***	***N/M check***	***Seis N check***	***Stirrups***	***V/T check rc***	***V/T check steel***
7	0	0.89	1.25	4d16 0+0 d16	0.79	0.67	2+2d10/5 L=55	0.29	0.08
	165	0.89	1.25	4d16 0+0 d16	0.78	0.67	2+2d10/15 L=220	0.29	0.23
	330	0.89	1.25	4d16 0+0 d16	0.78	0.66	2+2d10/5 L=55	0.29	0.08
71	330	0.89	1	4d16 0+0 d16	0.45	0.44	2+2d10/8 L=56	0.34	0.15
	495	0.89	1	4d16 0+0 d16	0.45	0.44	2+2d10/15 L=218	0.34	0.28
	660	1.79	1	4d16 2+2 d16	0.85	0.43	2+2d10/8 L=56	0.34	0.15
111	660	0.89	0.71	4d16 0+0 d16	0.72	0.21	2+2d10/12 L=62	0.23	0.14
	825	0.89	0.71	4d16 0+0 d16	0.13	0.21	2+2d10/15 L=205	0.23	0.17
	990	0.89	0.71	4d16 0+0 d16	0.2	0.2	2+2d10/12 L=62	0.23	0.14
M_C = 12 X = 1500.0 Y = 919.8									
Column	***Elevation***	***%Af***	***Slend. Ratio***	***Long. Reinf.***	***N/M check***	***Seis N check***	***Stirrups***	***V/T check rc***	***V/T check steel***
8	0	0.89	0.91	4d16 0+0 d16	0.36	0.38	2+2d10/8 L=56	0.28	0.1
	165	0.89	0.91	4d16 0+0 d16	0.2	0.37	2+2d10/15 L=218	0.28	0.19
	330	0.89	0.91	4d16 0+0 d16	0.41	0.37	2+2d10/8 L=56	0.28	0.1
72	330	0.89	0.73	4d16 0+0 d16	0.54	0.24	2+2d10/12 L=62	0.3	0.15
	495	0.89	0.73	4d16 0+0 d16	0.14	0.24	2+2d10/15 L=205	0.3	0.18
	660	0.89	0.73	4d16 0+0 d16	0.51	0.24	2+2d10/12 L=62	0.3	0.15
112	660	0.89	0.51	4d16 0+0 d16	0.68	0.11	2+2d10/12 L=62	0.28	0.12
	825	0.89	0.51	4d16 0+0 d16	0.1	0.11	2+2d10/15 L=205	0.28	0.14
	990	0.89	0.51	4d16 0+0 d16	0.81	0.1	2+2d10/12 L=62	0.28	0.12
M_C = 13 X = 0.0 Y = 1319.8									
Column	***Elevation***	***%Af***	***Slend. Ratio***	***Long. Reinf.***	***N/M check***	***Seis N check***	***Stirrups***	***V/T check rc***	***V/T check steel***
1	0	0.89	0.68	4d16 0+0 d16	0.33	0.22	2+2d10/12 L=62	0.24	0.14
	165	0.89	0.68	4d16 0+0 d16	0.12	0.22	2+2d10/15 L=205	0.24	0.16
	330	0.89	0.68	4d16 0+0 d16	0.35	0.21	2+2d10/12 L=62	0.25	0.14
65	330	0.89	0.55	4d16 0+0 d16	0.42	0.14	2+2d10/12 L=62	0.26	0.13
	495	0.89	0.55	4d16 0+0 d16	0.08	0.14	2+2d10/15 L=205	0.26	0.15
	660	0.89	0.55	4d16 0+0 d16	0.43	0.14	2+2d10/12 L=62	0.26	0.13
105	660	0.89	0.38	4d16 0+0 d16	0.46	0.07	2+2d10/12 L=62	0.25	0.11
	825	0.89	0.38	4d16 0+0 d16	0.07	0.06	2+2d10/15 L=205	0.25	0.13
	990	0.89	0.38	4d16 0+0 d16	0.57	0.06	2+2d10/12 L=62	0.25	0.11
M_C = 14 X = 500.0 Y = 1319.8									
Column	***Elevation***	***%Af***	***Slend. Ratio***	***Long. Reinf.***	***N/M check***	***Seis N check***	***Stirrups***	***V/T check rc***	***V/T check steel***
2	0	0.89	0.94	4d16 0+0 d16	0.34	0.41	2+2d10/8 L=56	0.27	0.11
	165	0.89	0.94	4d16 0+0 d16	0.21	0.4	2+2d10/15 L=218	0.27	0.2

	330	0.89	0.94	4d16 0+0 d16	0.33	0.4	2+2d10/8 L=56	0.27	0.11
66	330	0.89	0.76	4d16 0+0 d16	0.35	0.27	2+2d10/12 L=62	0.27	0.15
	495	0.89	0.76	4d16 0+0 d16	0.15	0.26	2+2d10/15 L=205	0.27	0.18
	660	0.89	0.76	4d16 0+0 d16	0.36	0.26	2+2d10/12 L=62	0.27	0.15
106	660	0.89	0.53	4d16 0+0 d16	0.34	0.12	2+2d10/12 L=62	0.24	0.12
	825	0.89	0.53	4d16 0+0 d16	0.08	0.12	2+2d10/15 L=205	0.24	0.15
	990	0.89	0.53	4d16 0+0 d16	0.4	0.12	2+2d10/12 L=62	0.24	0.12
M_C = 15 X = 1000.0 Y = 1319.8									
Column	***Elevation***	***%Af***	***Slend. Ratio***	***Long. Reinf.***	***N/M check***	***Seis N check***	***Stirrups***	***V/T check rc***	***V/T check steel***
3	0	0.89	0.94	4d16 0+0 d16	0.34	0.41	2+2d10/8 L=56	0.27	0.11
	165	0.89	0.94	4d16 0+0 d16	0.21	0.4	2+2d10/15 L=218	0.27	0.2
	330	0.89	0.94	4d16 0+0 d16	0.33	0.4	2+2d10/8 L=56	0.27	0.11
67	330	0.89	0.76	4d16 0+0 d16	0.35	0.27	2+2d10/12 L=62	0.27	0.15
	495	0.89	0.76	4d16 0+0 d16	0.15	0.26	2+2d10/15 L=205	0.27	0.18
	660	0.89	0.76	4d16 0+0 d16	0.36	0.26	2+2d10/12 L=62	0.27	0.15
107	660	0.89	0.53	4d16 0+0 d16	0.34	0.12	2+2d10/12 L=62	0.24	0.12
	825	0.89	0.53	4d16 0+0 d16	0.08	0.12	2+2d10/15 L=205	0.24	0.15
	990	0.89	0.53	4d16 0+0 d16	0.4	0.12	2+2d10/12 L=62	0.24	0.12
M_C = 16 X = 1500.0 Y = 1319.8									
Column	***Elevation***	***%Af***	***Slend. Ratio***	***Long. Reinf.***	***N/M check***	***Seis N check***	***Stirrups***	***V/T check rc***	***V/T check steel***
4	0	0.89	0.68	4d16 0+0 d16	0.33	0.22	2+2d10/12 L=62	0.24	0.14
	165	0.89	0.68	4d16 0+0 d16	0.12	0.22	2+2d10/15 L=205	0.24	0.16
	330	0.89	0.68	4d16 0+0 d16	0.35	0.21	2+2d10/12 L=62	0.25	0.14
68	330	0.89	0.55	4d16 0+0 d16	0.42	0.14	2+2d10/12 L=62	0.26	0.13
	495	0.89	0.55	4d16 0+0 d16	0.08	0.14	2+2d10/15 L=205	0.26	0.15
	660	0.89	0.55	4d16 0+0 d16	0.43	0.14	2+2d10/12 L=62	0.26	0.13
108	660	0.89	0.38	4d16 0+0 d16	0.46	0.07	2+2d10/12 L=62	0.25	0.11
	825	0.89	0.38	4d16 0+0 d16	0.07	0.06	2+2d10/15 L=205	0.25	0.13
	990	0.89	0.38	4d16 0+0 d16	0.57	0.06	2+2d10/12 L=62	0.25	0.11

Table 4.27 Columns properties

Column	***%Af***	***Slend. Ratio***	***N/M check***	***Seis N check***	***V/T check rc***	***V/T check steel***
	1.79	1.25	0.85	0.67	0.34	0.28

Table 4.28 Maximum values of columns verifications

The figures below graphically represent the results presented in the tables above.

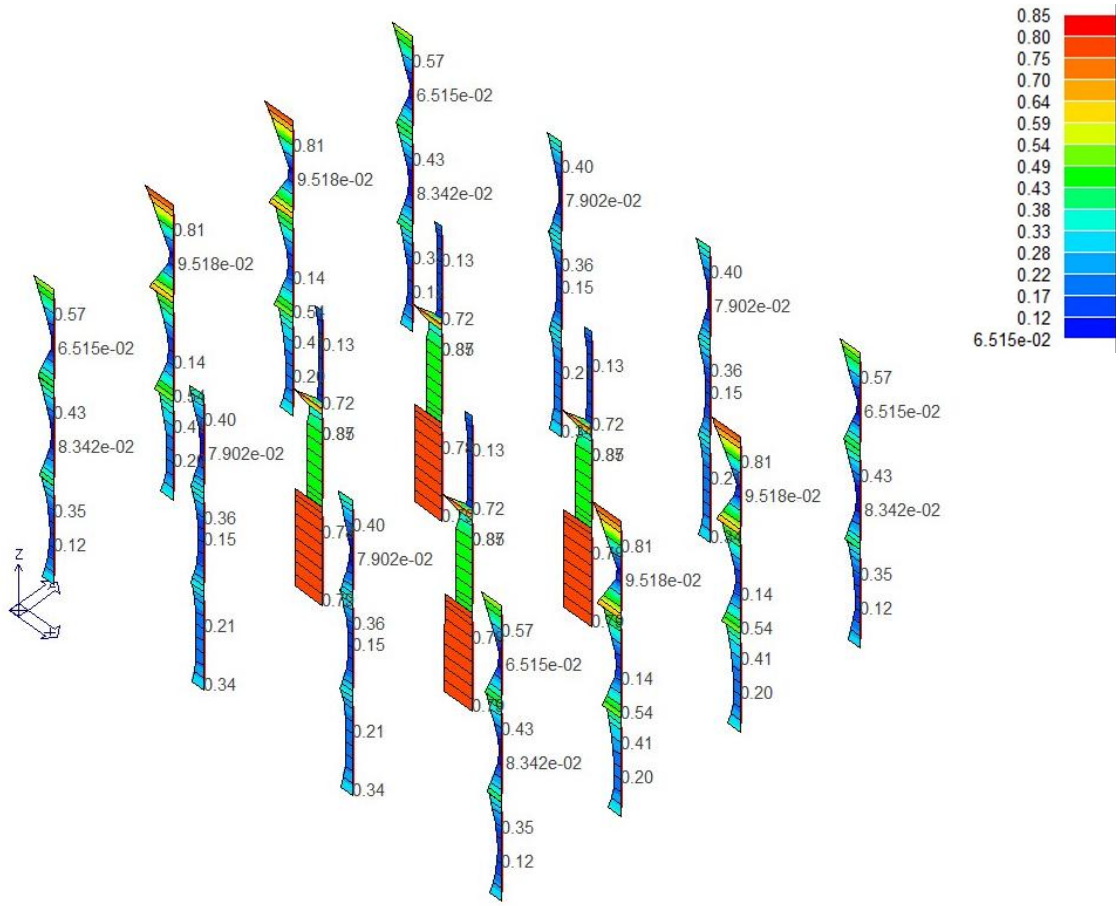


Figure 4.4 Check N/M

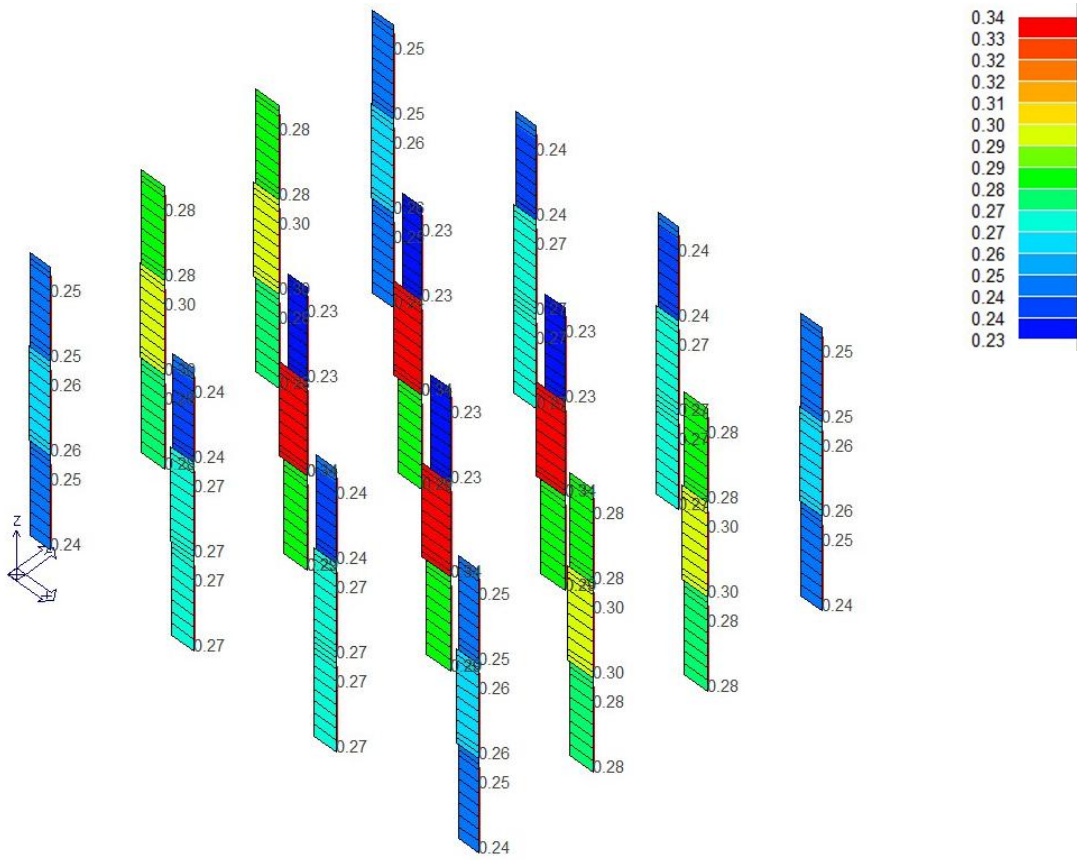


Figure 4.5 Check V/T concrete

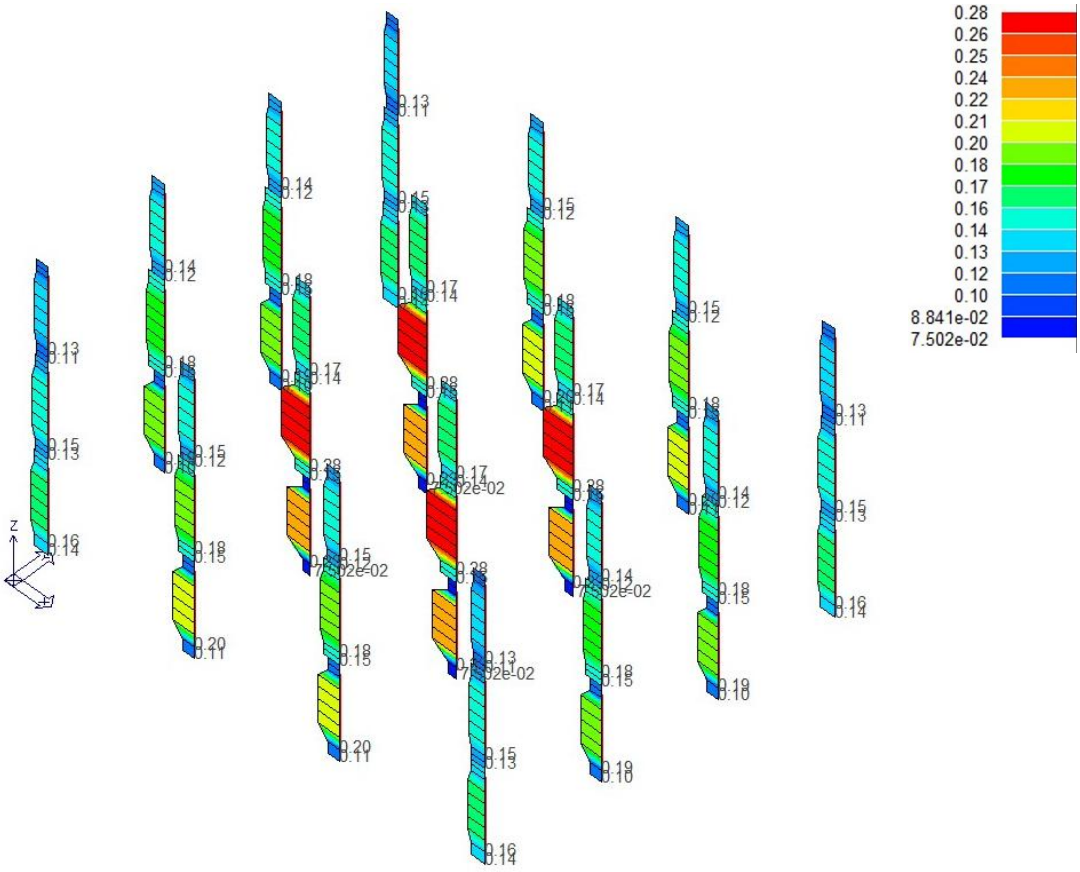


Figure 4.6 Check V/T steel

For checks on beam-column joints in new elements, there is a table with the symbols described below:

Node	Beam–column joint identification number
Status	Outcome of the checks
Column	Column identification number (D2)
Stirrup Ø	Diameter of joint stirrups
Spacing	Joint stirrup spacing
No. of legs 2 (3)	Number of stirrup legs for shear in direction 2 (3)
Bj2 (3)	Effective joint width for shear in direction 2 (3)
Hjc2 (3)	Distance between the outermost layers of column reinforcement for shear in direction 2 (3)
Check. 7.4.8	Ratio between joint shear demand Vjbd and shear resistance according to Section 7.4.8
Ash check	Ratio between the stirrup spacing calculated according to Section 7.4.4.3.1 and the stirrup spacing actually provided in the joint. If the value is equal to 1, the adopted spacing is derived from Section 7.4.4.3.1. If the value is less than 1, the adopted spacing is derived from the upper or lower column adjacent to the joint.
7.4.10	Check of stirrup spacing according to Eq. 7.4.10: • YES → spacing calculated using Eq. 7.4.10; • NO → spacing calculated using Eqs. 7.4.11 and/or 7.4.12; • NR → spacing calculation not required

Table 4.29 Legend for beam-column checks

Node	***Column***	***Diam***	***Spacing***	***n. br. 2***	***Bj2***	***Hjc2***	***n. br. 3***	***Bj3***	***Hjc3***	***7.4.8 C.***	***Ash C.***	***7.4.10***
		mm	*cm*		*cm*	*cm*		*cm*	*cm*			
2	1	12	12.5	2	30	21	2	30	21	0.5	0.6	SI
4	2	12	5	2	30	21	2	30	21	1	0.7	NO
6	3	12	5	2	30	21	2	30	21	1	0.7	NO
8	4	12	12.5	2	30	21	2	30	21	0.5	0.6	SI
10	5	12	8	2	30	21	2	30	21	0.8	0.9	NO
12	6	12	15	2	30	21	2	30	21	0	0	NR
14	7	12	15	2	30	21	2	30	21	0	0	NR
16	8	12	8	2	30	21	2	30	21	0.8	0.9	NO
18	9	12	8	2	30	21	2	30	21	0.8	0.9	NO
20	10	12	15	2	30	21	2	30	21	0	0	NR
22	11	12	15	2	30	21	2	30	21	0	0	NR
24	12	12	8	2	30	21	2	30	21	0.8	0.9	NO
26	13	12	12.5	2	30	21	2	30	21	0.5	0.6	SI
28	14	12	5	2	30	21	2	30	21	1	0.7	NO
30	15	12	5	2	30	21	2	30	21	1	0.7	NO
32	16	12	12.5	2	30	21	2	30	21	0.5	0.6	SI
33	65	12	12.5	2	30	21	2	30	21	0.4	0.8	NO
34	66	12	8	2	30	21	2	30	21	0.7	1	NO
35	67	12	8	2	30	21	2	30	21	0.7	1	NO
36	68	12	12.5	2	30	21	2	30	21	0.4	0.8	NO
37	69	12	5	2	30	21	2	30	21	0.7	0.6	NO
38	70	12	15	2	30	21	2	30	21	0	0	NR
39	71	12	15	2	30	21	2	30	21	0	0	NR
40	72	12	5	2	30	21	2	30	21	0.7	0.6	NO
41	73	12	5	2	30	21	2	30	21	0.7	0.6	NO
42	74	12	15	2	30	21	2	30	21	0	0	NR

43	75	12	15	2	30	21	2	30	21	0	0	NR
44	76	12	5	2	30	21	2	30	21	0.7	0.6	NO
45	77	12	12.5	2	30	21	2	30	21	0.4	0.8	NO
46	78	12	8	2	30	21	2	30	21	0.7	1	NO
47	79	12	8	2	30	21	2	30	21	0.7	1	NO
48	80	12	12.5	2	30	21	2	30	21	0.4	0.8	NO
49	105	12	12.5	2	30	21	2	30	21	0.4	0.8	NO
50	106	12	5	2	30	21	2	30	21	0.7	0.7	NO
51	107	12	5	2	30	21	2	30	21	0.7	0.7	NO
52	108	12	12.5	2	30	21	2	30	21	0.4	0.8	NO
53	109	12	5	2	30	21	2	30	21	0.7	0.7	NO
54	110	12	15	2	30	21	2	30	21	0	0	NR
55	111	12	15	2	30	21	2	30	21	0	0	NR
56	112	12	5	2	30	21	2	30	21	0.7	0.7	NO
57	113	12	5	2	30	21	2	30	21	0.7	0.7	NO
58	114	12	15	2	30	21	2	30	21	0	0	NR
59	115	12	15	2	30	21	2	30	21	0	0	NR
60	116	12	5	2	30	21	2	30	21	0.7	0.7	NO
61	117	12	12.5	2	30	21	2	30	21	0.4	0.8	NO
62	118	12	5	2	30	21	2	30	21	0.7	0.7	NO
63	119	12	5	2	30	21	2	30	21	0.7	0.7	NO
64	120	12	12.5	2	30	21	2	30	21	0.4	0.8	NO

Table 4.30 Nodes verifications

Node	***Step***	***7.4.8 Check***	***Ash check***
	5.00	0.97	0.99

Table 4.31 Maximum values of nodes verifications

For the sake of clarity, the above-mentioned checks prescribed by [18] NTC 2018 (Sections 7.4.8, 7.4.10, 7.4.11, and 7.4.12) are respectively presented below:

$$V_{jbd} \leq \eta * f_{cd} * b_j * \ h_{jc} * \sqrt{1 - \frac{v_d}{\eta}} \tag{13}$$

$$\frac{A_{sh} * f_{ywd}}{b_j * \ h_{jw}} \geq \frac{\left[\frac{V_{jbd}}{b_j * \ h_{jc}}\right]^2}{f_{ctd} + v_d * f_{cd}} - f_{ctd} \tag{14}$$

$$A_{sh} * f_{ywd} \geq \gamma_{Rd} * (A_{s1} + A_{s2}) * f_{yd} * (1 - 0.8\, v_d) \tag{15}$$

$$A_{sh} * f_{ywd} \geq \gamma_{Rd} * A_{s2} * f_{yd} * (1 - 0.8\, v_d) \tag{16}$$

For checks on the LS of the beams, there is a table with the symbols described below:

%Af	Percentage of reinforcement area with respect to the concrete area
Af bot.	Area of longitudinal reinforcement placed at the soffit
Af top	Area of longitudinal reinforcement placed at the top
Af long.	Total longitudinal reinforcement area
x/d	Ratio between the neutral axis depth and the effective depth
N/M check	Axial force–bending moment interaction check, ratio Ed/Rd: value ≤ 1 for a positive check
Stirrups	Data of the stirrup segment under verification: number of legs, diameter, spacing, segment length L
V/T rc/steel check	Shear/torsion check with ratio Ved/Vrd: value ≤ 1 for a positive check

Table 4.32

For beam checks, only the maximum values for each item described above are reported, as the table is conceptually the same as that for columns.

Similar to the latter, beams are also characterised by three D2 elements, for a total of 24 beams and 72 D2 elements.

Beam	***%Af***	***Af bot.***	***Af. top***	***Af long.***	***x/d***	***N/M check***	***V/T cls check***	***V/T st. check***
	0.67	20.10	20.10	0.0	0.24	0.98	0.49	0.45

Table 4.33 Maximum values of beams verification

For column and beam capacity design checks, a list is provided containing the symbols described below:

- Negative moment $M_i^-(M_f^-)$: Negative resistant bending moment at the initial end i (final end f) of the beam
- Positive moment $M_i^+(M_f^+)$: Positive resistant bending moment at the initial end i (final end f) of the beam
- Span for shear L_V: Design span adopted for the definition of shear generated by resistant moments
- $V_{M-i\,M+f}$: Shear generated by the negative resistant moment at end $i$and the positive resistant moment at end f
- $V_{M+i\,M-f}$: Shear generated by the positive resistant moment at end $i$and the negative resistant moment at end f
- A_s: Area of a single layer of diagonal reinforcement according to equation 7.4.2 (only for ductility class "A")
- $M_{2-2,i}(M_{2-2,f})$: Resistant bending moment about the 2-2 axis at the base i and at the top f, corresponding to the maximum moment under the design axial force
- $M_{3-3,i}(M_{3-3,f})$: Resistant bending moment about the 3-3 axis at the base i and at the top f, corresponding to the maximum moment under the design axial force
- Span for shear L_V: Design span adopted for the definition of shear generated by resistant moments
- $V_{M2-2}(V_{M3-3})$: Shear force generated by the resistant moments about the 2-2 axis (3-3 axis)

Here are reported only the maximum values:

Column	$M_{2-2,i}$	$M_{2-2,f}$	$M_{3-3,i}$	$M_{3-3,f}$	V_{M2-2}	V_{M3-3}
	kN m	*kN m*	*kN m*	*kN m*	*kN*	*kN*
	79.54	92.06	79.54	92.06	63.49	63.49

Table 4.34 Column design resistance values

Beam	M_i^-	M_i^+	M_f^-	M_f^+	$V_{M-i\,M+f}$	$V_{M+i\,M-f}$
	kN m	*kN m*	*kN m*	*kN m*	*kN*	*kN*
	93.29	50.62	93.29	50.62	30.62	30.62

Table 4.35 Beam design resistance values

As shown in the figures below, in the columns the acting bending moments in both directions remain below the corresponding resisting bending moments, confirming that the structural capacity is not exceeded.

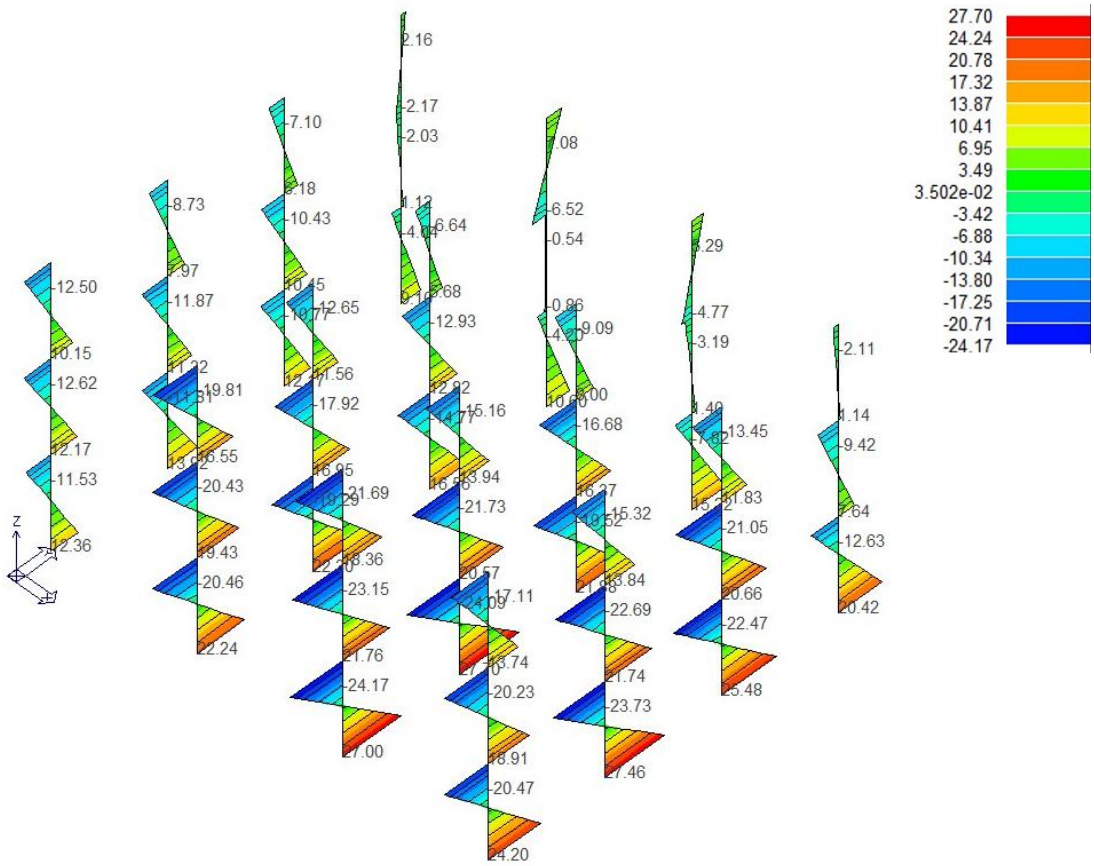


Figure 4.7 Maximum acting bending moment 2-2 [kN m] from combination ELS 66

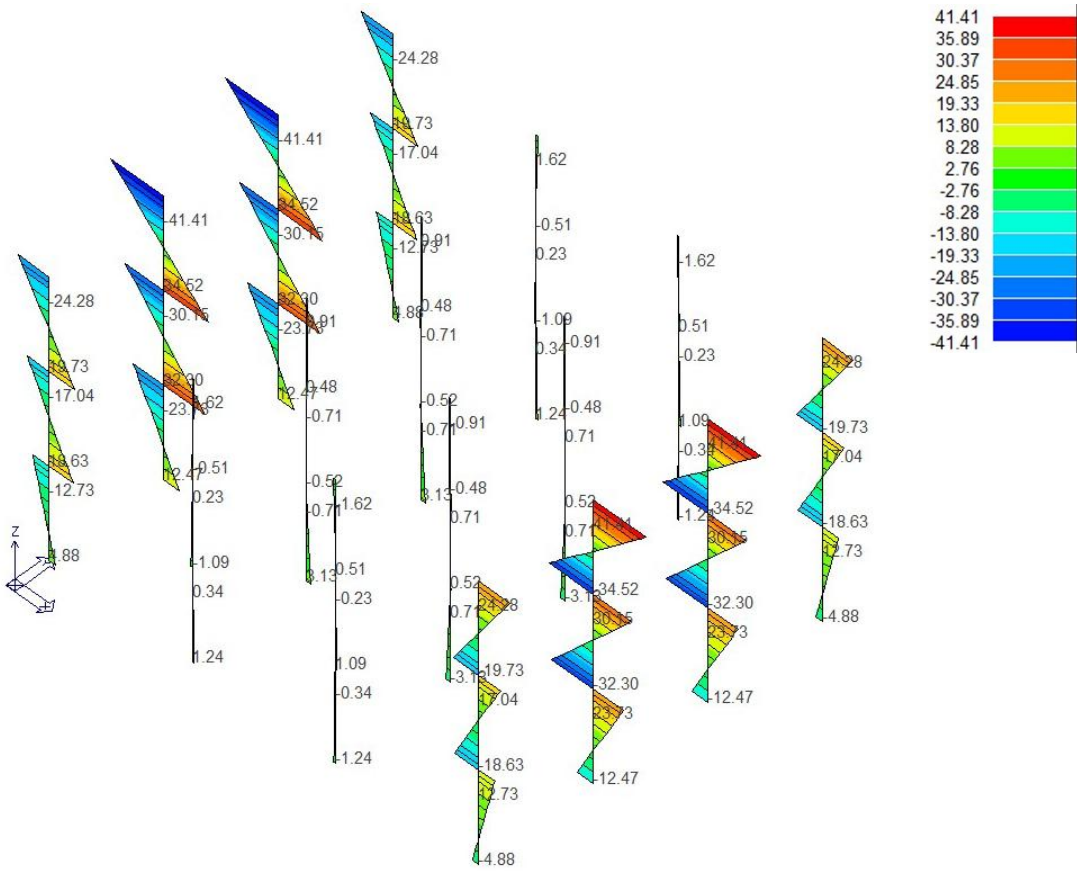


Figure 4.8 Maximum acting bending moment 3-3 [kN m] from combination ULS A1 11

After the description of the structural elements, the corresponding drawings are presented, which allow a clearer understanding of their geometry and the arrangement of the reinforcement.

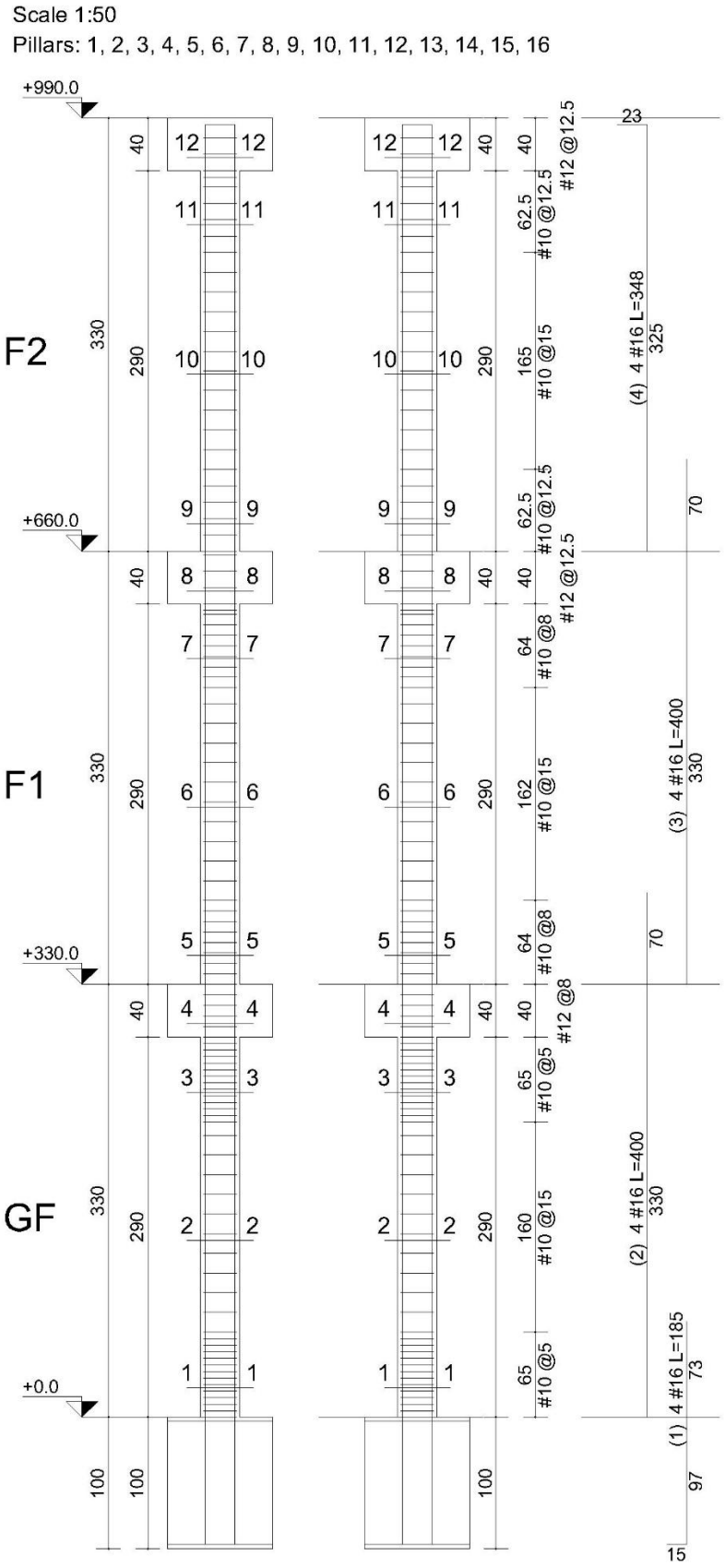
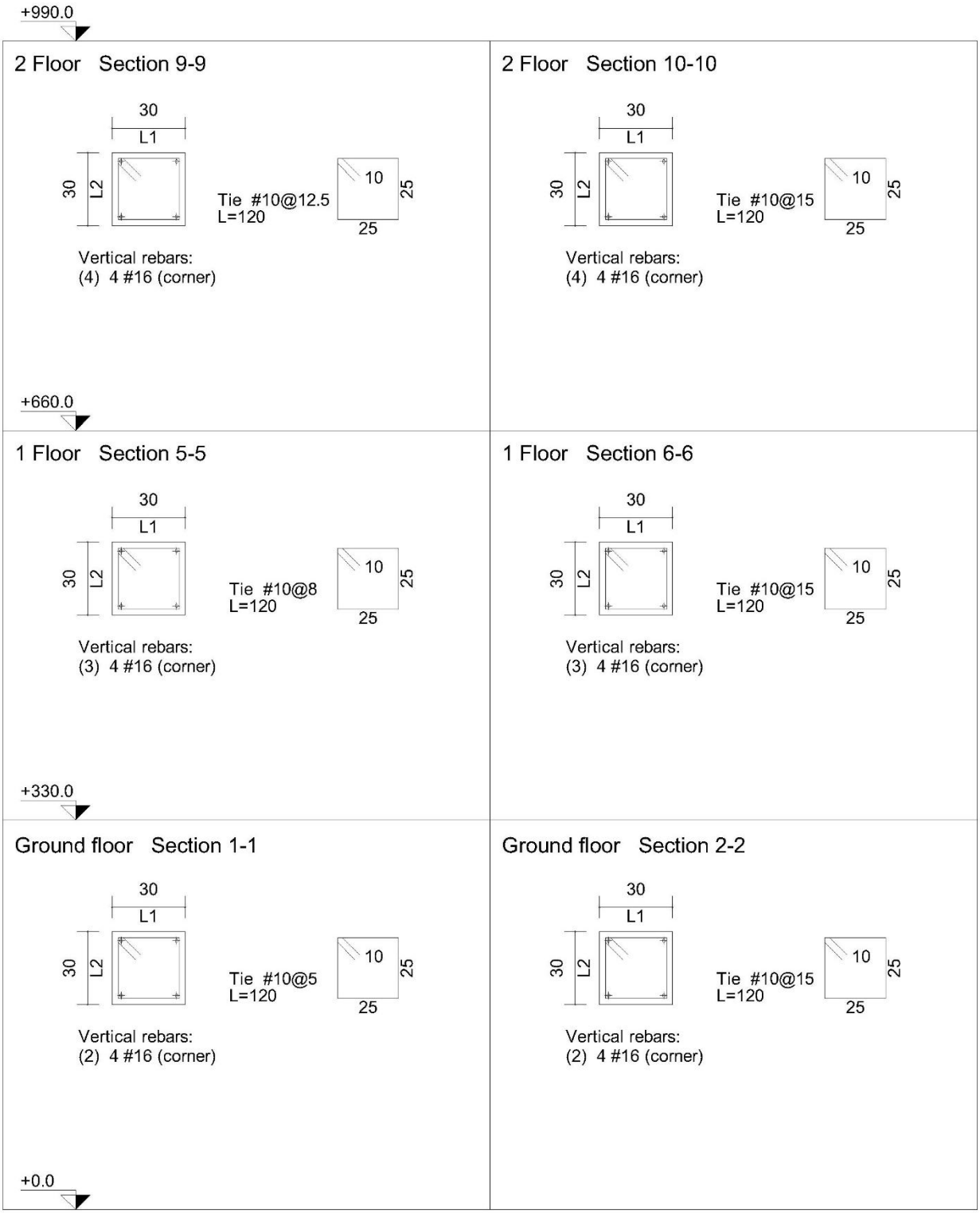


Figure 4.9 Column reinforcement layout

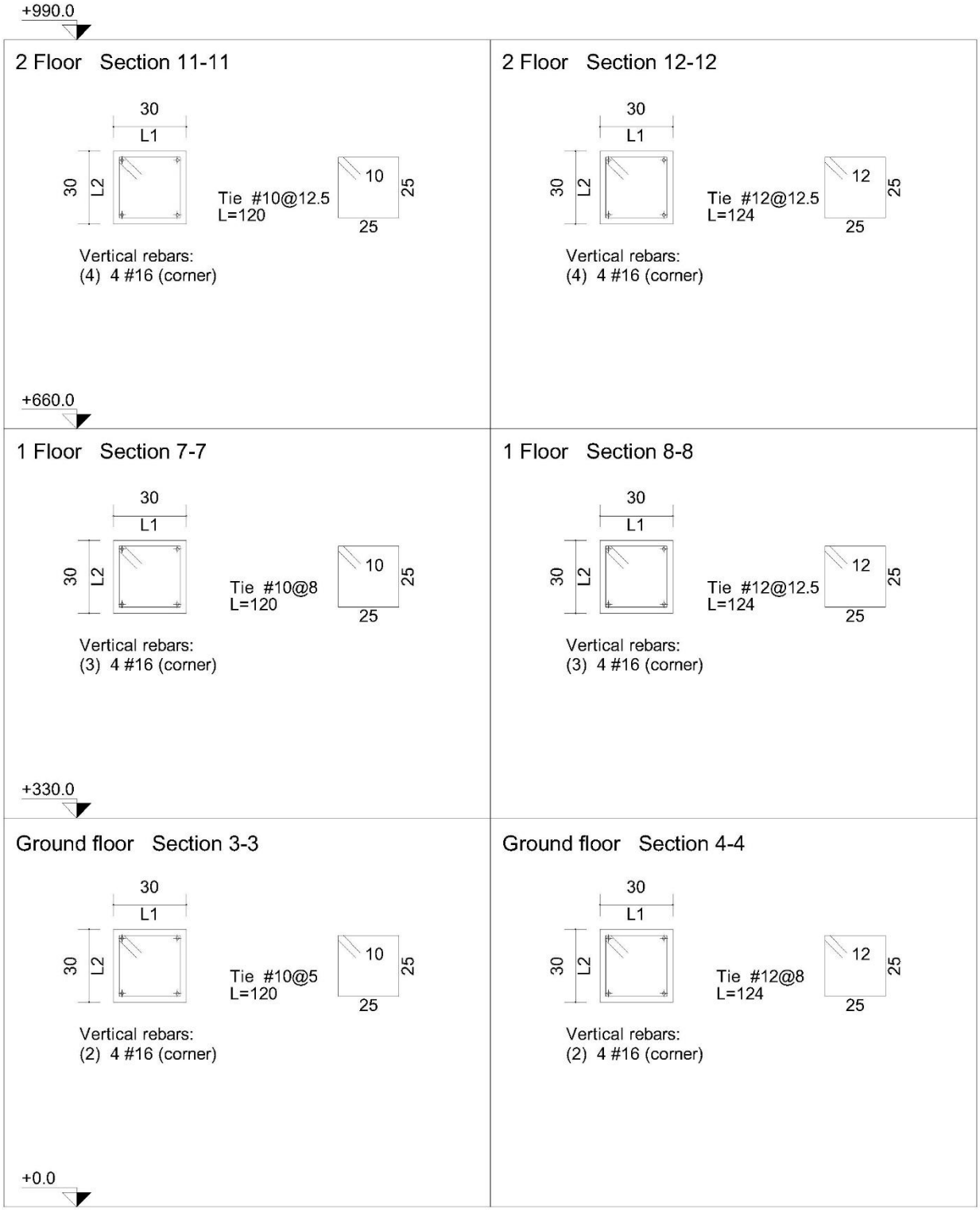
Scale 1:20



Pillars: 1, 2, 3, 4, 5, 6, 7, 8, 9, 10, 11, 12, 13, 14, 15, 16

Figure 4.10 Column reinforcement layout

Scale 1:20



Pillars: 1, 2, 3, 4, 5, 6, 7, 8, 9, 10, 11, 12, 13, 14, 15, 16

Figure 4.11 Column reinforcement layout

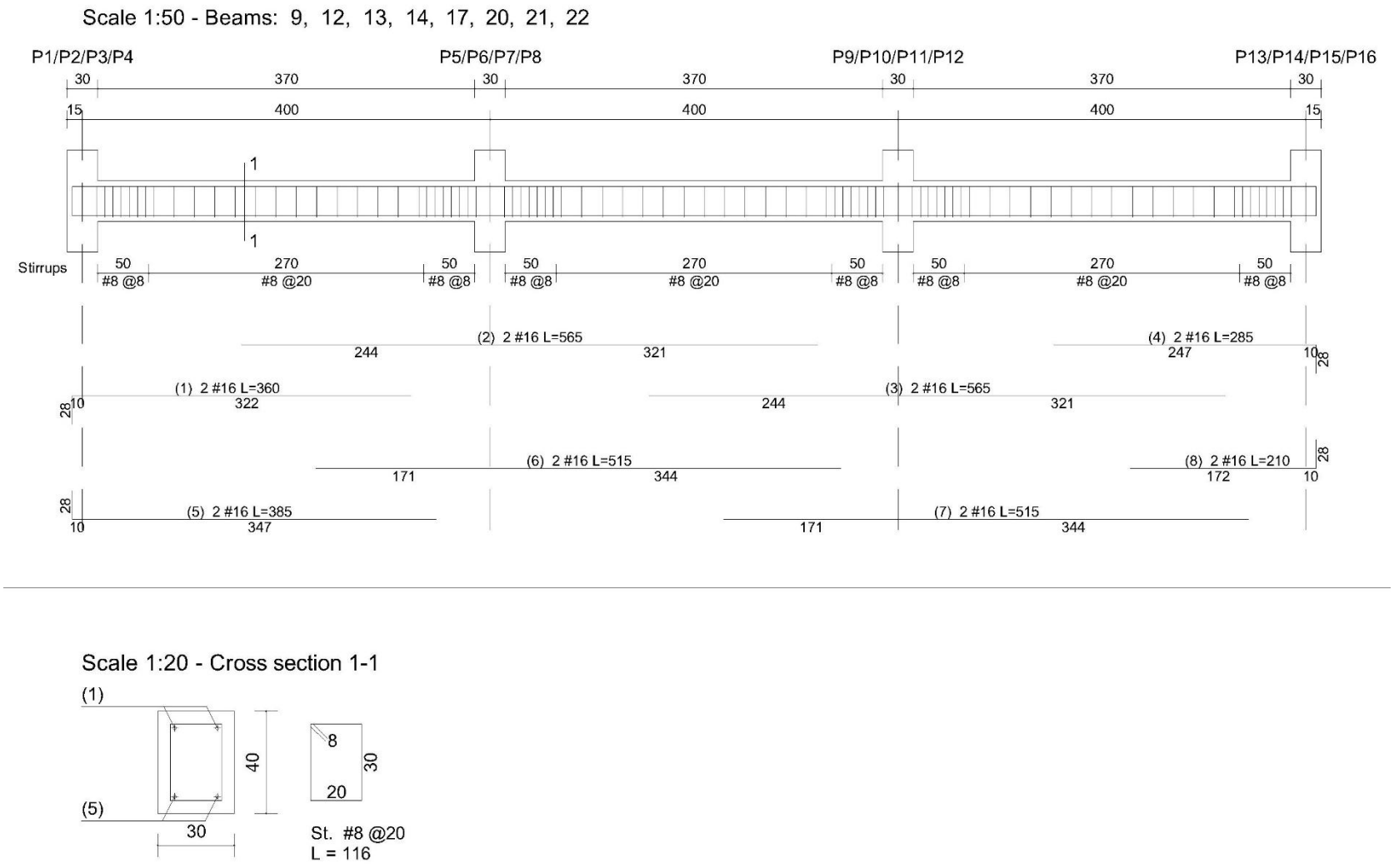


Figure 4.12 Beam reinforcement layout

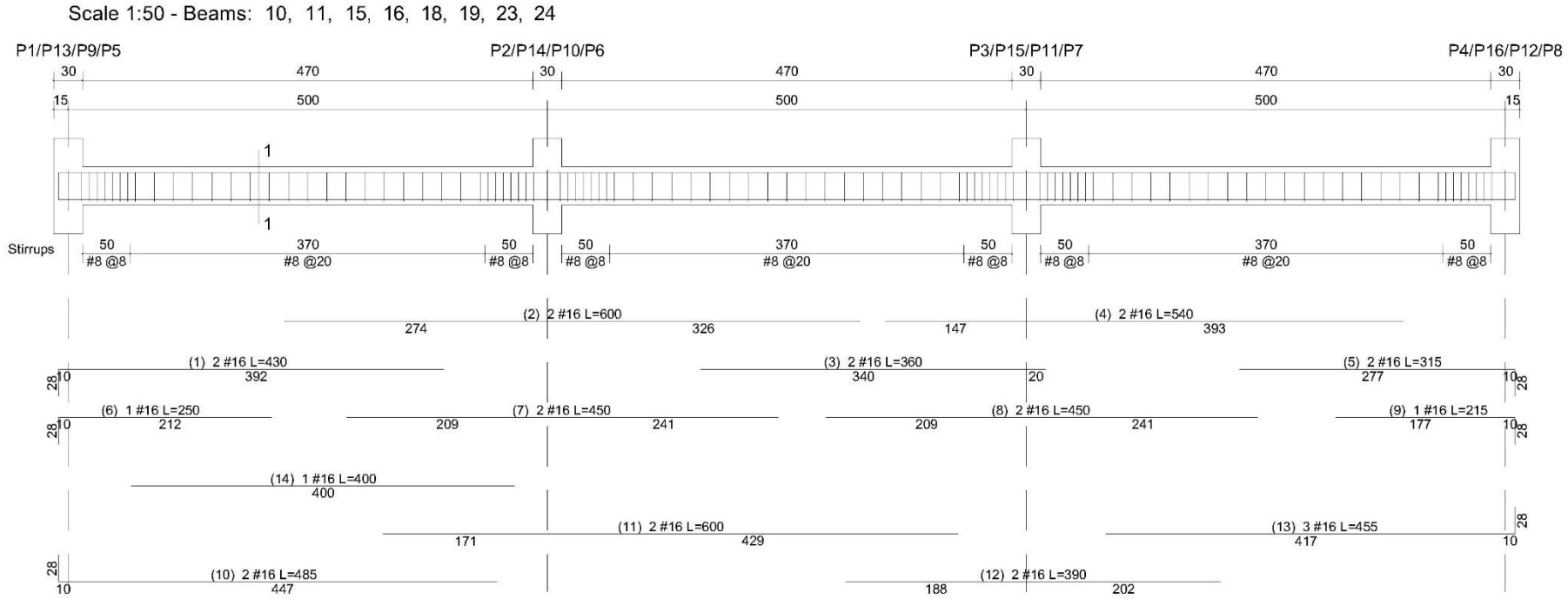
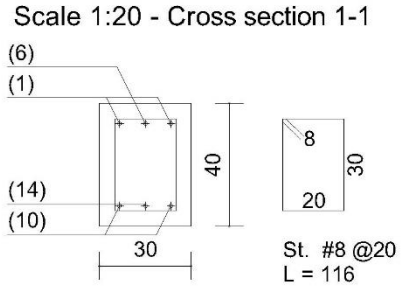
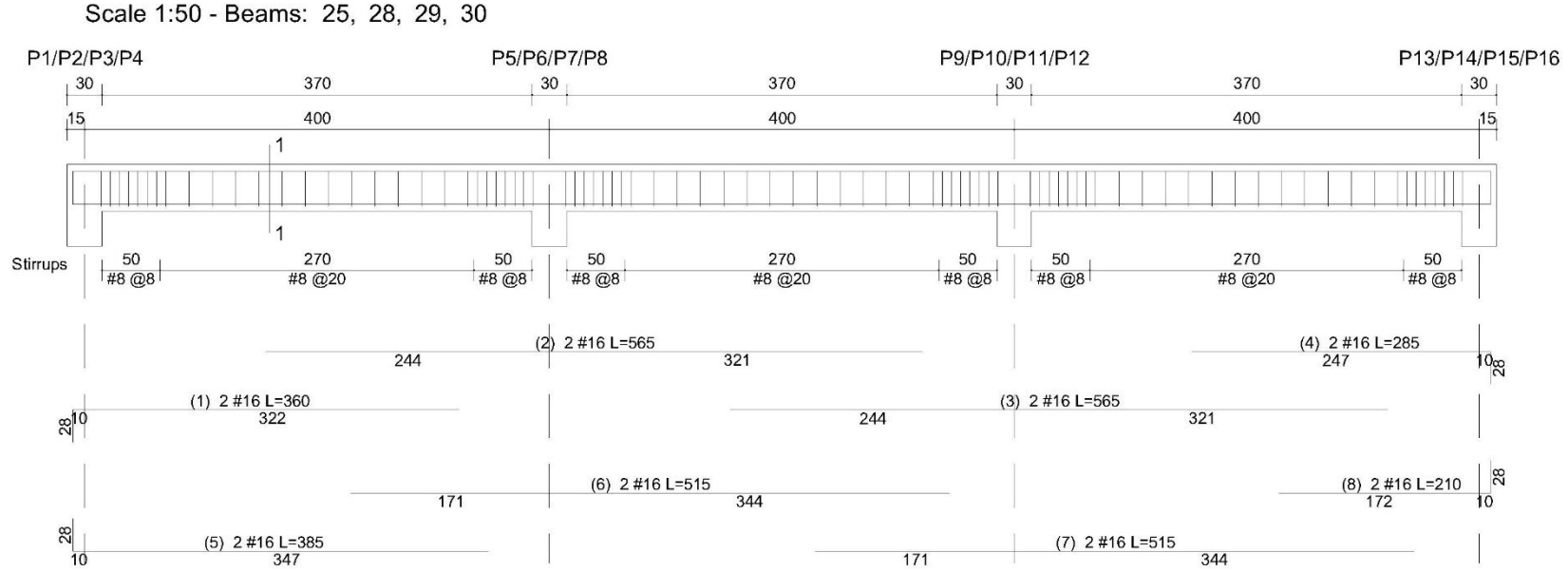


Figure 4.13 Beam reinforcement layout





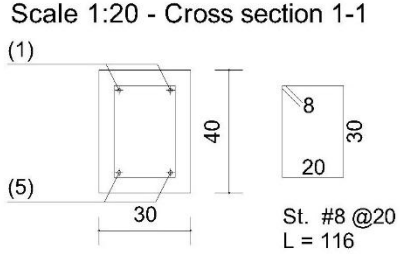


Figure 4.14 Beam reinforcement layout

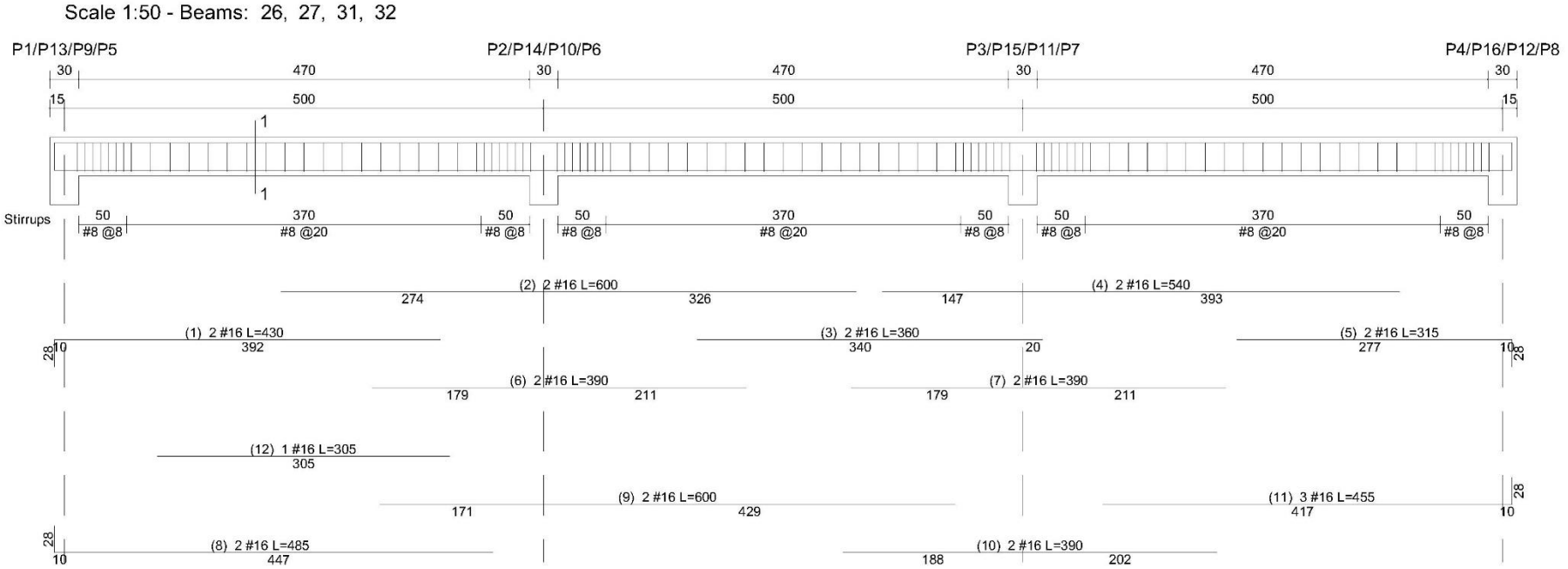
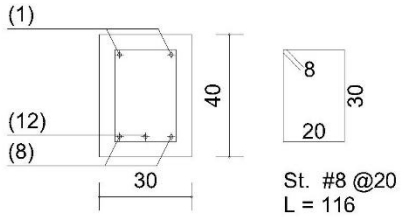


Figure 4.15 Beam reinforcement layout

Scale 1:20 - Cross section 1-1



4.3 Design of the structure located in L'Aquila

The same design and verification procedure previously described for the structure located in Turin is applied to the case study developed for the city of L'Aquila. Since the adopted methodology, modelling approach, and verification criteria remain substantially unchanged, only the most relevant design parameters and analysis results are presented in the following paragraphs. Detailed descriptions of each individual step and calculation are therefore omitted in order to avoid unnecessary repetition and to focus on the aspects that are most significant for the present case study. (Figure 4.16)

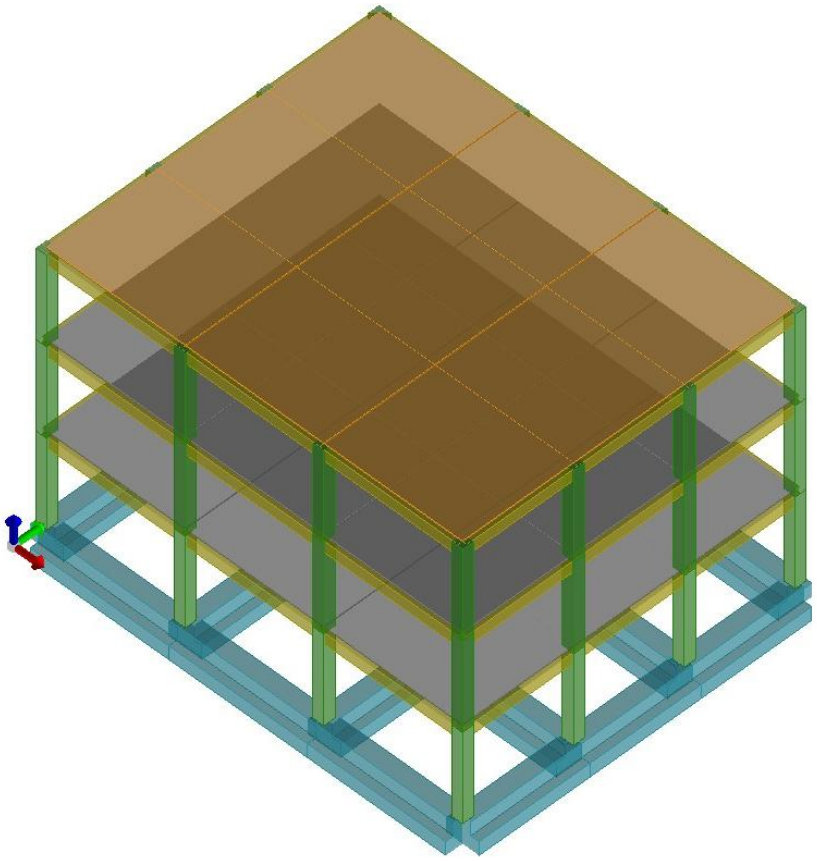


Figure 4.16 Structure located in L'Aquila

4.3.1 PROPERTIES OF STRUCTURAL ELEMENTS USED

The following table summarizes the main geometric and mechanical properties of the cross-sections adopted for the structural elements. In particular, the table reports the cross-sectional area, torsional and bending inertias, as well as the section moduli about the principal axes. The properties are provided for the different structural elements, including beams, columns, and foundations.

Id	Type	Area	A V2	A V3	Jt	J 2-2	J 3-3	W 2-2	W 3-3
		cm2	*cm2*	*cm2*	*cm4*	*cm4*	*cm4*	*cm3*	*cm3*
13	T: bi=12.00 ht=24.00 bs=50.00 hs=4.00	440.00	0.0	0.0	1.048e+04	4.455e+04	2.398e+04	1781.87	1551.37
17	Column Rettangular: b=40 h=40	1600.00	1333.33	1333.33	3.599e+05	2.133e+05	2.133e+05	1.067e+04	1.067e+04
18	Foundation Reverse T: bi=120	9000.00	0.0	0.0	8.166e+06	8.100e+06	6.875e+06	1.350e+05	1.179e+05

Id	Type	Area	A V2	A V3	Jt	J 2-2	J 3-3	W 2-2	W 3-3
		cm2	*cm2*	*cm2*	*cm4*	*cm4*	*cm4*	*cm3*	*cm3*
	ht=100 bs=60 hi=50								
19	Beam Rettangular: b=30 h=40	1200.00	1000.00	1000.00	1.946e+05	9.000e+04	1.600e+05	6000.00	8000.00

Table 4.36 Geometric and section properties of structural elements

4.3.2 LOAD CASE SCHEMATIZATION

- ***Snow load calculation:***
  The snow load on roofs is calculated based on the following parameters:
  - Zone: macro area resulting from the subdivision of the national territory;
  - Exp.: topographical area exposed to wind;
  - Ce: wind exposure coefficient;
  - TR: design return period expressed in years;
  - as: site altitude;
  - qsk: characteristic value of snow load on the ground (for Tr = 50 years);

Zone	Exposure	Ce	TR	as	qsk
Alpine II	Normal zone	1,00	50 years	714 m	279,29

Table 4.37 Snow load

Considering the parameters reported above, the snow load is: Qnk = 2.18 kN/mq

- ***Wind load calculation:***
  Wind velocity is calculated with reference to the following parameters:
  - Zone: macro-area derived from the subdivision of the national territory (NTC – Table 3.3.I);
  - Vb,0: basic wind velocity of the zone (NTC – Table 3.3.I);
  - a0: base altitude of the zone (NTC – Table 3.3.I);
  - ks: parameter depending on the zone where the structure is located (NTC – Table 3.3.I);
  - as: site altitude;
  - TR: design return period expressed in years;
  - Vb: reference wind velocity calculated as follows:
    $Vb = Vb,0 \quad for \quad as \leq a0$
    $Vb = Vb,0 \cdot [1 + ks\,((as / a0) - 1)] \quad for \quad a0 < as \leq 1500\ m$
    for as > 1500 m, values shall be obtained from appropriate documentation or proven investigations; such values shall not be lower than those prescribed for as = 1500 m;
  - Cr: return coefficient as a function of the return period TR;
  - Vr: reference wind velocity corresponding to the return period TR.

Zone	Vb,0	a0	ks	as	TR	Vb	Cr	Vr
3	27 m/s	500 m	0,37	714 m	50 years	31,28 m/s	1,000	31,28 m/s

Table 4.38 Wind load

Reference dynamic pressure

$$q_r = \frac{\rho V_r^2}{2} = 0.61\ kN/mq \tag{17}$$

where: ρ is the air density (conventionally assumed constant and equal to 1.25 kg/m³).

Exposure: Category V – Inland areas up to 750 m above sea level
From which the parameters of Table 3.3.II of the NTC are derived:

Kr	z0	zmin
0.23	0.70 m	12 m

Table 4.39

Terrain roughness class: A (NTC – Table 3.3.III)
Urban areas with at least 15% of the surface covered by buildings whose average height exceeds 15 m.

Wind action on structures is determined by the following parameters:

- Cp: pressure coefficient;
- Cd: dynamic coefficient;
- Ct: topographic coefficient;
- Ce: exposure coefficient (function of *z*, *z0* and *Ct*);
- z: height above ground level.

Cp	Cd	Ct	Ce	z
1.00	1.00	1.00	1.48	9.90 m

Table 4.40 Wind calculation parameters

Wind pressure:

$$p = q_r \, C_e \, C_p \, C_d = 0.90 \frac{kN}{mq} \tag{18}$$

4.3.3 SEISMIC ACTION EVALUATION

The seismic analysis was repeated for the same structural configuration assuming this different site location. Since the seismic input parameters vary according to the geographical area, the resulting seismic actions and design forces differ from those previously obtained. The updated seismic data are presented below.

Use class	Life Vn [year]	Use Coeff.	Period Vr [year]	Kind of soil	Kind of surface
II	50.0	1.0	50.0	B	T1

Table 4.41 Structure parameters

From the seismic hazard parameters the code computes:

- S factor for soil and kind of surface as: $S = S_s * S_t$
- F_0 maximum amplification factor for orizontal acceleration spectrum
- F_V maximum amplification factor for vertical acceleration spectrum
- T_B initial period for costant acceleration
- T_C initial period for costant velocity

- T_D initial period for costant displacement

The horizontal acceleration spectrum, S_e, is definied by the espressions below which are reproduced here for clarity:

$$0 \leq T < T_B \qquad S_e(T) = a_g * S * \eta * F_0 * \left[\frac{T}{T_B} + \frac{1}{\eta * F_0} * \left(1 - \frac{T}{T_B}\right)\right] \tag{4}$$

$$T_B \leq T < T_C \qquad S_e(T) = a_g * S * \eta * F_0 \tag{5}$$

$$T_C \leq T < T_D \qquad S_e(T) = a_g * S * \eta * F_0 * \left(\frac{T_C}{T}\right) \tag{6}$$

$$T_D \leq T \qquad S_e(T) = a_g * S * \eta * F_0 * \left(\frac{T_C * T_D}{T^2}\right) \tag{7}$$

Subsoil category	S_s	T_B	T_C	T_D
A, B, C, D, E	1,0	0,05 s	0,15 s	1,0 s

Table 4.42 Seismic spectrum parameters

LS	P_{ver}	T_r	a_g	F_0	$T * c$
		Years	*g*		*sec*
SLO	81.0	30.1	0.079	2.399	0.270
SLD	63.0	50.3	0.104	2.330	0.280
SLV	10.0	474.6	0.261	2.360	0.350
SLC	5.0	974.8	0.334	2.400	0.360

Table 4.43 Seismic parameters for the considered limit states

LS	a_g	S	F_0	F_v	T_B	T_C	T_D
	g				*sec*	*sec*	*sec*
SLO	0.079	1.200	2.399	0.910	0.129	0.386	1.916
SLD	0.104	1.200	2.330	1.015	0.132	0.397	2.017
SLV	0.261	1.154	2.360	1.626	0.158	0.475	2.642
SLC	0.334	1.079	2.400	1.872	0.162	0.486	2.936

Table 4.44 Seismic response spectrum parameters

Mode	**Frequency**	**Period**	**X effective M x g**	**%**	**Y effective M x g**	**%**	**Z effective M x g**	**%**	**RZ effective M x g**	**%**
	1/sec	*sec*	*kN*		*kN*		*kN*		*kN m*	
1	1.74	0.58	4752.00	86	0.0	0	0.0	0	0.0	0
2	1.77	0.57	0.0	0	4764.00	86	0.0	0	0.0	0
3	2.19	0.46	0.0	0	0.0	0	0.0	0	1940.00	87
4	5.97	0.17	632.00	11	0.0	0	0.0	0	0.0	0
5	6.16	0.16	0.0	0	6294.00	11	0.0	0	0.0	0
6	6.99	0.14	1.73e-06	0	1.07e-07	0	0.0	0	228.00	10

Table 4.45 Modal properties of the structure

4.3.4 LEGEND OF SEISMIC ANALYSIS RESULTS

The structure is classified as a new building with regularity both in plan and in height. The adopted ductility class is CD "B". The structural system is made of reinforced concrete and consists of frame structures, coupled wall structures, and mixed systems. The αu/α1 ratio has been defined according to the value specified by the applicable code provisions, with reference to multi-storey and multi-bay frame structures

a_u/a_1	1.300
$q_0 = 3.000\ a_u/a_1$	3.900
k_w	1.000
K_R	1.0
$q_D = q_0 \bullet k_w \bullet K_R$	3.900

Table 4.46 Seismic behavior factor parameters

	Dissipative
q SLU x	3.900
q SLU y	3.900
q SLU z	1.500

Table 4.47 Behaviour factors for ULS

4.3.5 VERIFICATION OF REINFORCED CONCRETE BEAM AND COLUMN ELEMENTS

For the present case, the results obtained are reported below, adopting the same notation and verification criteria previously described. The column numbering corresponds to that shown in Figure 4.3, which refers to the structure located in Turin.

M_C = 1 X = 0.0 Y = 119.8									
Column	***Elevation***	***%Af***	***Slend. Ratio***	***Long. Reinf.***	***N/M check***	***S. N check***	***Stirrups***	***V/T check rc***	***V/T check steel***
	cm						L=cm		
13	0	1.27	0.41	4d18 2+2 d18	0.89	0.2	2+2d8/10 L=60	0.55	0.44
	165	1.27	0.41	4d18 2+2 d18	0.27	0.19	2+2d8/20 L=210	0.55	0.88
	330	1.27	0.41	4d18 2+2 d18	0.43	0.19	2+2d8/10 L=60	0.55	0.44
77	330	1.27	0.33	4d18 2+2 d18	0.47	0.12	2+2d8/12 L=62	0.52	0.51
	495	1.27	0.33	4d18 2+2 d18	0.06	0.12	2+2d8/20 L=205	0.52	0.82
	660	1.27	0.33	4d18 2+2 d18	0.56	0.11	2+2d8/12 L=62	0.52	0.51
117	660	1.27	0.23	4d18 2+2 d18	0.24	0.05	2+2d8/12 L=62	0.45	0.45
	825	1.27	0.23	4d18 2+2 d18	0.11	0.05	2+2d8/20 L=205	0.45	0.72
	990	1.27	0.23	4d18 2+2 d18	0.45	0.04	2+2d8/12 L=62	0.45	0.45
M_C = 2 X = 500.0 Y = 119.8									
Column	***Elevation***	***%Af***	***Slend. Ratio***	***Long. Reinf.***	***N/M check***	***Seis N check***	***Stirrups***	***V/T check rc***	***V/T check steel***
14	0	1.27	0.55	4d18 2+2 d18	0.86	0.3	2+2d8/5 L=55	0.57	0.24
	165	1.27	0.55	4d18 2+2 d18	0.2	0.29	2+2d8/20 L=220	0.57	0.94
	330	1.27	0.55	4d18 2+2 d18	0.52	0.29	2+2d8/5 L=55	0.57	0.24
78	330	1.27	0.45	4d18 2+2 d18	0.61	0.19	2+2d8/12 L=62	0.54	0.55

	495	1.27	0.45	4d18 2+2 d18	0.06	0.18	2+2d8/20 L=205	0.54	0.89
	660	1.27	0.45	4d18 2+2 d18	0.67	0.18	2+2d8/12 L=62	0.54	0.55
118	660	1.27	0.32	4d18 2+2 d18	0.36	0.08	2+2d8/12 L=62	0.45	0.47
	825	1.27	0.32	4d18 2+2 d18	0.1	0.08	2+2d8/20 L=205	0.45	0.76
	990	1.27	0.32	4d18 2+2 d18	0.56	0.08	2+2d8/12 L=62	0.45	0.47
M_C = 3 X = 1000.0 Y = 119.8									
Column	***Elevation***	***%Af***	***Slend. Ratio***	***Long. Reinf.***	***N/M check***	***Seis N check***	***Stirrups***	***V/T check rc***	***V/T check steel***
15	0	1.27	0.55	4d18 2+2 d18	0.86	0.3	2+2d8/5 L=55	0.57	0.24
	165	1.27	0.55	4d18 2+2 d18	0.2	0.29	2+2d8/20 L=220	0.57	0.94
	330	1.27	0.55	4d18 2+2 d18	0.52	0.29	2+2d8/5 L=55	0.57	0.24
79	330	1.27	0.45	4d18 2+2 d18	0.61	0.19	2+2d8/12 L=62	0.54	0.55
	495	1.27	0.45	4d18 2+2 d18	0.06	0.18	2+2d8/20 L=205	0.54	0.89
	660	1.27	0.45	4d18 2+2 d18	0.67	0.18	2+2d8/12 L=62	0.54	0.55
119	660	1.27	0.32	4d18 2+2 d18	0.36	0.08	2+2d8/12 L=62	0.45	0.47
	825	1.27	0.32	4d18 2+2 d18	0.1	0.08	2+2d8/20 L=205	0.45	0.76
	990	1.27	0.32	4d18 2+2 d18	0.56	0.08	2+2d8/12 L=62	0.45	0.47
M_C = 4 X = 1500.0 Y = 119.8									
Column	***Elevation***	***%Af***	***Slend. Ratio***	***Long. Reinf.***	***N/M check***	***Seis N check***	***Stirrups***	***V/T check rc***	***V/T check steel***
16	0	1.27	0.41	4d18 2+2 d18	0.89	0.2	2+2d8/10 L=60	0.55	0.44
	165	1.27	0.41	4d18 2+2 d18	0.27	0.19	2+2d8/20 L=210	0.55	0.88
	330	1.27	0.41	4d18 2+2 d18	0.43	0.19	2+2d8/10 L=60	0.55	0.44
80	330	1.27	0.33	4d18 2+2 d18	0.47	0.12	2+2d8/12 L=62	0.52	0.51
	495	1.27	0.33	4d18 2+2 d18	0.06	0.12	2+2d8/20 L=205	0.52	0.82
	660	1.27	0.33	4d18 2+2 d18	0.56	0.11	2+2d8/12 L=62	0.52	0.51
120	660	1.27	0.23	4d18 2+2 d18	0.24	0.05	2+2d8/12 L=62	0.45	0.45
	825	1.27	0.23	4d18 2+2 d18	0.11	0.05	2+2d8/20 L=205	0.45	0.72
	990	1.27	0.23	4d18 2+2 d18	0.45	0.04	2+2d8/12 L=62	0.45	0.45
M_C = 5 X = 0.0 Y = 519.8									
Column	***Elevation***	***%Af***	***Slend. Ratio***	***Long. Reinf.***	***N/M check***	***Seis N check***	***Stirrups***	***V/T check rc***	***V/T check steel***
9	0	1.27	0.53	4d18 2+2 d18	0.87	0.27	2+2d8/8 L=56	0.55	0.37
	165	1.27	0.53	4d18 2+2 d18	0.23	0.26	2+2d8/20 L=218	0.55	0.93
	330	1.27	0.53	4d18 2+2 d18	0.58	0.26	2+2d8/8 L=56	0.55	0.37
73	330	1.27	0.43	4d18 2+2 d18	0.69	0.17	2+2d8/12 L=62	0.53	0.54
	495	1.27	0.43	4d18 2+2 d18	0.06	0.17	2+2d8/20 L=205	0.53	0.87
	660	1.27	0.43	4d18 2+2 d18	0.74	0.16	2+2d8/12 L=62	0.53	0.54
113	660	1.27	0.31	4d18 2+2 d18	0.42	0.08	2+2d8/12 L=62	0.47	0.47
	825	1.27	0.31	4d18 2+2 d18	0.11	0.07	2+2d8/20 L=205	0.47	0.75
	990	1.27	0.31	4d18 2+2 d18	0.62	0.07	2+2d8/12 L=62	0.47	0.47
M_C = 6 X = 500.0 Y = 519.8									
Column	***Elevation***	***%Af***	***Slend. Ratio***	***Long. Reinf.***	***N/M check***	***Seis N check***	***Stirrups***	***V/T check rc***	***V/T check steel***
10	0	1.27	0.71	4d18 2+2 d18	0.74	0.39	2+2d8/5 L=55	0.49	0.24
	165	1.27	0.71	4d18 2+2 d18	0.16	0.38	2+2d8/20 L=220	0.49	0.97
	330	1.27	0.71	4d18 2+2 d18	0.48	0.38	2+2d8/5 L=55	0.49	0.24

74	330	1.27	0.58	4d18 2+2 d18	0.53	0.25	2+2d8/8 L=56	0.5	0.38
	495	1.27	0.58	4d18 2+2 d18	0.1	0.25	2+2d8/20 L=218	0.51	0.94
	660	1.27	0.58	4d18 2+2 d18	0.58	0.25	2+2d8/8 L=56	0.51	0.38
114	660	1.27	0.42	4d18 2+2 d18	0.33	0.12	2+2d8/12 L=62	0.44	0.5
	825	1.27	0.42	4d18 2+2 d18	0.08	0.12	2+2d8/20 L=205	0.44	0.8
	990	1.27	0.42	4d18 2+2 d18	0.47	0.11	2+2d8/12 L=62	0.44	0.5
M_C = 7 X = 1000.0 Y = 519.8									
Column	***Elevation***	***%Af***	***Slend. Ratio***	***Long. Reinf.***	***N/M check***	***Seis N check***	***Stirrups***	***V/T check rc***	***V/T check steel***
11	0	1.27	0.71	4d18 2+2 d18	0.74	0.39	2+2d8/5 L=55	0.49	0.24
	165	1.27	0.71	4d18 2+2 d18	0.16	0.38	2+2d8/20 L=220	0.49	0.97
	330	1.27	0.71	4d18 2+2 d18	0.48	0.38	2+2d8/5 L=55	0.49	0.24
75	330	1.27	0.58	4d18 2+2 d18	0.53	0.25	2+2d8/8 L=56	0.5	0.38
	495	1.27	0.58	4d18 2+2 d18	0.1	0.25	2+2d8/20 L=218	0.51	0.94
	660	1.27	0.58	4d18 2+2 d18	0.58	0.25	2+2d8/8 L=56	0.51	0.38
115	660	1.27	0.42	4d18 2+2 d18	0.33	0.12	2+2d8/12 L=62	0.44	0.5
	825	1.27	0.42	4d18 2+2 d18	0.08	0.12	2+2d8/20 L=205	0.44	0.8
	990	1.27	0.42	4d18 2+2 d18	0.47	0.11	2+2d8/12 L=62	0.44	0.5
M_C = 8 X = 1500.0 Y = 519.8									
Column	***Elevation***	***%Af***	***Slend. Ratio***	***Long. Reinf.***	***N/M check***	***Seis N check***	***Stirrups***	***V/T check rc***	***V/T check steel***
12	0	1.27	0.53	4d18 2+2 d18	0.87	0.27	2+2d8/8 L=56	0.55	0.37
	165	1.27	0.53	4d18 2+2 d18	0.23	0.26	2+2d8/20 L=218	0.55	0.93
	330	1.27	0.53	4d18 2+2 d18	0.58	0.26	2+2d8/8 L=56	0.55	0.37
76	330	1.27	0.43	4d18 2+2 d18	0.69	0.17	2+2d8/12 L=62	0.53	0.54
	495	1.27	0.43	4d18 2+2 d18	0.06	0.17	2+2d8/20 L=205	0.53	0.87
	660	1.27	0.43	4d18 2+2 d18	0.74	0.16	2+2d8/12 L=62	0.53	0.54
116	660	1.27	0.31	4d18 2+2 d18	0.42	0.08	2+2d8/12 L=62	0.47	0.47
	825	1.27	0.31	4d18 2+2 d18	0.11	0.07	2+2d8/20 L=205	0.47	0.75
	990	1.27	0.31	4d18 2+2 d18	0.62	0.07	2+2d8/12 L=62	0.47	0.47
M_C = 9 X = 0.0 Y = 919.8									
Column	***Elevation***	***%Af***	***Slend. Ratio***	***Long. Reinf.***	***N/M check***	***Seis N check***	***Stirrups***	***V/T check rc***	***V/T check steel***
5	0	1.27	0.53	4d18 2+2 d18	0.87	0.27	2+2d8/8 L=56	0.55	0.37
	165	1.27	0.53	4d18 2+2 d18	0.23	0.26	2+2d8/20 L=218	0.55	0.93
	330	1.27	0.53	4d18 2+2 d18	0.58	0.26	2+2d8/8 L=56	0.55	0.37
69	330	1.27	0.43	4d18 2+2 d18	0.69	0.17	2+2d8/12 L=62	0.53	0.54
	495	1.27	0.43	4d18 2+2 d18	0.06	0.17	2+2d8/20 L=205	0.53	0.87
	660	1.27	0.43	4d18 2+2 d18	0.74	0.16	2+2d8/12 L=62	0.53	0.54
109	660	1.27	0.31	4d18 2+2 d18	0.42	0.08	2+2d8/12 L=62	0.47	0.47
	825	1.27	0.31	4d18 2+2 d18	0.11	0.07	2+2d8/20 L=205	0.47	0.75
	990	1.27	0.31	4d18 2+2 d18	0.62	0.07	2+2d8/12 L=62	0.47	0.47
M_C = 10 X = 500.0 Y = 919.8									
Column	***Elevation***	***%Af***	***Slend. Ratio***	***Long. Reinf.***	***N/M check***	***Seis N check***	***Stirrups***	***V/T check rc***	***V/T check steel***
6	0	1.27	0.71	4d18 2+2 d18	0.74	0.39	2+2d8/5 L=55	0.49	0.24

	165	1.27	0.71	4d18 2+2 d18	0.16	0.38	2+2d8/20 L=220	0.49	0.97
	330	1.27	0.71	4d18 2+2 d18	0.48	0.38	2+2d8/5 L=55	0.49	0.24
70	330	1.27	0.58	4d18 2+2 d18	0.53	0.25	2+2d8/8 L=56	0.5	0.38
	495	1.27	0.58	4d18 2+2 d18	0.1	0.25	2+2d8/20 L=218	0.51	0.94
	660	1.27	0.58	4d18 2+2 d18	0.58	0.25	2+2d8/8 L=56	0.51	0.38
110	660	1.27	0.42	4d18 2+2 d18	0.33	0.12	2+2d8/12 L=62	0.44	0.5
	825	1.27	0.42	4d18 2+2 d18	0.08	0.12	2+2d8/20 L=205	0.44	0.8
	990	1.27	0.42	4d18 2+2 d18	0.47	0.11	2+2d8/12 L=62	0.44	0.5
M_C = 11 X = 1000.0 Y = 919.8									
Column	***Elevation***	***%Af***	***Slend. Ratio***	***Long. Reinf.***	***N/M check***	***Seis N check***	***Stirrups***	***V/T check rc***	***V/T check steel***
7	0	1.27	0.71	4d18 2+2 d18	0.74	0.39	2+2d8/5 L=55	0.49	0.24
	165	1.27	0.71	4d18 2+2 d18	0.16	0.38	2+2d8/20 L=220	0.49	0.97
	330	1.27	0.71	4d18 2+2 d18	0.48	0.38	2+2d8/5 L=55	0.49	0.24
71	330	1.27	0.58	4d18 2+2 d18	0.53	0.25	2+2d8/8 L=56	0.5	0.38
	495	1.27	0.58	4d18 2+2 d18	0.1	0.25	2+2d8/20 L=218	0.51	0.94
	660	1.27	0.58	4d18 2+2 d18	0.58	0.25	2+2d8/8 L=56	0.51	0.38
111	660	1.27	0.42	4d18 2+2 d18	0.33	0.12	2+2d8/12 L=62	0.44	0.5
	825	1.27	0.42	4d18 2+2 d18	0.08	0.12	2+2d8/20 L=205	0.44	0.8
	990	1.27	0.42	4d18 2+2 d18	0.47	0.11	2+2d8/12 L=62	0.44	0.5
M_C = 12 X = 1500.0 Y = 919.8									
Column	***Elevation***	***%Af***	***Slend. Ratio***	***Long. Reinf.***	***N/M check***	***Seis N check***	***Stirrups***	***V/T check rc***	***V/T check steel***
8	0	1.27	0.53	4d18 2+2 d18	0.87	0.27	2+2d8/8 L=56	0.55	0.37
	165	1.27	0.53	4d18 2+2 d18	0.23	0.26	2+2d8/20 L=218	0.55	0.93
	330	1.27	0.53	4d18 2+2 d18	0.58	0.26	2+2d8/8 L=56	0.55	0.37
72	330	1.27	0.43	4d18 2+2 d18	0.69	0.17	2+2d8/12 L=62	0.53	0.54
	495	1.27	0.43	4d18 2+2 d18	0.06	0.17	2+2d8/20 L=205	0.53	0.87
	660	1.27	0.43	4d18 2+2 d18	0.74	0.16	2+2d8/12 L=62	0.53	0.54
112	660	1.27	0.31	4d18 2+2 d18	0.42	0.08	2+2d8/12 L=62	0.47	0.47
	825	1.27	0.31	4d18 2+2 d18	0.11	0.07	2+2d8/20 L=205	0.47	0.75
	990	1.27	0.31	4d18 2+2 d18	0.62	0.07	2+2d8/12 L=62	0.47	0.47
M_C = 13 X = 0.0 Y = 1319.8									
Column	***Elevation***	***%Af***	***Slend. Ratio***	***Long. Reinf.***	***N/M check***	***Seis N check***	***Stirrups***	***V/T check rc***	***V/T check steel***
1	0	1.27	0.41	4d18 2+2 d18	0.89	0.2	2+2d8/10 L=60	0.55	0.44
	165	1.27	0.41	4d18 2+2 d18	0.27	0.19	2+2d8/20 L=210	0.55	0.88
	330	1.27	0.41	4d18 2+2 d18	0.43	0.19	2+2d8/10 L=60	0.55	0.44
65	330	1.27	0.33	4d18 2+2 d18	0.47	0.12	2+2d8/12 L=62	0.52	0.51
	495	1.27	0.33	4d18 2+2 d18	0.06	0.12	2+2d8/20 L=205	0.52	0.82
	660	1.27	0.33	4d18 2+2 d18	0.56	0.11	2+2d8/12 L=62	0.52	0.51
105	660	1.27	0.23	4d18 2+2 d18	0.23	0.05	2+2d8/12 L=62	0.45	0.45
	825	1.27	0.23	4d18 2+2 d18	0.11	0.05	2+2d8/20 L=205	0.45	0.72
	990	1.27	0.23	4d18 2+2 d18	0.45	0.04	2+2d8/12 L=62	0.45	0.45
M_C = 14 X = 500.0 Y = 1319.8									
Column	***Elevation***	***%Af***	***Slend. Ratio***	***Long. Reinf.***	***N/M check***	***Seis N check***	***Stirrups***	***V/T check rc***	***V/T check steel***

2	0	1.27	0.55	4d18 2+2 d18	0.86	0.3	2+2d8/5 L=55	0.57	0.24
	165	1.27	0.55	4d18 2+2 d18	0.2	0.29	2+2d8/20 L=220	0.57	0.94
	330	1.27	0.55	4d18 2+2 d18	0.52	0.29	2+2d8/5 L=55	0.57	0.24
66	330	1.27	0.45	4d18 2+2 d18	0.61	0.19	2+2d8/12 L=62	0.54	0.55
	495	1.27	0.45	4d18 2+2 d18	0.06	0.18	2+2d8/20 L=205	0.54	0.89
	660	1.27	0.45	4d18 2+2 d18	0.67	0.18	2+2d8/12 L=62	0.54	0.55
106	660	1.27	0.32	4d18 2+2 d18	0.36	0.08	2+2d8/12 L=62	0.45	0.47
	825	1.27	0.32	4d18 2+2 d18	0.1	0.08	2+2d8/20 L=205	0.45	0.76
	990	1.27	0.32	4d18 2+2 d18	0.56	0.08	2+2d8/12 L=62	0.45	0.47
M_C = 15 X = 1000.0 Y = 1319.8									
Column	***Elevation***	***%Af***	***Slend. Ratio***	***Long. Reinf.***	***N/M check***	***Seis N check***	***Stirrups***	***V/T check rc***	***V/T check steel***
3	0	1.27	0.55	4d18 2+2 d18	0.86	0.3	2+2d8/5 L=55	0.57	0.24
	165	1.27	0.55	4d18 2+2 d18	0.2	0.29	2+2d8/20 L=220	0.57	0.94
	330	1.27	0.55	4d18 2+2 d18	0.52	0.29	2+2d8/5 L=55	0.57	0.24
67	330	1.27	0.45	4d18 2+2 d18	0.61	0.19	2+2d8/12 L=62	0.54	0.55
	495	1.27	0.45	4d18 2+2 d18	0.06	0.18	2+2d8/20 L=205	0.54	0.89
	660	1.27	0.45	4d18 2+2 d18	0.67	0.18	2+2d8/12 L=62	0.54	0.55
107	660	1.27	0.32	4d18 2+2 d18	0.36	0.08	2+2d8/12 L=62	0.45	0.47
	825	1.27	0.32	4d18 2+2 d18	0.1	0.08	2+2d8/20 L=205	0.45	0.76
	990	1.27	0.32	4d18 2+2 d18	0.56	0.08	2+2d8/12 L=62	0.45	0.47
M_C = 16 X = 1500.0 Y = 1319.8									
Column	***Elevation***	***%Af***	***Slend. Ratio***	***Long. Reinf.***	***N/M check***	***Seis N check***	***Stirrups***	***V/T check rc***	***V/T check steel***
4	0	1.27	0.41	4d18 2+2 d18	0.89	0.2	2+2d8/10 L=60	0.55	0.44
	165	1.27	0.41	4d18 2+2 d18	0.27	0.19	2+2d8/20 L=210	0.55	0.88
	330	1.27	0.41	4d18 2+2 d18	0.43	0.19	2+2d8/10 L=60	0.55	0.44
68	330	1.27	0.33	4d18 2+2 d18	0.47	0.12	2+2d8/12 L=62	0.52	0.51
	495	1.27	0.33	4d18 2+2 d18	0.06	0.12	2+2d8/20 L=205	0.52	0.82
	660	1.27	0.33	4d18 2+2 d18	0.56	0.11	2+2d8/12 L=62	0.52	0.51
108	660	1.27	0.23	4d18 2+2 d18	0.23	0.05	2+2d8/12 L=62	0.45	0.45
	825	1.27	0.23	4d18 2+2 d18	0.11	0.05	2+2d8/20 L=205	0.45	0.72
	990	1.27	0.23	4d18 2+2 d18	0.45	0.04	2+2d8/12 L=62	0.45	0.45

Table 4.48 Columns properties

Column	***%Af***	***Slend. Ratio***	***N/M check***	***Seis N check***	***V/T check rc***	***V/T check steel***
	1.27	0.71	0.89	0.39	0.57	0.97

Table 4.49 Maximum values of columns verifications

The figures below graphically represent the results presented in the tables above.

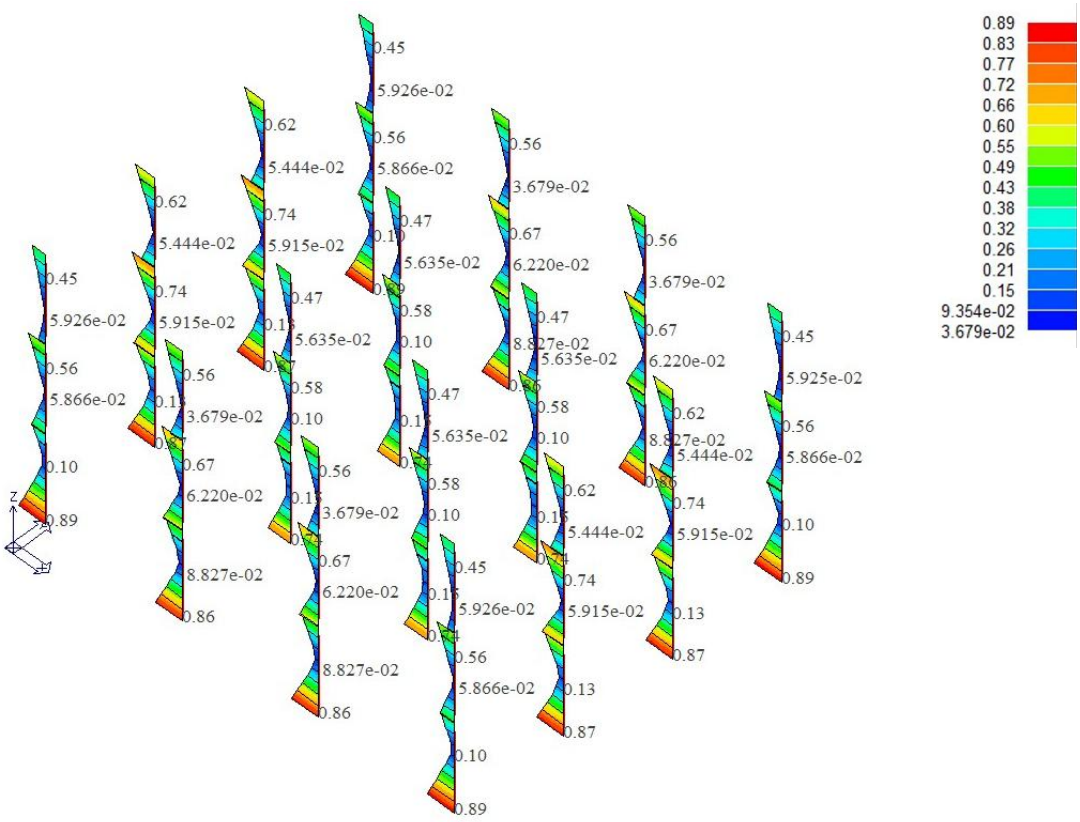


Figure 4.17 Check N/M

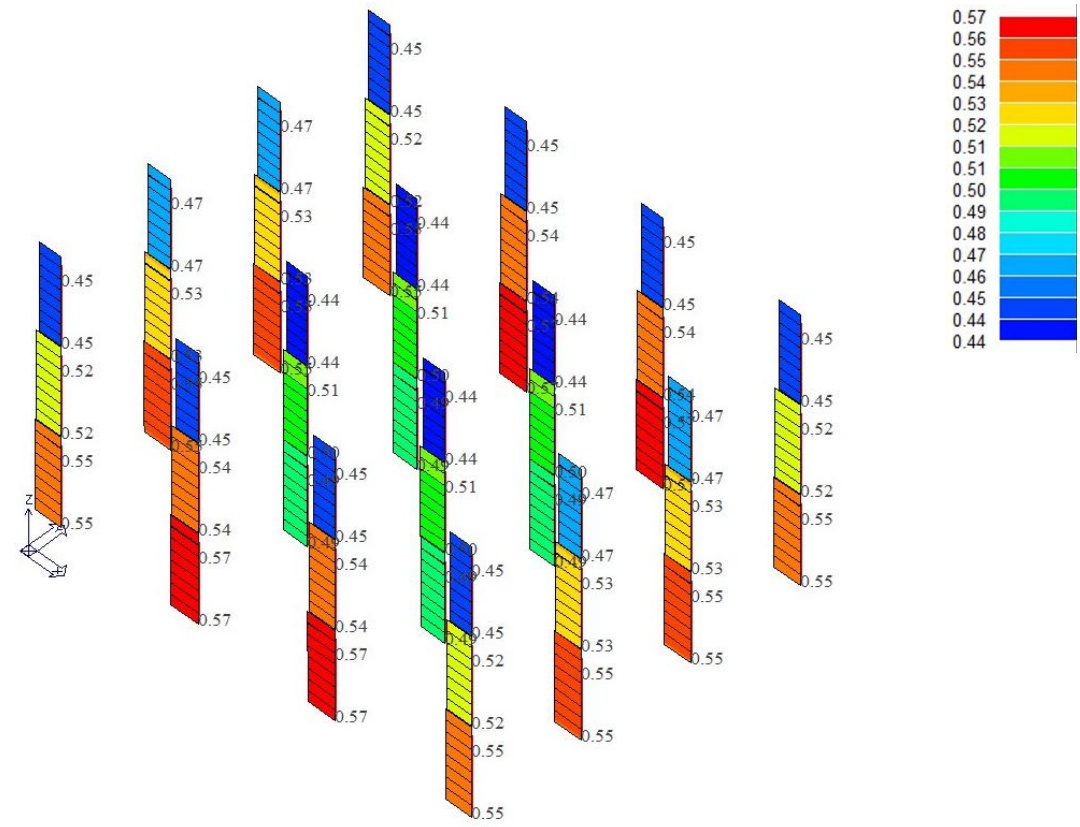


Figure 4.18 Check V/T concrete

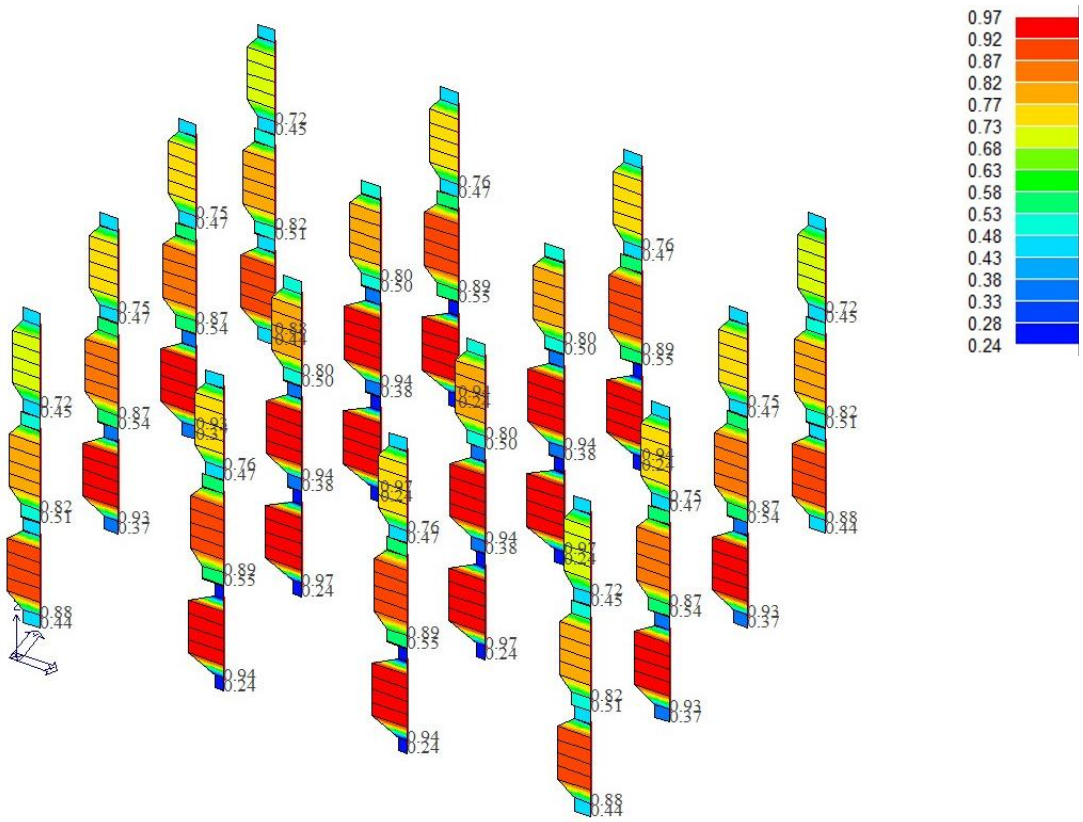


Figure 4.19 Check V/T steel

For beam checks, only the maximum values for each item described above are reported, as the table is conceptually the same as that for columns.

Similar to the latter, beams are also characterised by three D2 elements, for a total of 24 beams and 72 D2 elements.

Beam	***%Af***	***Af bot.***	***Af. top***	***Af long.***	***x/d***	***N/M check***	***V/T cls check***	***V/T st. check***
	1.05	28.27	28.27	0.0	0.31	0.95	0.57	0.51

Table 4.50 Maximum values of beams verifications

For column and beam capacity design checks, here are reported only the maximum values of the actions.

Column	$M_{2-2,i}$	$M_{2-2,f}$	$M_{3-3,i}$	$M_{3-3,f}$	V_{M2-2}	V_{M3-3}
	kN m	*kN m*	*kN m*	*kN m*	*kN*	*kN*
	185.79	185.20	185.79	185.20	140.72	140.72

Table 4.51 Column design resistance values

As shown in the figures below, the acting bending moments in both directions remain below the corresponding resisting bending moments, confirming that the structural capacity is not exceeded.

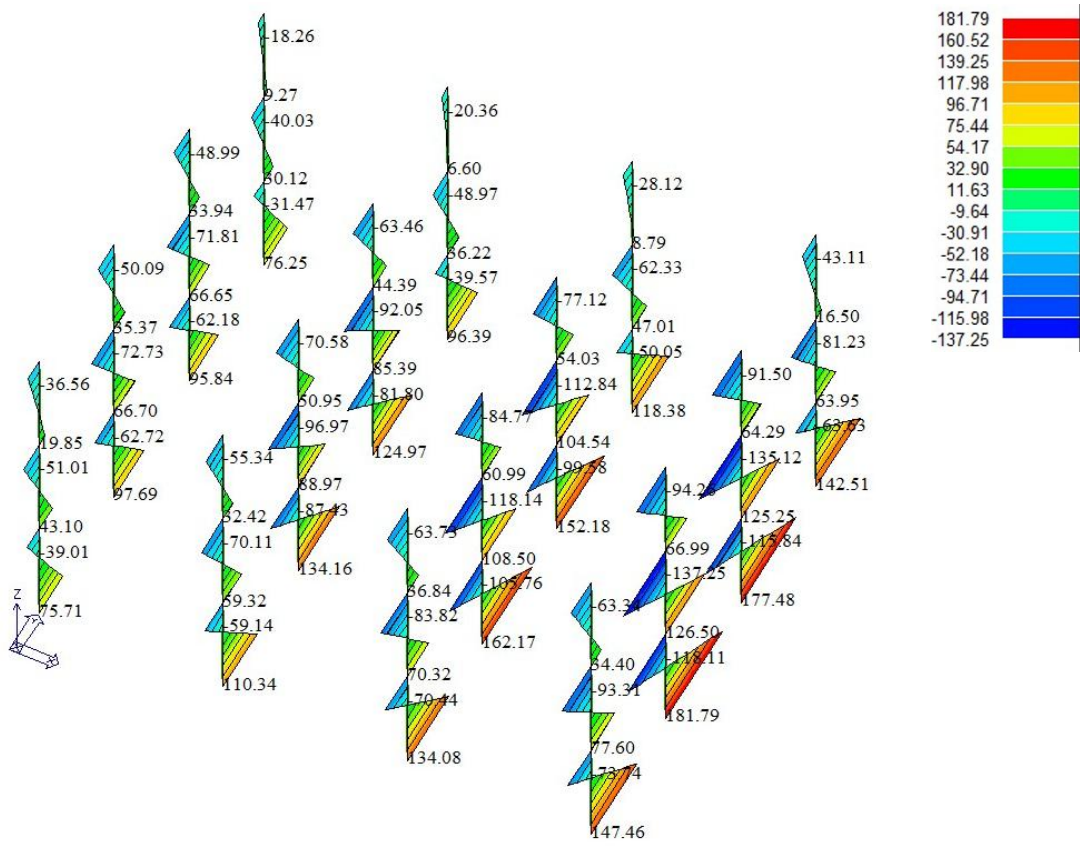


Figure 4.20 Maximum acting bending moment 2-2 [kN m] from combination ELS 66

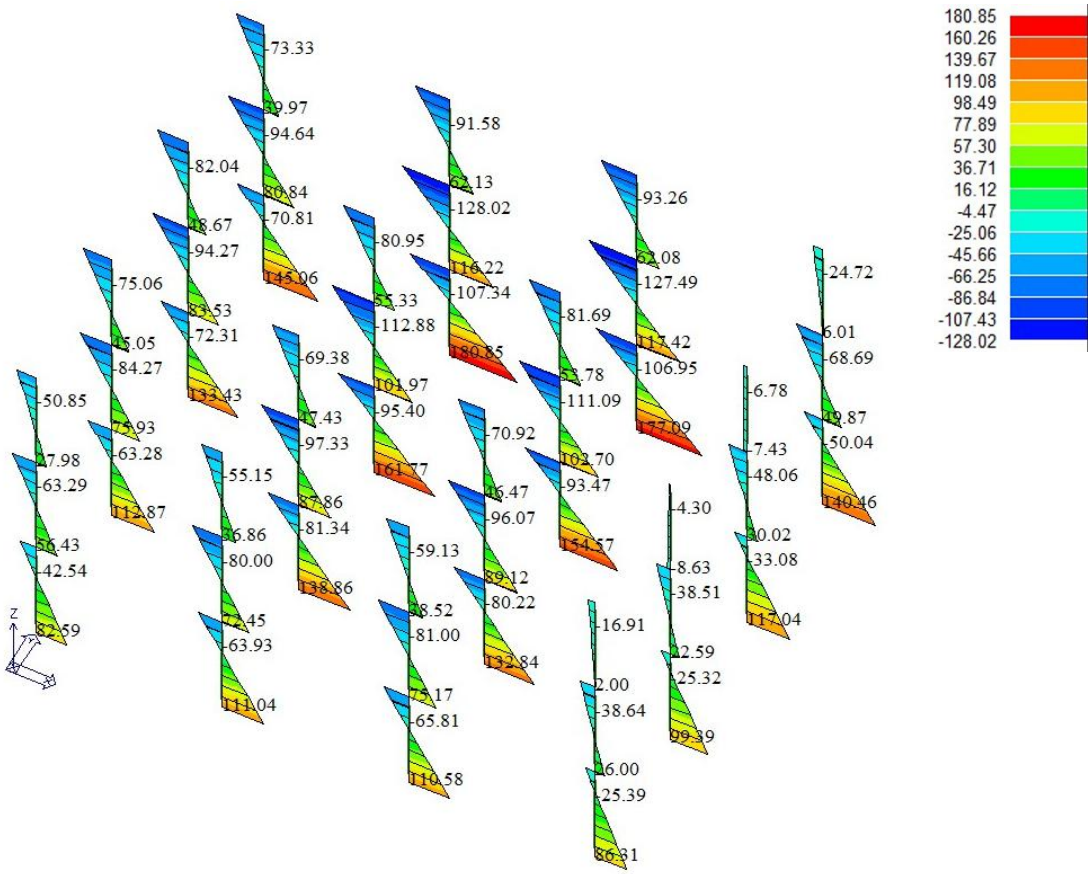


Figure 4.21 Maximum acting bending moment 3-3 [kN m] from combination ELS 62

Beam	M_i^-	M_i^+	M_f^-	M_f^+	$V_{M-i\,M+f}$	$V_{M+i\,M-f}$
	kN m	*kN m*	*kN m*	*kN m*	*kN*	*kN*
	138.00	107.00	139.00	107.00	75.07	75.07

Table 4.52 Beams design resistance values

For checks on beam-column joints in new elements, the following are the results obtained for the present case; the corresponding notation has been previously introduced.

Node	Step	7.4.8 Check	Ash check
	5.00	0.98	0.95

Table 4.53 Maximum values of nodes verifications

After the description of the structural elements, the corresponding drawings are presented, which allow a clearer understanding of their geometry and the arrangement of the reinforcement.

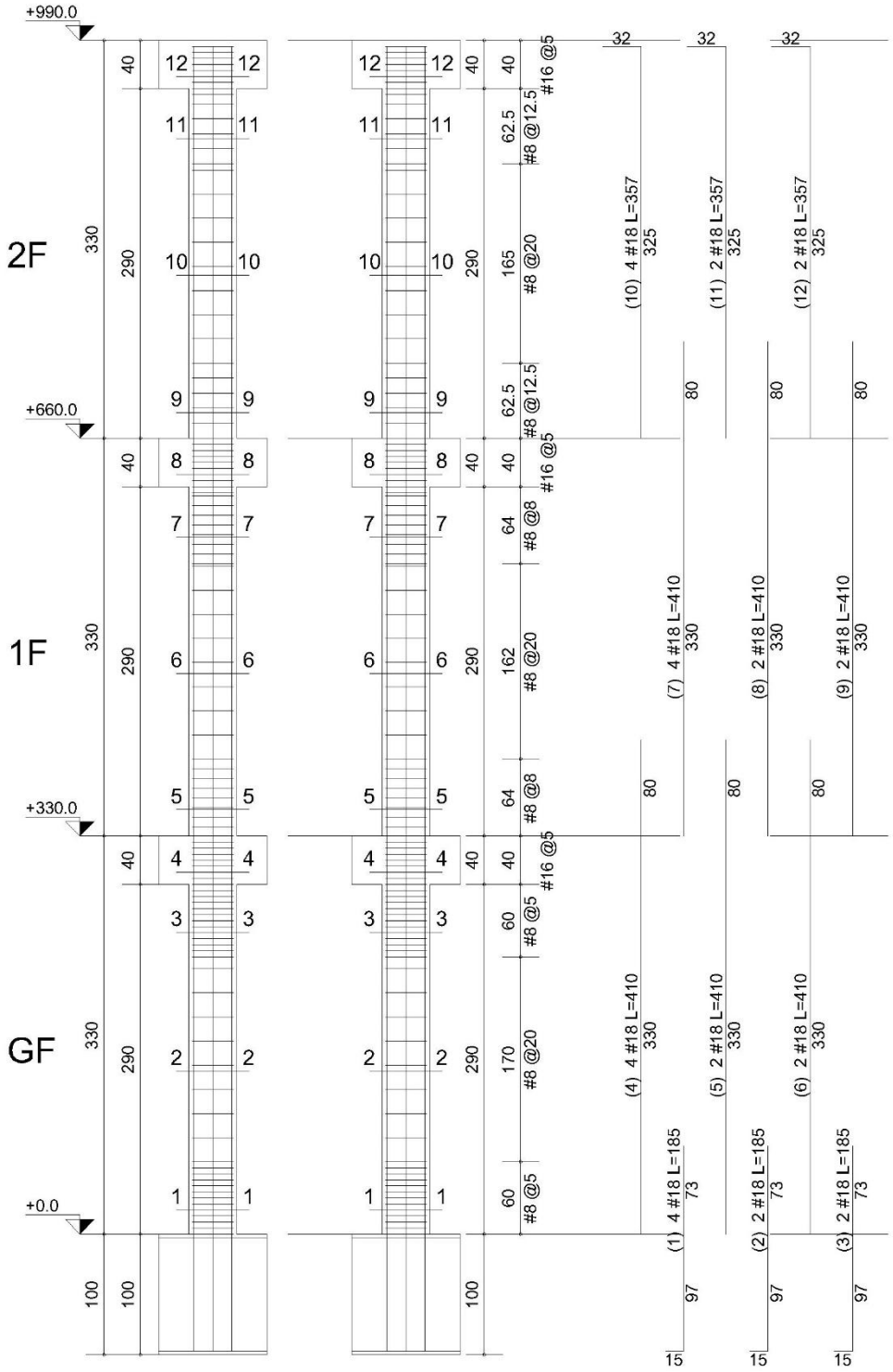
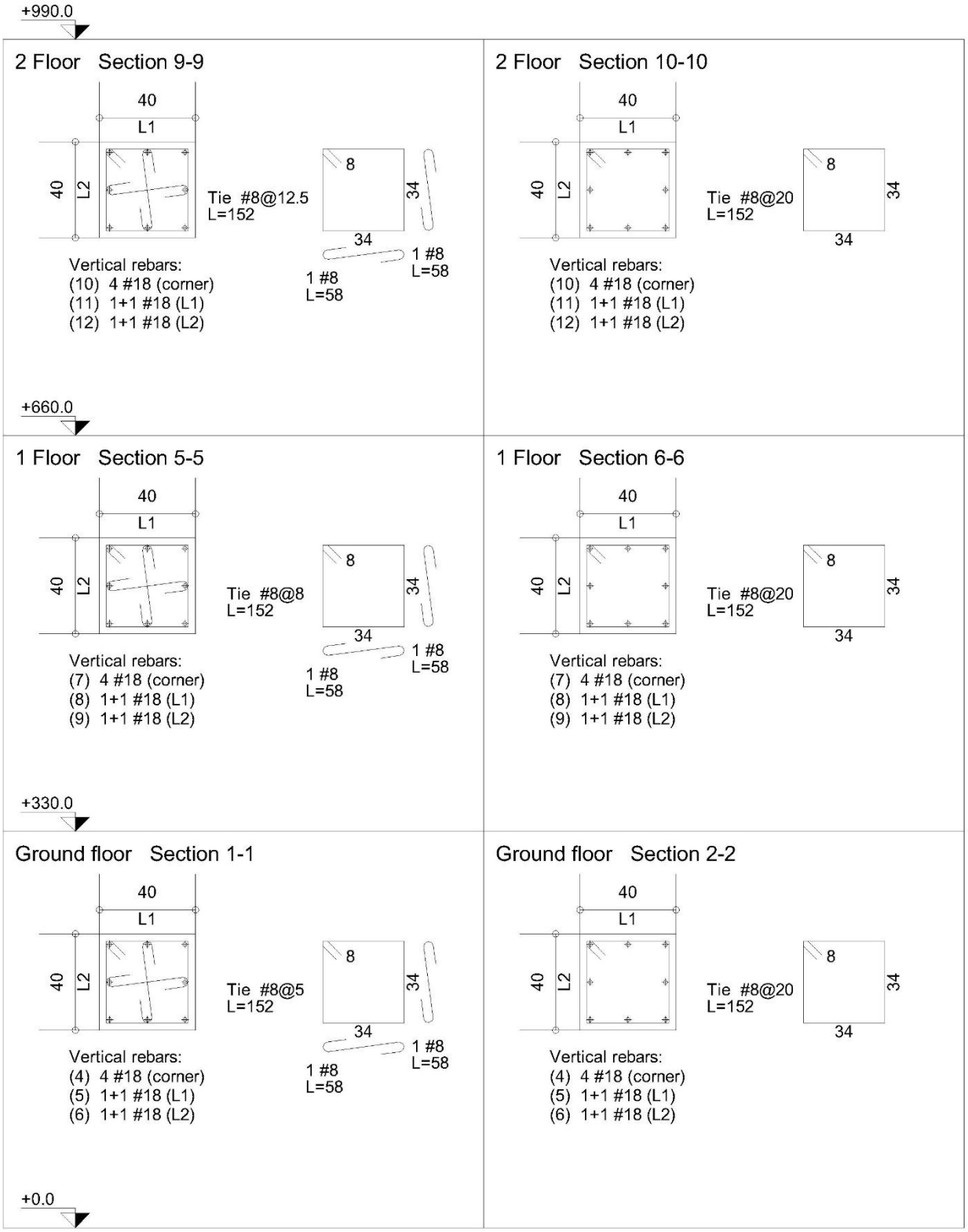


Figure 4.22 Column reinforcement layout

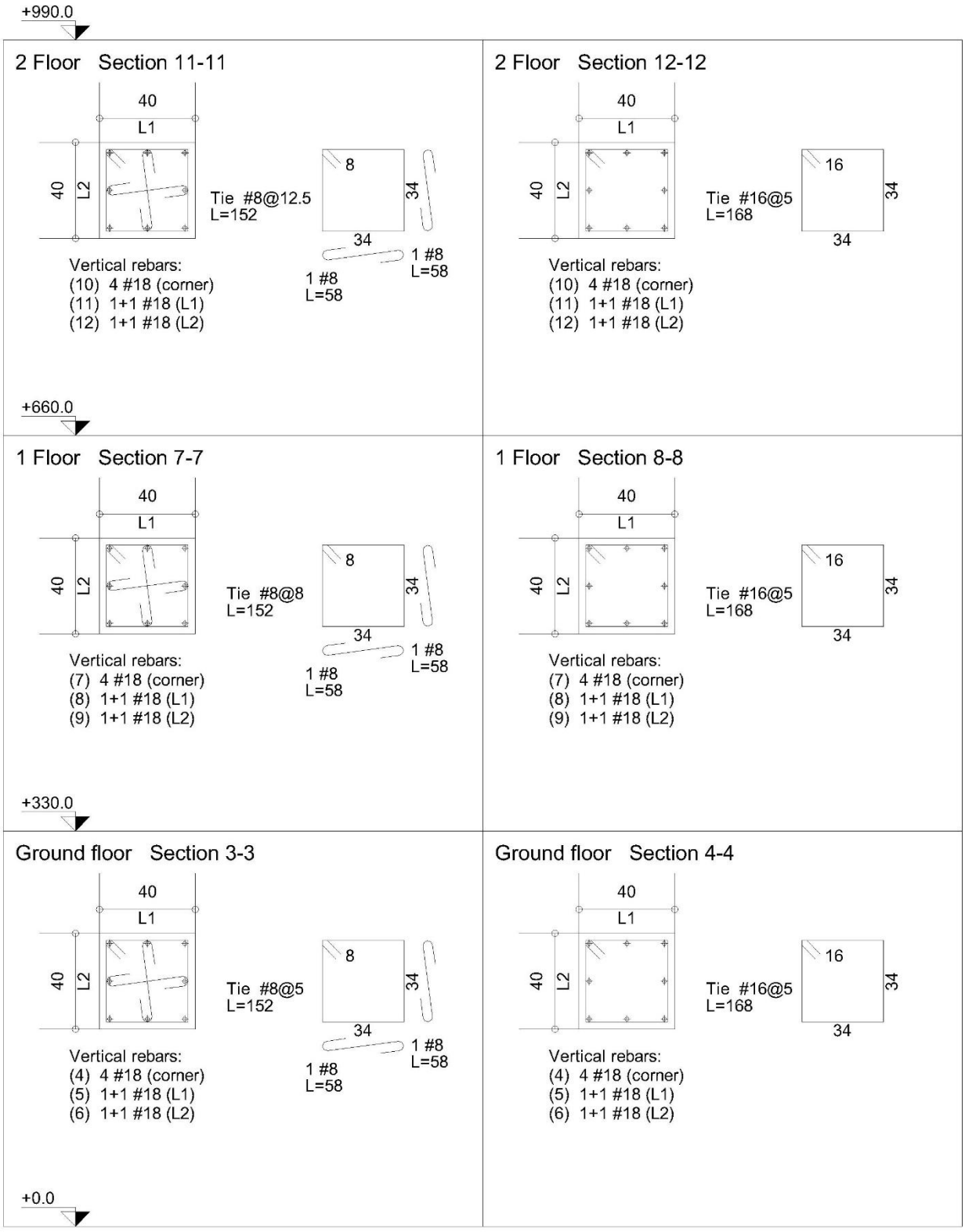
Scale 1:20



Pillars: 1, 2, 3, 4, 5, 6, 7, 8, 9, 10, 11, 12, 13, 14, 15, 16

Figure 4.23 Column reinforcement layout

Scale 1:20



Pillars: 1, 2, 3, 4, 5, 6, 7, 8, 9, 10, 11, 12, 13, 14, 15, 16

Figure 4.24 Column reinforcement layout

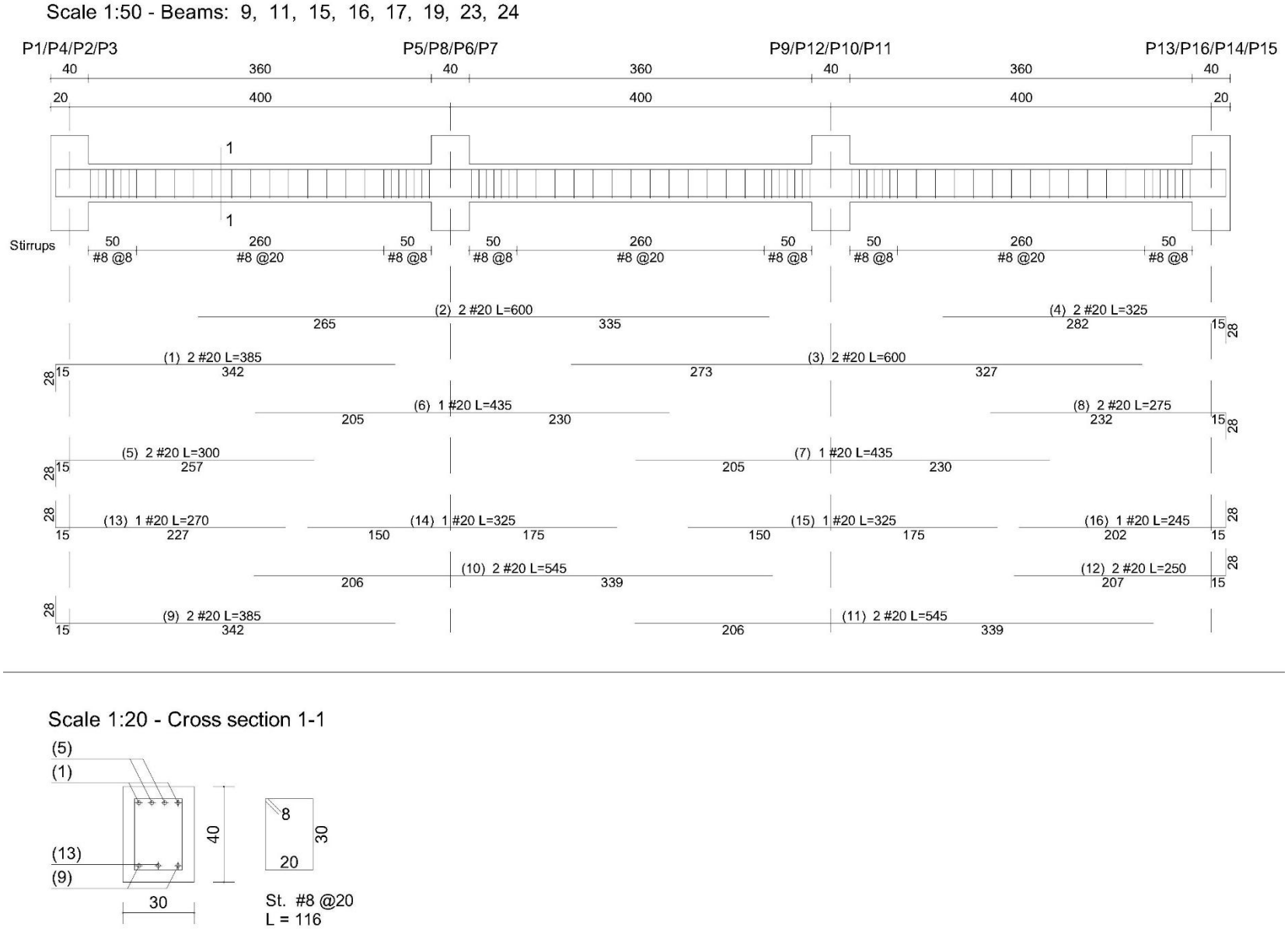
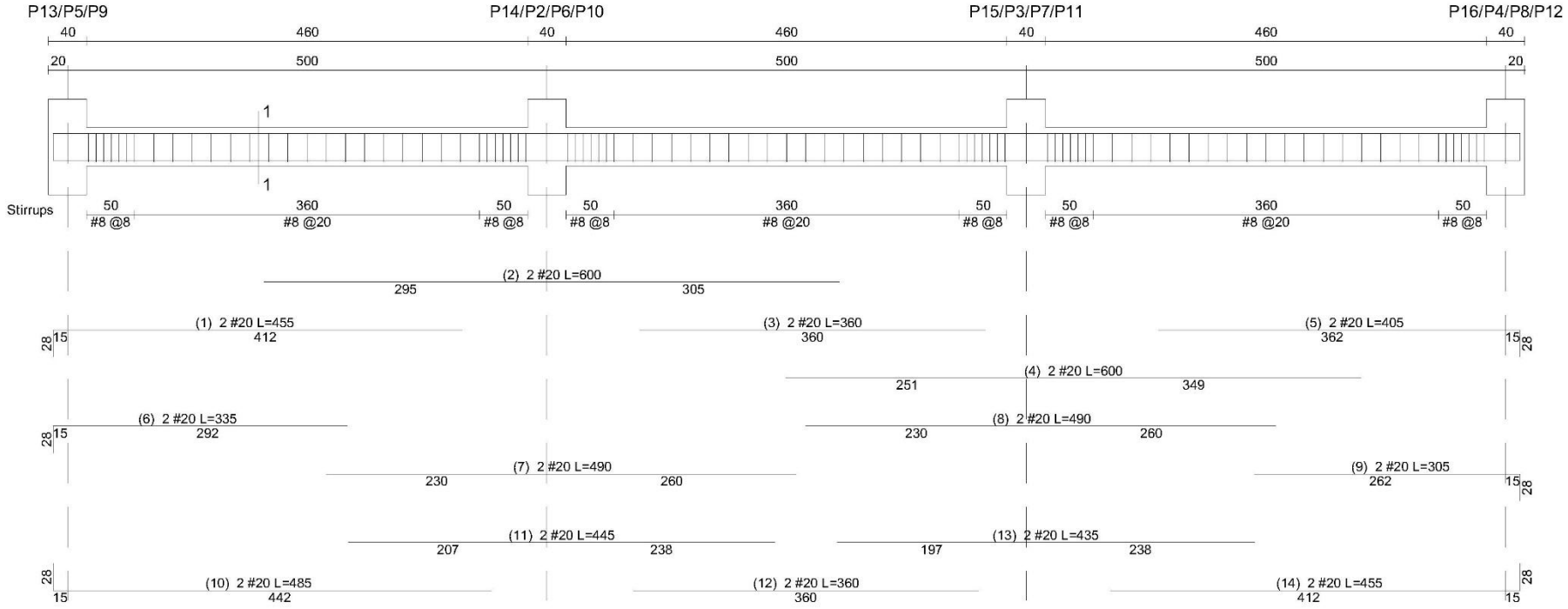


Figure 4.25 Beam reinforcement layout

Scale 1:50 - Beams: 10, 12, 13, 14, 18, 20, 21, 22



Scale 1:20 - Cross section 1-1

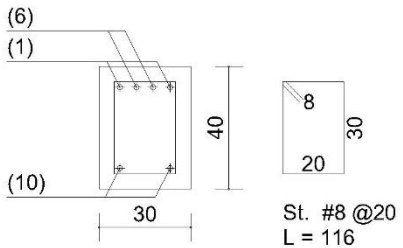


Figure 4.26 Beam reinforcement layout

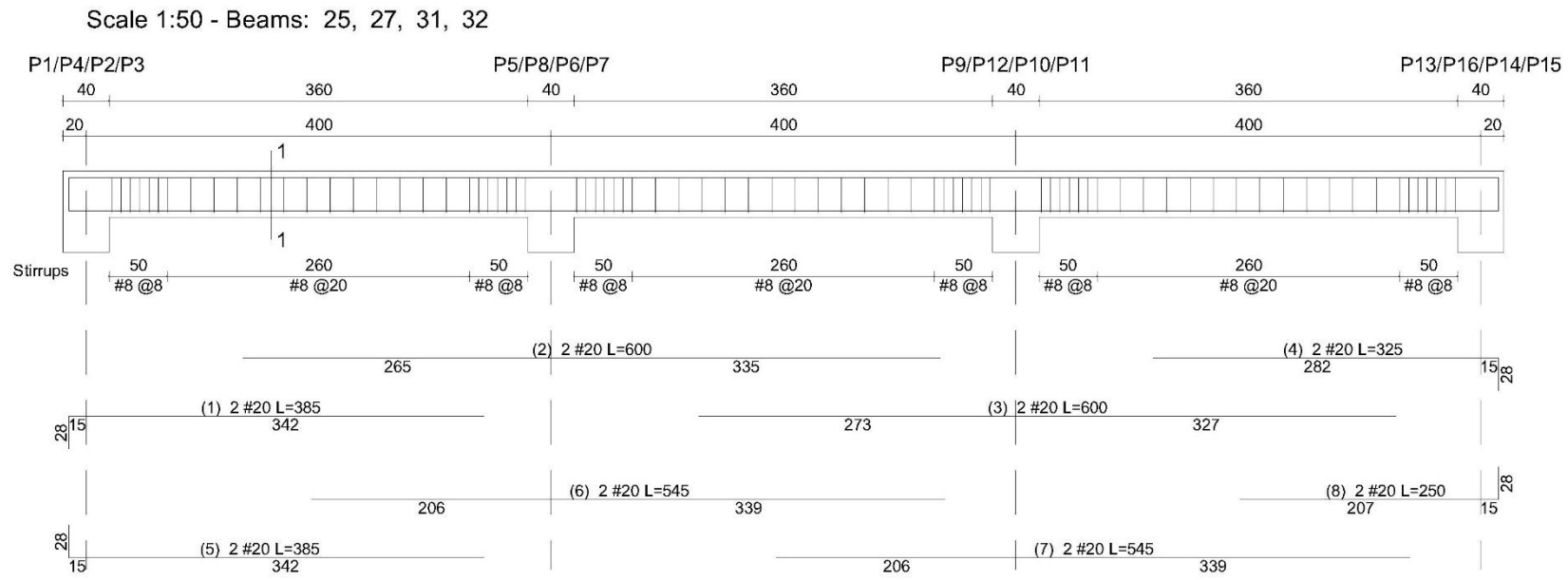
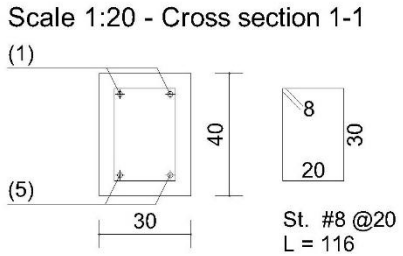


Figure 4.27 Beam reinforcement layout



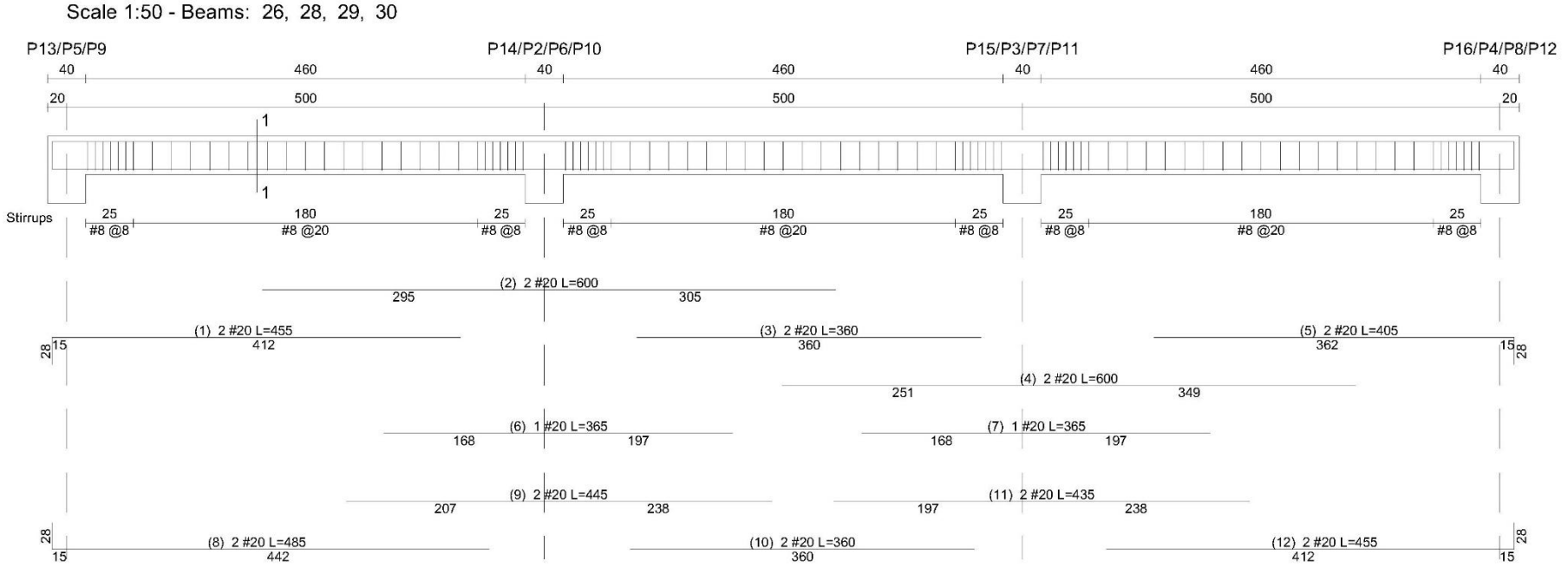
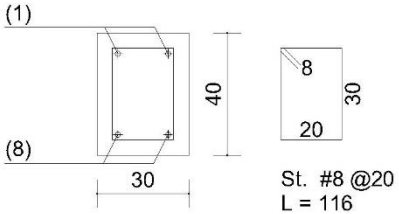


Figure 4.28 Beam reinforcement layout



5 ANALYSIS OF THE PROGRESSIVE COLLAPSE OF STRUCTURES

This chapter presents the structural models developed within the ELS software and the simulations carried out to investigate the behaviour of the previously described structures following the loss of one or more columns. The aim is to highlight the differences in the results obtained for the two structural configurations, Turin and L'Aquila, with particular attention to the possible reasons behind the different responses observed after the removal of columns located in the same position in both models.

Progressive collapse is a phenomenon in which the failure of a primary structural element leads to the failure of adjacent structural elements, triggering a chain reaction that can result in partial or total collapse of the structure.

A common approach to assess the susceptibility of a building to progressive collapse is to remove a critical structural component, such as a column, and evaluate the structural response. If the structure is capable of redistributing the loads and bridging over the removed element, the building may remain stable, although significant deformations and deflections can occur. Conversely, if the structure is unable to develop alternative load paths, the local failure may propagate to neighboring elements, leading to a progressive collapse of part or all of the building.

The analyses presented in this study were performed as dynamic simulations, considering the sudden removal of the selected column. This approach allows the evaluation of the structural response over time, including inertial effects, load redistribution, and the development of transient displacements. The dynamic behaviour of the structure was therefore assessed by monitoring the response following the columns removal event.

The code used to performed the analysis is the UFC 4-023-03. ASCE 7 defines two approaches to resist progressive collapse: Indirect Design and Direct Design method.

The first approach is also called **Tie Forces method** (Figure 5.1), because it prescribes a tensile force strength of the floor or roof system, to ensure the transfer of load from the damaged portion of the structure to the undamaged one. The designer has to make sure that there is the continuity for the load path in the floor, beams and columns. This method is not so much used because is indirect and it causes the utilization of very large cross section.

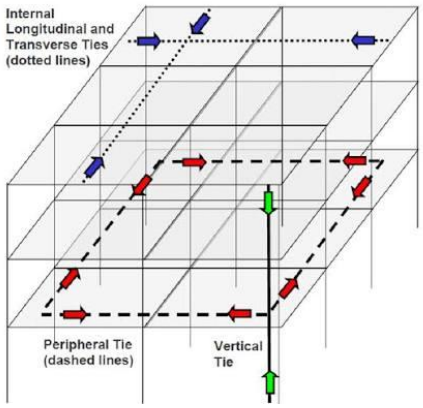


Figure 5.1 Tie Force method (From: [19])

The second approach instead, is known as **Alternate Load Path method**. It requires that the structure be capable of bridging over a missing structural element, ensuring that the resulting damage remains localized [19].
Although the Alternate Load Path (ALP) approach allows for local structural damage, it requires the structure to be capable of developing alternative load paths to redistribute the applied loads. In this way, the initial damage can be confined to the affected area, thereby reducing the risk of progressive propagation and preventing the collapse of the entire structure.
As an illustrative example, Figure 5.2 shows the sudden removal of an interior column. Under these circumstances, the structural system is required to develop alternative load paths to ensure the continuity of load transfer. One of the primary mechanisms that enables this redistribution is catenary action, through which beams, by developing tensile forces, are able to continue supporting the vertical loads even after the loss of the original support. This mechanism plays a key role in limiting the spread of damage and preventing the so-called domino effect, which could ultimately lead to the progressive collapse of the structure. [20]

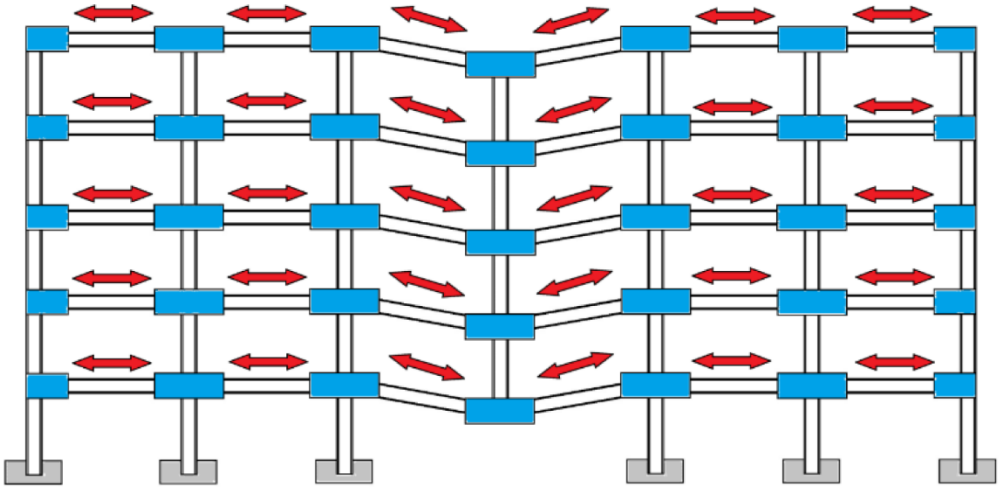


Figure 5.2 Alternate Load Path method (From: [20])

The theoretical background presented in Chapter 4 was essential for the development of the numerical model in the ELS software. The structural elements were assigned the mechanical and geometrical properties previously described, in order to ensure the reliability of the simulations. Regarding the accuracy of the results, a refined mesh was adopted in the column removal zone to improve the reliability of the numerical response.

A total of 6 analyses were performed. The first set of simulations describes the structural response following the loss of a single column, while the subsequent analyses consider the removal of multiple columns.

It is of particular interest to observe the evolution of vertical displacements (along the Z-axis) following column removal, as well as the axial force distribution, which is also time-dependent throughout the dynamic analysis.

5.1 Analysis performed on ELS

This chapter presents and discusses the results obtained from the numerical simulations performed on the structural models. The objective of the analyses is to investigate the structural response under the different

progressive collapse scenarios considered, with particular attention to the evolution of damage, the redistribution of internal forces, the development of deformations, and the vertical displacement of the slab after the removal of the columns.

Each simulation is examined individually to highlight the main aspects of the structural behaviour following the initiation of the collapse. The evolution of the response is analysed through the interpretation of the relevant output parameters, including internal forces, displacements, and the sequence of structural failures. Finally, a comparative discussion of the different simulation cases is presented to evaluate the influence of the considered collapse scenarios on the overall structural performance. The comparison allows the identification of similarities and differences in the structural response, providing a comprehensive assessment of the robustness of the analysed structure and its ability to redistribute loads after the loss of a primary load-bearing member.

Before defining the progressive collapse scenarios, the structural models were completed by assigning to each structural member the geometric and mechanical properties previously obtained from the PRO_SAP design models. These properties include the cross-sectional dimensions, material characteristics, and reinforcement details adopted for the numerical analyses.

The gravity loads are applied to both structures by converting the surface loads into an equivalent density assigned to the material of the slab. The structural permanent loads G_1, non-structural permanent loads G_2, and live loads Q were considered according to the load combination adopted for the analyses, according to UFC 4-023-03:

$$1.2 * (G_1 + G_2) + 0.5 * Q \tag{19}$$

The resulting total surface load was subsequently converted into a volumetric load by dividing the obtained value by the slab thickness t resulting in a value expressed in kN/m^3. This value was then converted into kg/m^3

$$q = \frac{1.2 * (G_1 + G_2) + 0.5 * Q}{t} \tag{20}$$

The resulting density was then directly assigned to the slab material, replacing the original density of concrete. In this way, the combined effect of the permanent and live loads considered in the adopted load combination was represented in the numerical model through the self-weight of the slab, without introducing additional surface loads. This approach allows the loads to be uniformly distributed over the entire slab area while ensuring that the considered gravitational actions are properly represented in the numerical analysis.

The numerical values resulting from the procedure described above are reported in the following table.

G_1	4.85	kN/m^2
G_2	2.32	kN/m^2
Q	2	kN/m^2
$1.2 * (G_1 + G_2) + 0.5 * Q$	9.6	kN/m^2
t	0.2	m
d	48	kN/m^3
ρ	4802	kg/m^3

Table 5.1 Equivalent density calculation

Before presenting the results obtained, the following section provides the images of the structures modelled in ELS, together with the related observations and considerations, as well as the floor plans of the buildings showing the numbering of the columns. (Figure 5.5).

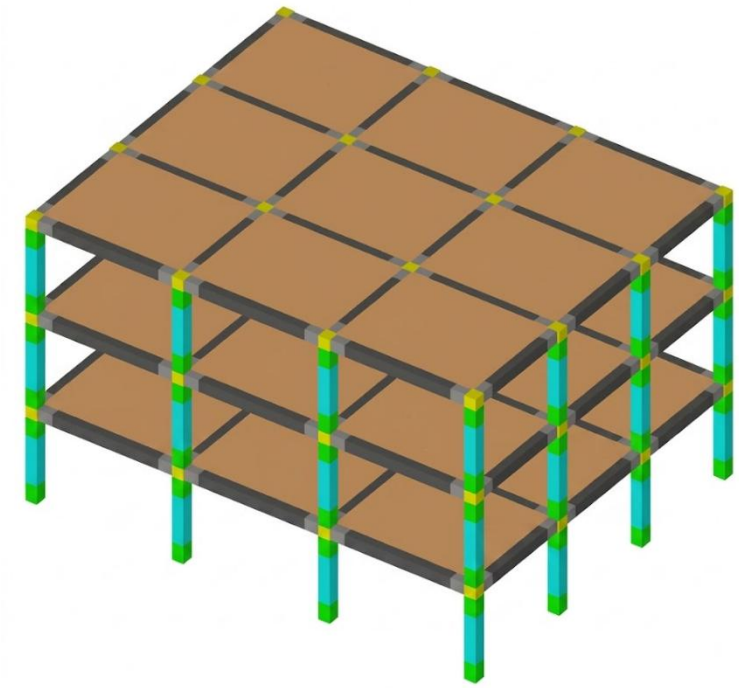


Figure 5.3 Structure located in L'Aquila

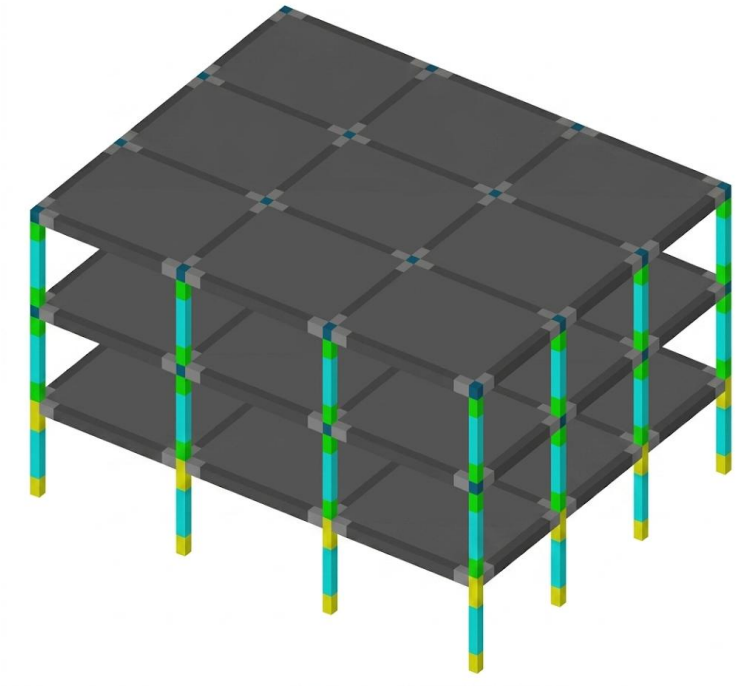


Figure 5.4 Structure located in Turin

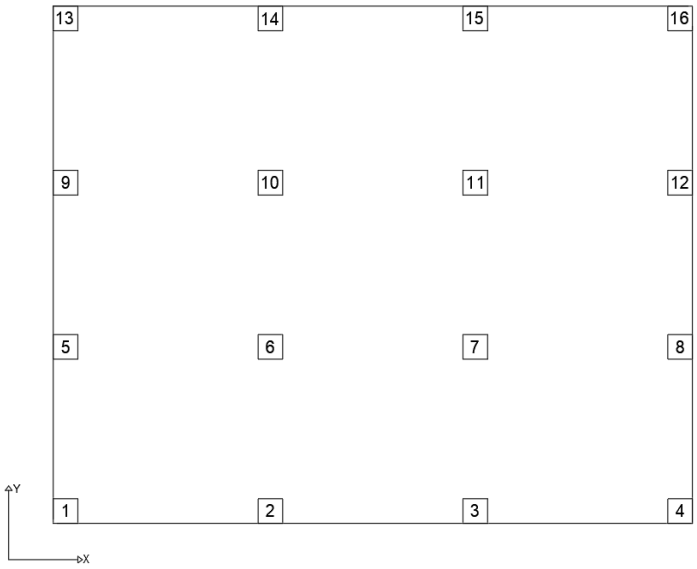


Figure 5.5 Columns numbering on ELS

It can be observed that the columns and beams appear to be subdivided into several segments, as indicated by the different colours visible in the figures. This subdivision results from the need to ensure full consistency between the model implemented in ELS and the structural model previously designed and verified using PRO_SAP. To this end, the structural members were discretized into portions characterized by different properties, according to the specific reinforcement details defined in the design model. In particular, for each segment, the characteristics relating to the spacing and diameter of the stirrups, as well as the arrangement, number, and position of the longitudinal reinforcement bars running along the structural members, were defined. This approach allowed the actual distribution of the reinforcement to be accurately reproduced in the ELS model and, consequently, provided a more reliable representation of the mechanical properties and structural behaviour of the members.

5.2 Description of analysed scenario

This section presents the displacement plots along the Z-axis of the slab following the removal of one or more columns, together with an analysis and discussion of the results obtained. The aim of the analysis is to highlight the differences between the two structures when the same columns are removed, as well as to provide a comparison within each individual structure by evaluating the percentage increase in displacement resulting from the removal of one or more columns.

The dynamic analyses were performed considering a total simulation time of 0.5 s, which was deemed sufficient to capture the structural response following the sudden removal of the column. For each analysis, the simulation time was discretized into 61 frames, corresponding to the time steps at which the software provides the analysis results. This makes it possible to evaluate how the structure responds over time. Another important aspect to describe before presenting the results is the mesh used. The beams and columns of the structure were discretized into four elements along their main longitudinal direction and into two elements along the other two directions. A finer mesh was adopted locally for the columns adjacent to the removed one, in order to obtain a more accurate representation of the structural response in the area directly affected by the column removal. This local mesh refinement provides a more accurate representation of the structural response

near the removed column, providing more reliable results for the subsequent assessment of the structural response. As an example, shows the mesh adopted for the L'Aquila structure in the case of single-column removal, illustrating the local refinement around the damaged area.

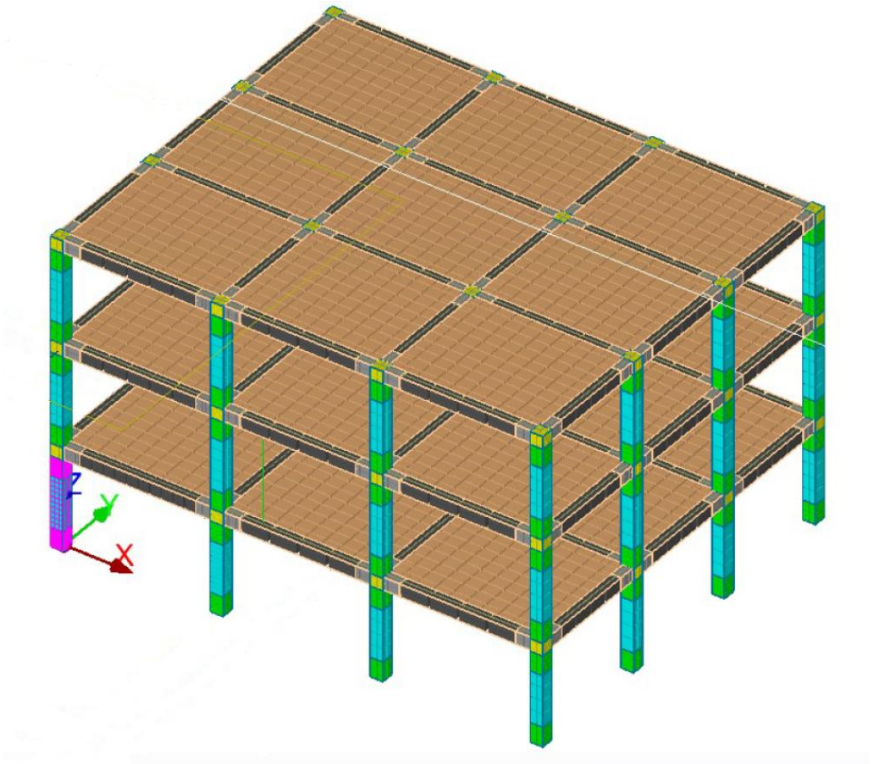


Figure 5.6 Local refinement of the mesh around the columns adjacent to the removed column

Having described the boundary conditions used in the analyses, the results can now be presented: for the structure located in L'Aquila the time history of the vertical displacement (Z-direction) of the node located immediately above the removed portion of Column 1 is reported in the following figures.

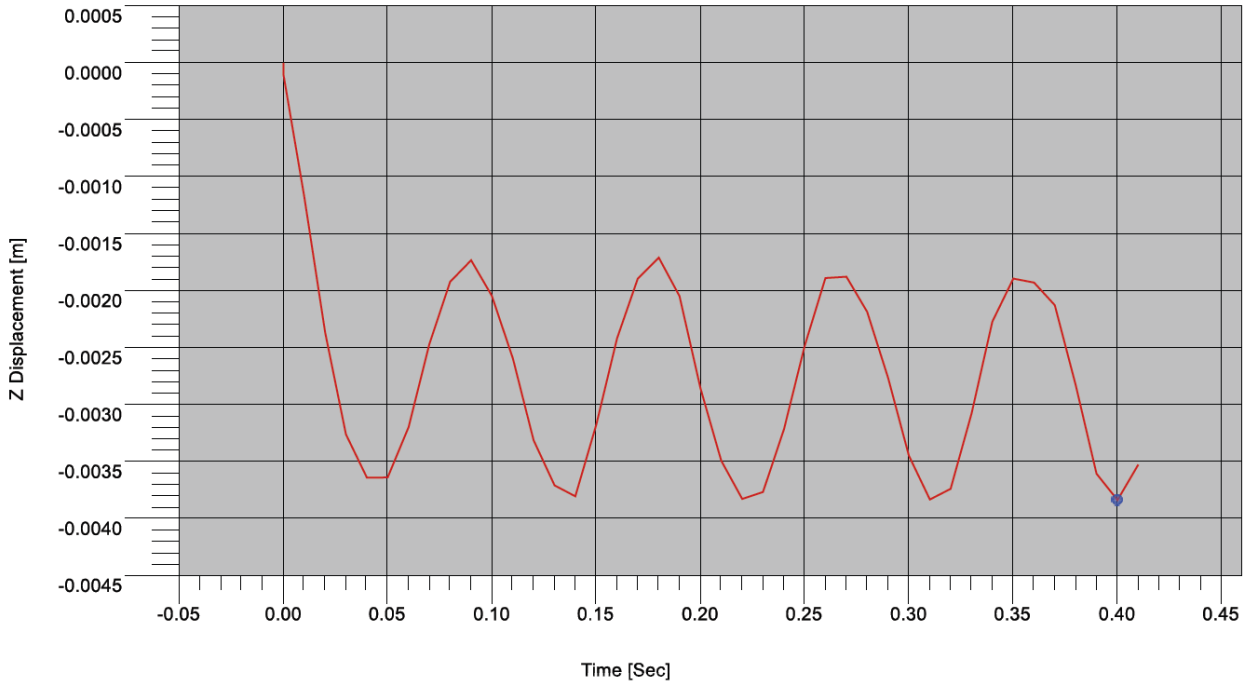


Figure 5.7 L'Aquila - Displacement after the removal of Column 1

The graph shown in Figure 5.7 illustrates the evolution of the vertical displacement, along the Z-axis, of the floor's control point as a function of time. At the initial instant, the displacement is close to zero, whilst following the removal of the column, an immediate negative change in displacement is observed, associated with the downward deflection of the slab. Subsequently, the structure exhibits oscillatory behaviour, characterised by alternating phases of greater and lesser displacement. The maximum downward displacement values progressively reach values of the order of 3.5–3.9 mm, whilst the intermediate values generally remain within the range of approximately 1.7 to 2.0 mm. This oscillatory behaviour is indicative of the structure's dynamic response following the sudden loss of the column and the resulting redistribution of internal forces. In the final stage of the analysis, specifically at frame 51, the control point reaches the maximum displacement of approximately 3.9 mm.

To highlight the difference compared with the structure in Turin, we can now see what happens in this case under the same boundary conditions: the peak occurs slightly earlier, at frame 28 to be precise, and the maximum deflection recorded is 5.9 mm.

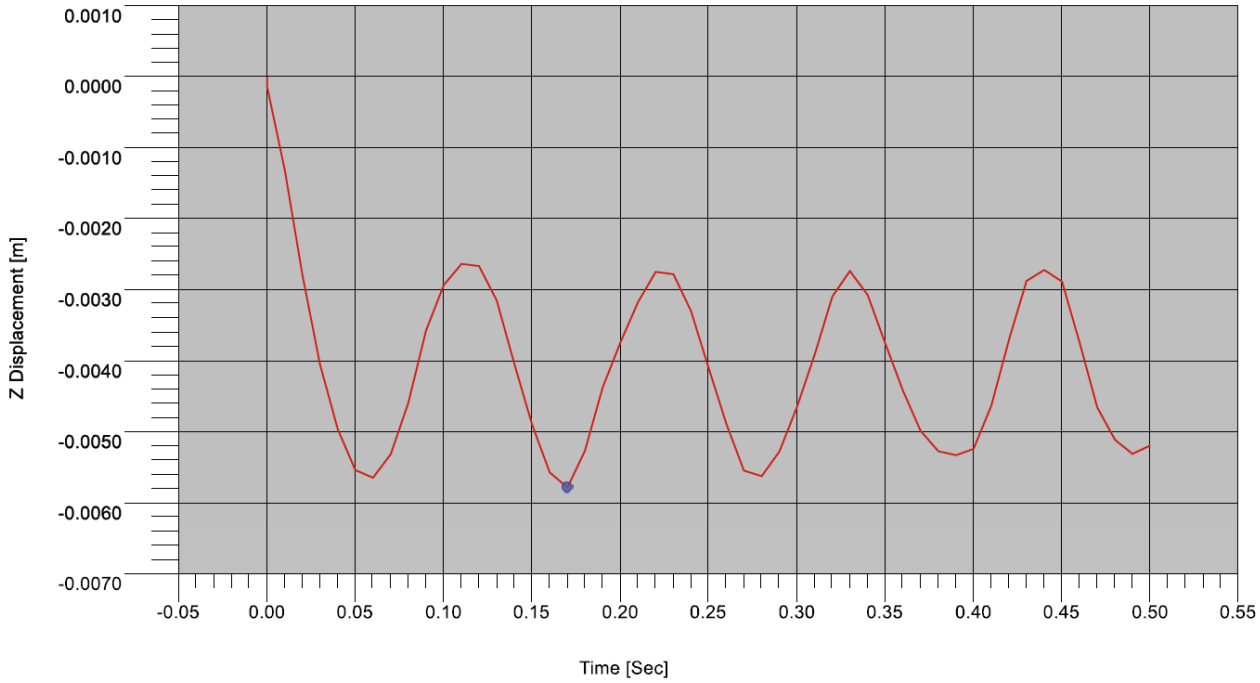


Figure 5.8 Turin - Displacement after the removal of Column 1

A qualitatively similar oscillatory response can be observed following the removal of the corner column. Despite the similarity in the qualitative behaviour of the response, a significant difference can be observed in the value of the vertical displacement. In the Turin structure, the maximum downward displacement reaches approximately 5.9 mm at frame 28, whereas in the L'Aquila structure, the maximum recorded value is approximately 3.9 mm at frame 51. Consequently, the L'Aquila structure exhibits a maximum downward displacement approximately 34% lower than that recorded for the Turin structure. This difference indicates a less deformable response of the L'Aquila structure following the sudden removal of the corner column. It is also interesting to note that the maximum downward displacement is reached at a different frame in the two structures, indicating a different evolution of the dynamic response following the removal of the load-bearing element.

The difference between the two structures becomes even more pronounced in the case of the removal of two columns, specifically columns 1 and 2 (Figure 5.5). In this case, two peripheral columns supporting the slab are simultaneously removed, resulting in a greater loss of load bearing capacity and, consequently, a more significant redistribution of the internal forces towards the surrounding structural members. Compared with the removal of the single corner column, it is possible to observe a significant increase in the vertical downward displacement. For the L'Aquila structure, the maximum displacement increases from 3.9 mm to approximately 14 mm, whereas for the Turin structure, it increases from 5.9 mm to approximately 25 mm. The observed behaviour therefore highlights how the simultaneous removal of two peripheral columns leads to a significantly more severe structural response compared with the removal of a single column, resulting in an increase in the deformability of the system and a greater demand for internal force redistribution, as discussed in greater detail in Section 5.3. Furthermore, also in this case, the L'Aquila structure exhibits a lower maximum downward displacement than the Turin structure, with the difference increasing from approximately 34% in the case of single-column removal to approximately 44% in the case of two column removal.

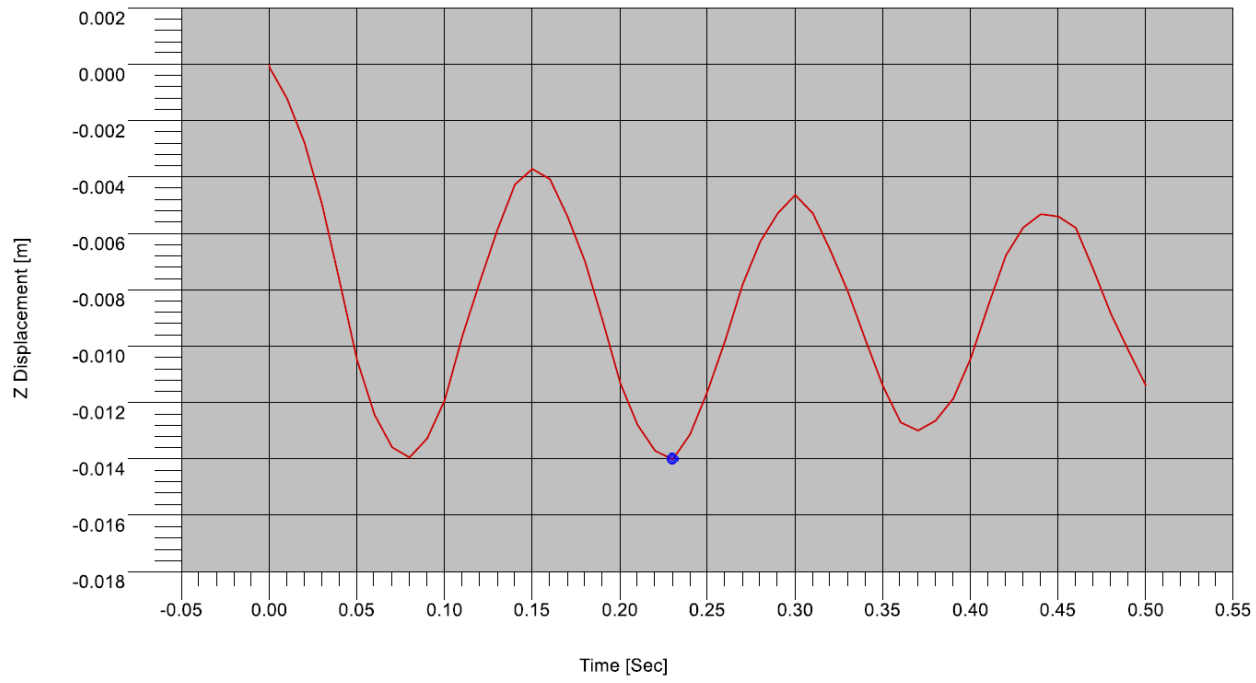


Figure 5.9 L'Aquila - Displacement after the removal of Column 1 and 2 at frame 34

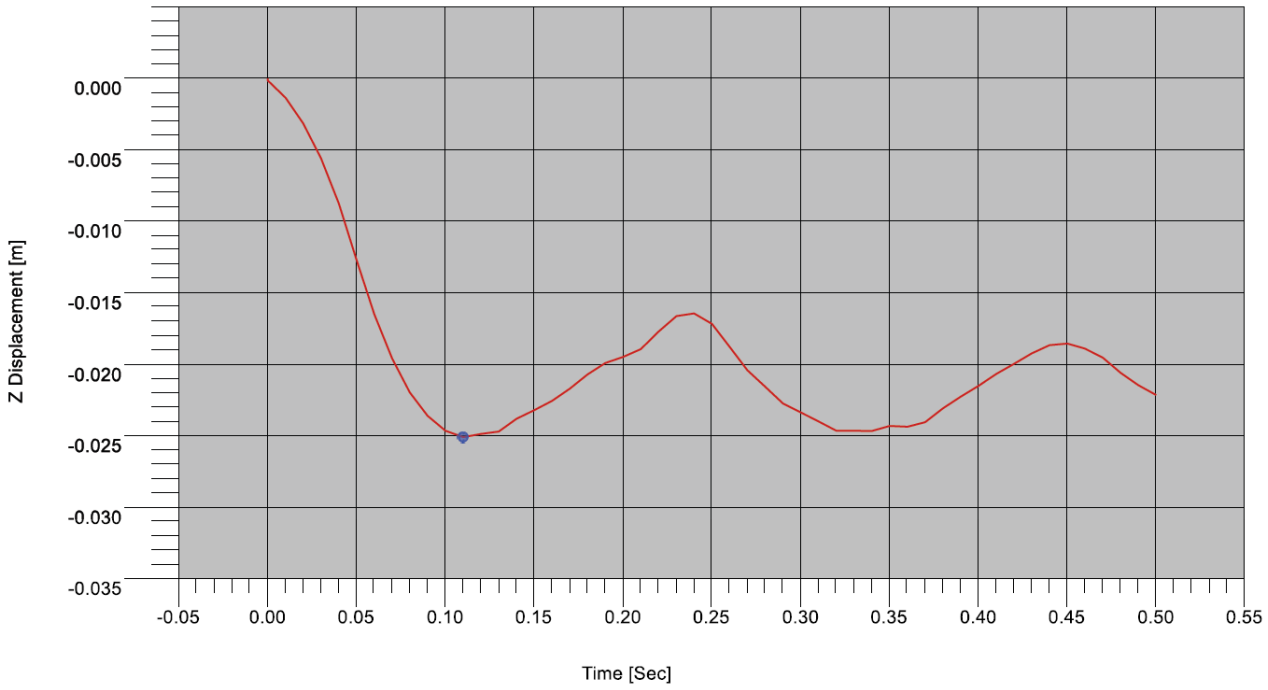


Figure 5.10 Turin - Displacement after the removal of Column 1 and 2 at frame 22

In addition to the difference in displacement magnitude, the two structures also exhibit distinct dynamic characteristics. In the Turin structure, the maximum displacement of approximately 25 mm is reached at around 0.11 s, whereas in the L'Aquila structure, the maximum displacement of approximately 14 mm is reached later,

at around 0.23 s. This indicates a different evolution of the transient response following the sudden removal of the two load bearing elements.

A further difference can be observed in the oscillation period. Following the initial downward displacement, the Turin structure exhibits a longer oscillation period, of approximately 0.22 – 0.23 s, compared with approximately 0.15 s for the L'Aquila structure. Interestingly, the longer period in Turin is not associated with substantially larger oscillation amplitudes. After the initial displacement, the amplitude of the oscillations around the mean displaced position remains relatively limited in both structures, with the amplitude in L'Aquila being slightly higher. This difference is evident from the mean level around which the subsequent oscillations develop. In the Turin structure, the response remains centred at a displacement of approximately −20 mm, whereas the L'Aquila structure oscillates around a substantially less negative displacement, approximately −9 to −10 mm. These differences indicate that the two structures have a different dynamic response and different levels of deformation following the loss of the two peripheral load bearing elements.

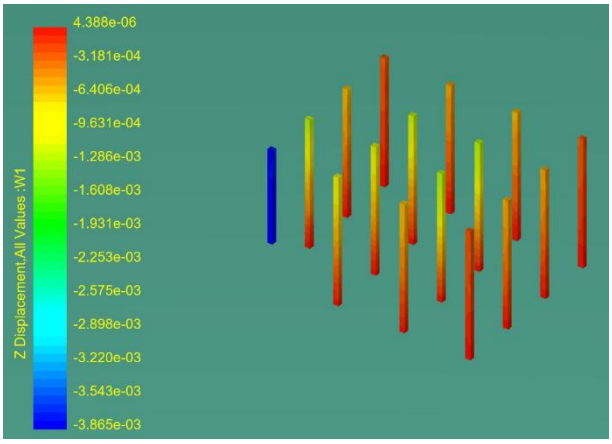


Figure 5.11 L'Aquila – Displacement contour plot after the removal of column 1

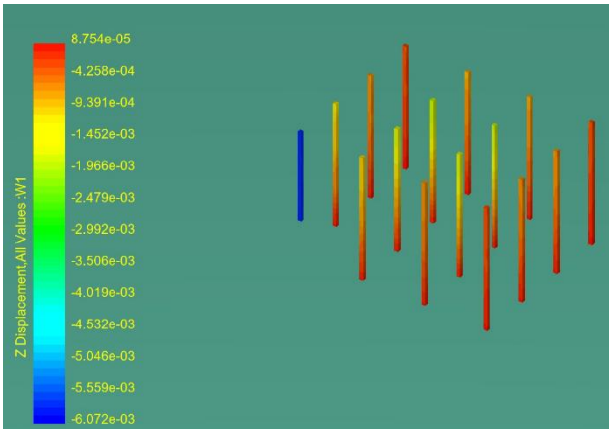


Figure 5.12 Turin – Displacement contour plot after the removal of column 1

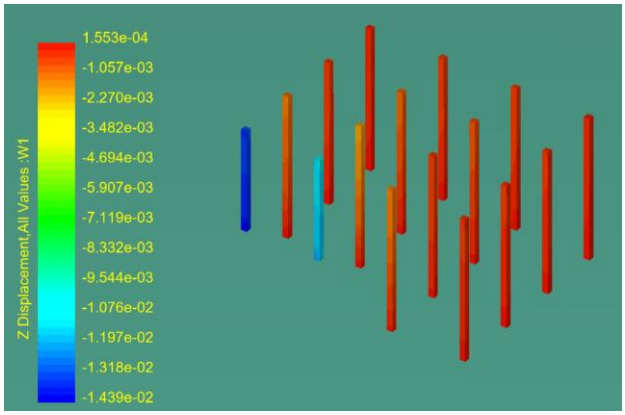


Figure 5.13 L'Aquila – Displacement contour plot after the removal of column 1 and 2

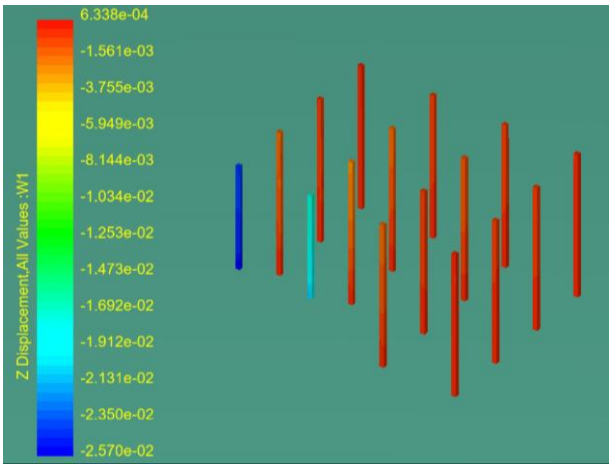


Figure 5.14 Turin – Displacement contour plot after the removal of column 1 and 2

A comparison of the simulations shows that, following the removal of the columns, the structure designed for L'Aquila exhibits a greater maximum slab deflection than that observed for the Turin structure. This behaviour can be attributed to the greater overall stiffness of the structure designed for the site with the higher seismic hazard.

The larger cross-sections of the structural elements and the greater quantity of reinforcement, adopted to meet high seismic requirements, facilitate a more effective redistribution of loads to adjacent elements, limiting the deformations resulting from the sudden failure of a column. Although the design was not specifically carried out with progressive collapse in mind, the increased strength resulting from seismic design also has beneficial effects in relation to this scenario. Columns with larger cross-sections increase the lateral and vertical stiffness of the frame. The increase in flexural stiffness EI is shown below, moving from 30x30 columns for the Turin structure to 40x40 columns in L'Aquila.

In fact, the area increases from 900 cm² to 1600 cm², and the moment of inertia of a square cross-section is given by $I = b^4/12$ therefore, the 40×40 column is approximately three times stiffer than the 30×30 one:

$$\frac{I_{40}}{I_{30}} = \frac{40^4}{30^4} = 3.16$$

Greater reinforcement, on the other hand, increases the structural capacity and, above all, the ability of the members to develop continuous forces. This makes the structure more robust in the event of the loss of a load bearing member.

The most interesting aspect is that the difference between the two structures increases as the damage becomes more severe:

- **Removal of one column**
    - Turin: **5.9 mm**
    - L'Aquila: **3.9 mm**
    - Difference: approximately **34% lower deflection in L'Aquila**.
- **Removal of two columns**
    - Turin: **25 mm**
    - L'Aquila: **14 mm**
    - Difference: approximately **44% lower deflection**.

This indicates that the structure designed for L'Aquila is not simply stiffer, but retains a greater ability to redistribute loads as damage increases. This is precisely what one would expect from a structure designed for a high-seismicity zone, where regulatory requirements lead to more robust elements with a greater capacity to withstand exceptional conditions.

While in the cases described above, involving the removal of one and two columns, the two structures showed different capacities to limit slab deflections and redistribute internal forces, with more favorable behavior observed for the structure designed for L'Aquila, the simultaneous removal of three columns, specifically those on the first floor at positions 1, 2, and 5 (Figure 5.5), leads to a significantly more critical condition. In this case, both structures exhibit a rapid increase in deflection, reaching approximately 30 cm within the first 0.5 s, with no subsequent tendency toward stabilization, as shown in the following figures. A deflection of this

magnitude, developing over such a short time interval, indicates a loss of structural stability and can be interpreted as the development of a collapse mechanism.

The fact that a similar degree of settlement was achieved for both structures can be attributed to the severity of the scenario under consideration. The simultaneous removal of three columns results in such a significant loss of load-bearing capacity that it exceeds the structures' ability to redistribute loads, making the difference in stiffness that characterized the cases involving the removal of one and two columns less significant. Once the collapse mechanism has been triggered, the response is predominantly governed by the loss of equilibrium and the resulting dynamic behaviour of the structure. The greater stiffness and strength of the structure designed for L'Aquila are therefore not sufficient to prevent collapse in the event of the simultaneous removal of three columns, unlike in the less severe cases described previously.

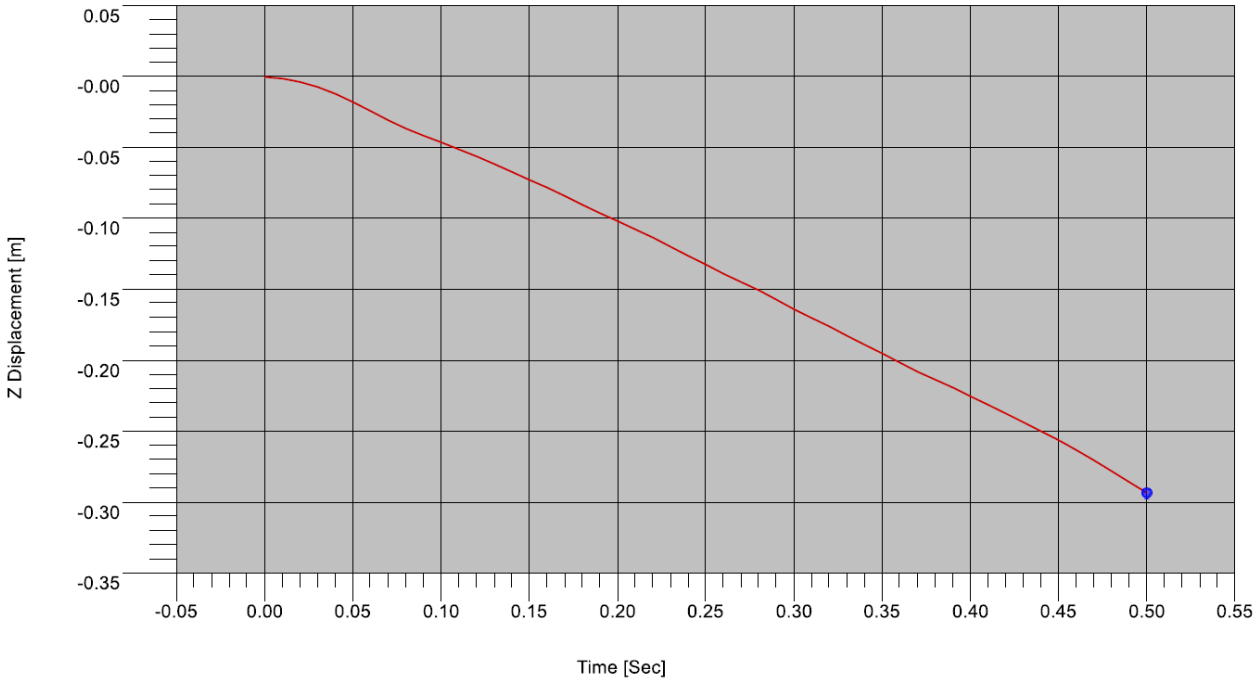


Figure 5.15 Turin – Displacement after the removal of three columns

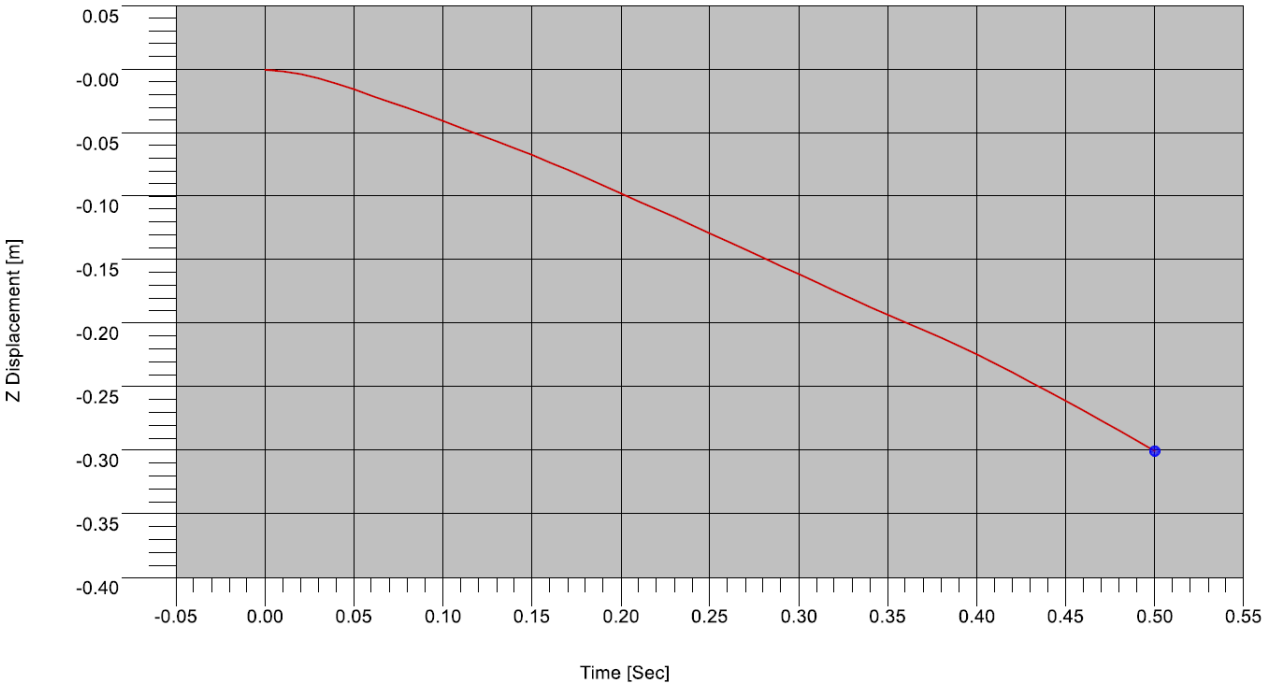


Figure 5.16 L'Aquila – Displacement after the removal of three columns

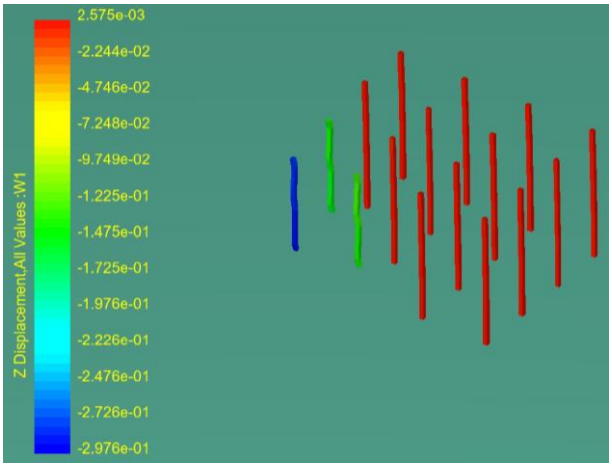


Figure 5.17 Turin – Displacement contour plot after the removal of three columns

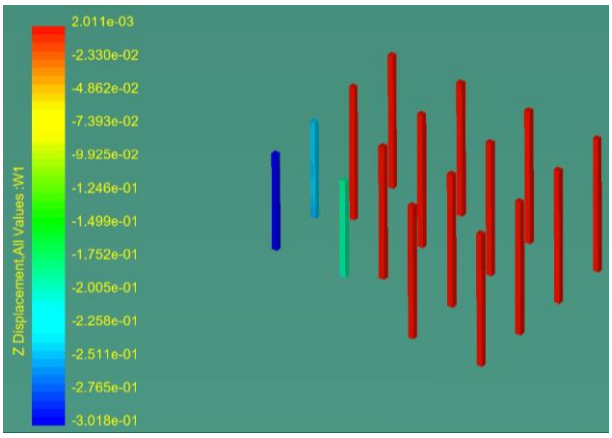


Figure 5.18 L'Aquila – Displacement contour plot after the removal of three columns

5.3 Normal straining action distribution

An analysis of the normal straining actions on the remaining columns allows for a more detailed understanding of the structure's behaviour following the removal of one or more vertical load-bearing elements. In particular, attention has been focused on the columns under the greatest stress, as these are the ones most heavily involved in the redistribution of vertical loads.

The removal of one or more columns results in a sudden change in the load transfer path and, consequently, a redistribution of stresses in the remaining columns can be observed. The stresses vary from one frame to the next, exhibiting an oscillatory behaviour associated with the structure's dynamic response. This aspect is particularly significant as the maximum normal stress does not coincide with the moment when the floor slab reaches its maximum deflection.

The comparison between the structure designed for Turin and that designed for L'Aquila is particularly significant in this respect as well. The L'Aquila structure, characterised by larger cross-sections of the structural elements and a greater quantity of reinforcement, has a greater capacity to support and redistribute the vertical forces resulting from the removal of the columns. This behaviour is consistent with the lower maximum deflections obtained in the simulations.

Overall, the analysis of the normal straining actions therefore complements the assessment of deflections and provides a more comprehensive picture of the behaviour of the two structures following the loss of vertical load-bearing elements. The smaller deflections observed for the L'Aquila structure, combined with its ability to redistribute vertical loads among the remaining columns, highlight a greater capacity to develop alternative load-transfer paths. Although the structure was not specifically designed to resist progressive collapse, the greater stiffness, larger cross-sections and increased amount of reinforcement resulting from seismic design contribute positively to its robustness against the damage scenarios considered.

A noticeable difference is related to the distribution of the straining actions depending on the number of columns removed. In the case of the removal of a single column, the distribution is more uniform. As can be observed in the following figures, the four central columns are, to a similar extent, the most highly stressed columns in both structures. A peak value of −825 kN is recorded for the L'Aquila structure, compared with −683 kN for the Turin structure.

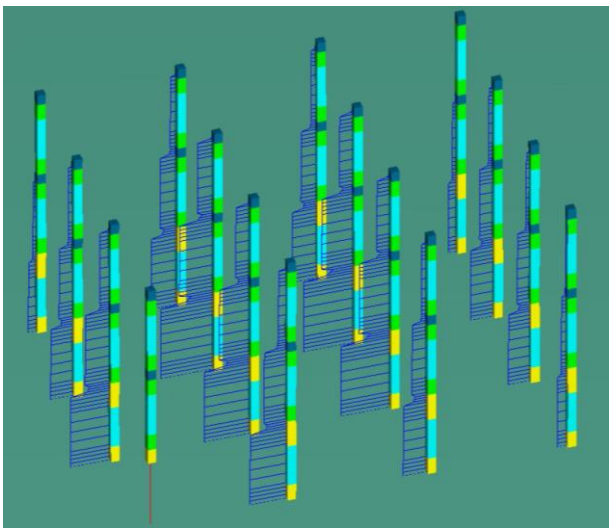


Figure 5.19 Turin - Distribution of axial straining actions in the columns following column removal

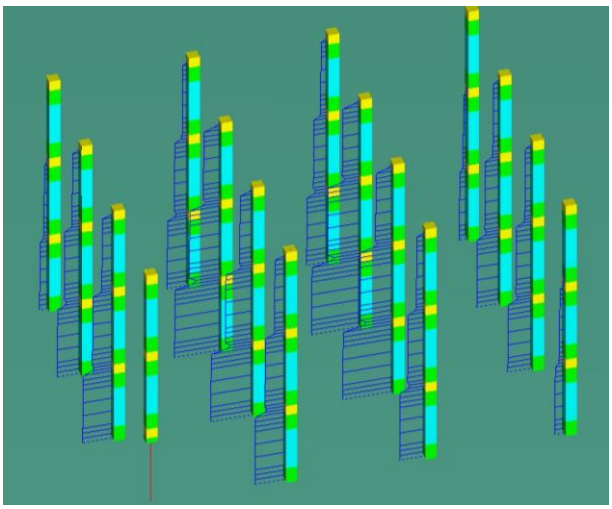


Figure 5.20 L'Aquila - Distribution of axial straining actions in the columns following column removal

When two columns are removed, the maximum peak is instead recorded at the base of Column 6, which is also a central column, followed by Column 5. As a perimeter column, Column 5 experiences lower values. In this case, the peak value is −1401 kN for the L'Aquila structure and −1040 kN for the Turin structure.

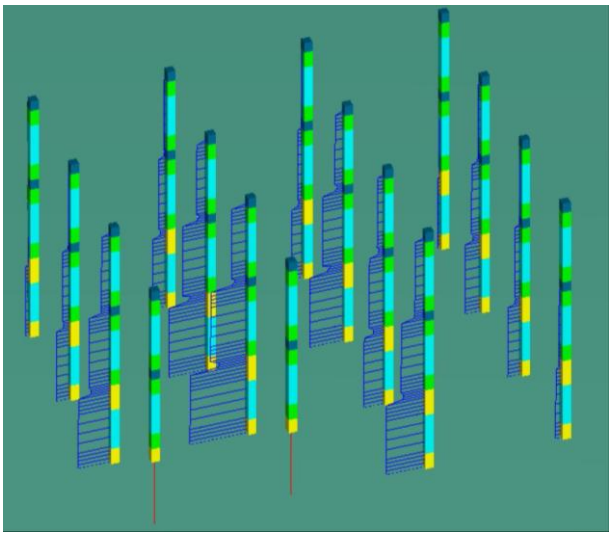


Figure 5.21 Turin - Distribution of axial straining actions in the columns following the removal of two columns

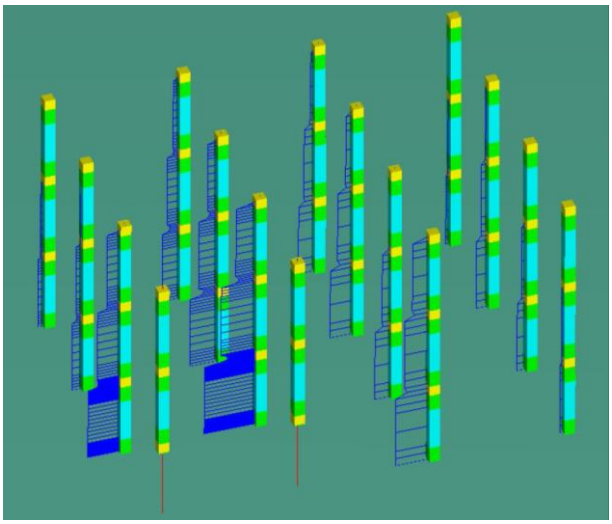


Figure 5.22 L'Aquila - Distribution of axial straining actions in the columns following the removal of two columns

The central columns exhibit the highest axial force values, mainly due to their larger tributary areas compared with perimeter and corner columns. Considering the adopted structural grid of 5 × 4 m, an internal column is associated with a tributary area of approximately 20 m², whereas a perimeter column has a tributary area of approximately 10 m². Consequently, internal columns are subjected to higher vertical loads, which are further increased by the accumulation of loads transferred from the upper floors, an effect that is particularly significant for columns located on the lower floors.

It is important, however, to distinguish between the absolute value of the axial force and its variation following the removal of a column. Columns located in the vicinity of the removed element, particularly perimeter columns, may experience a greater increase in axial force, as they directly participate in the redistribution of the load previously carried by the removed column. Despite this increase, their absolute axial force may remain lower than that of the central columns due to their smaller initial tributary area. Therefore, a central column may exhibit the highest absolute axial force, while a perimeter column may experience a greater increase in axial force following column removal.

An example illustrating this behavior can be observed in the structure located in L'Aquila following the removal of the corner column. As previously stated, a maximum axial force of -825 kN is recorded in the central columns, whereas the adjacent perimeter column, specifically Column 5, reaches an axial force of -700 kN at its base. Before the removal of Column 1, the central columns were subjected to an axial force of approximately -728 kN, while the perimeter column under consideration was subjected to an axial force of approximately -400 kN. These values demonstrate that, in terms of absolute value, the central columns remain the most highly loaded, however the perimeter columns experience the greater increase in axial force as a result of the column removal.

The columns located farther from the removed elements, on the other hand, exhibit a smaller increase in axial forces, confirming that the redistribution of internal forces primarily affects the structural elements located close to the removal area, while its effects on more distant parts of the structure is progressively reduced.

This distinction is particularly significant in the analysis of progressive collapse, as it allows both the level of stress experienced by the structural elements and the actual redistribution of loads and development of alternative load-transfer paths to be assessed.

6 CONCLUSIONS

The events that first drew engineers' attention to progressive collapse, Ronan Point in 1968, the Alfred P. Murrah Building in Oklahoma City, the Twin Towers in 2001, share a common feature: a localised failure that was allowed, by the absence of adequate structural continuity, to propagate far beyond its original cause. This thesis compared two versions of the same reinforced concrete building, one designed for the low seismic hazard of Turin, the other for the higher hazard of L'Aquila, to determine whether seismic design incidentally improves robustness against progressive collapse. Using dynamic simulations in ELS, both structures were subjected to the sudden removal of one, two, and three columns.

For the removal of a single corner column, the seismically designed L'Aquila structure deflected about 34% less than its Turin counterpart (3.9 mm against 5.9 mm); for the removal of two adjacent columns, the difference grew to about 44% (14 mm against 25 mm). The explanation lies in the larger cross-sections and heavier reinforcement that seismic detailing requires: a 40×40 cm column is roughly three times stiffer than the 30×30 cm section used where seismic demand is minimal, and this additional stiffness translates directly into a greater ability to bridge over a lost support.

The distribution of axial forces in the surviving columns tells the same story from a different angle. After the loss of a single corner column, the most heavily loaded central columns reached a peak axial force of -825 kN in L'Aquila against -683 kN in Turin; with two columns removed, the peak recorded at the base of Column 6 (Figure 5.5) rose to -1401 kN and -1040 kN respectively. Higher forces in the more robust structure may appear counterintuitive, but they are in fact the signature of a more effective redistribution: the stiffer, more heavily reinforced members of the L'Aquila frame are able to attract and carry a larger share of the load released by the removed element, which is precisely why the resulting deflections are smaller. It is also worth distinguishing between the absolute value of the axial force and its increase. In L'Aquila, the perimeter Column 5 went from roughly -400 kN to -700 kN after the removal of Column 1, a far larger relative increase than that experienced by the central columns, which rose from about -728 kN to -825 kN, confirming that redistribution is concentrated in the members immediately adjacent to the damaged area and decays rapidly with distance from it.

The qualification is important, though, and it is arguably the most instructive result of the study. Once three columns were removed simultaneously, the advantage all but disappeared: both structures developed a rapid, unstabilised deflection of around 30 cm within half a second, consistent with the onset of a genuine collapse mechanism. Seismic design, in other words, raises the threshold of damage a structure can absorb, but it does not remove that threshold.

Several choices made to keep the analysis tractable also mark its boundaries, and point to where it could usefully be extended. Rather than applying the design loads as discrete surface actions, the combination 1.2*(G1 + G2) + 0.5*Q was converted into an equivalent density of 4802 kg/m³ assigned to the slab material, so that the gravity loads were carried entirely as self-weight. This is a convenient and widely adopted simplification, but it has three consequences worth stating. Non-structural permanent loads such as partitions and perimeter infill walls, if present, which in reality act along defined lines and often bear directly on the beams, are instead smeared uniformly over the slab area, so the local peaks in bending moment and shear associated with their actual position are lost. The inertial mass mobilised in the dynamic analysis is the factored one, slightly higher than the mass physically present, which has some influence on the oscillation period and on the amplitude of the peaks discussed above. Finally, the live load is treated as rigidly bound to the slab rather than simply resting on it.

Finally, the comparison could be extended to buildings with a larger number of storeys and different structural configurations and alternative construction materials. The present study considers a relatively small reinforced concrete structure, for which the load redistribution paths remain relatively simple. In taller or more irregular buildings, redundancy, continuity and alternative load paths may play a more significant role, potentially changing the relationship between seismic design and robustness against progressive collapse. Such an extension would help establish whether the conclusions reached in this thesis are specific to the case study or reflect a broader structural behaviour.

7 BIBLIOGRAPHY

[1] ASCE, «Minimum design loads for buildings and other structures,» Washington, DC, 2005.

[2] J. a. E. J. Agarwal, «Recent developments in robustness and relation with risk,» *Structures and Buildings,* vol. 161, pp. 183-188, 2008.

[3] BSI, Eurocode — Basis of structural design: Incorporating corrigenda December 2008 and April 2010, London, 2010.

[4] HM, The Building Regulations 2010: Structure, A3: Disproportionate collapse, H. Government, A cura di, London, 2010.

[5] Starossek, Progressive Collapse of Structures, Second Edition a cura di, London: ICE Publishing, 2017, p. 19.

[6] F. Fu, Structural Analysis and Design to Prevent Disproportionate Collapse, C. Press, A cura di, Boca Raton, FL, 2016.

[7] L. Sheng, «Tearing behavior of PVC-coated fabric with double initial crack,» *Thin-Walled Structures,* vol. 211, 2025.

[8] S.-f. Gong, L. Yuan e W.-l. Jin, «Buckle propagation of offshore pipelines under external pressure,» *Marine Structures,* vol. 29, pp. 115-130, 2012.

[9] C. Pearson e N. Delatte, «Ronan Point Apartment Tower Collapse and its Effect on Building Codes,» *Journal of Performance of Constructed Facilities,* pp. 172 - 176, 2005.

[10] W. G. Corley, P. F. S. Mlakar, M. A. Sozen e C. H. Thornton, «The Oklahoma City Bombing: Summary and Recommendations for Multihazard Mitigation,» Reston, 1996.

[11] https://www.fbi.gov/news/stories/the-oklahoma-city-bombing-20-years-later. [Online].

[12] M. Al-Bazoon e J. S. Arora, «Design of Structures Subjected to Blast Loads: Analysis and Design Review,» *Misan Journal of Engineering Sciences,* vol. 3, pp. 16-37, 2024.

[13] S. Shyam-Sunder, R. Gann, . Grosshandler, H. Lew, R. Bukowski, F. Sadek, F. Gayle, J. Gross, T. McAllister, J. Averill, J. Lawson, H. Nelson e S. Cauffman, Federal Building and Fire Safety Investigation of the World Trade Center Disaster: Final Report on the Collapse of the World Trade Center Towers, U. D. o. C. National Institute of Standards and Technology (NIST), A cura di, Gaithersburg, 2005.

[14] https://www.nist.gov/. [Online].

[15] https://www.britannica.com/editor/The-Editors-of-Encyclopaedia-Britannica/4419. [Online].

[16] K. Meguro e H. S. Tagel-Din, «Applied Element Method Used for Large Displacement Structural Analysis,» *Journal of Natural Disaster Science,* vol. 24, pp. 25-34, 2002.

[17] L. Applied Science International, «Extreme Loading® for Structures: Theoretical Manual,» 2022.

[18] M. d. I. e. d. Trasporti, Norme Tecniche per le Costruzioni, Rome, 2018.

[19] D. o. Defense, «Unified Facilities Criteria (UFC) 4-023-03: Design of Buildings to Resist Progressive Collapse,» Department of Defense, Washington, DC, 2009.

[20] Faridmehr Iman, Osman Mohd Hanim, Tahir Mahmood Bin Md, Farokhi Nejad Ali, Hodjati Reza, «Seismic and progressive collapse assessment of SidePlate moment connection system,» *Structural Engineering and Mechanics,* pp. 35-54, January 2015.

[21] J. G. M. Wood, «Pipers Row Car Park, Wolverhampton: Quantitative Study of the Causes of the Partial Collapse on 20th March 1997».